UNITED NATIONS EDUCATIONAL, SCIENTIFIC AND CULTURAL ORGANIZATION
INTERNATIONAL ATOMIC ENERGY AGENCY
INTERNATIONAL CENTRE FOR THEORETICAL PHYSICS
I.C.T.P., P.O. BOX 586, 34100 TRIESTE, ITALY, CABLE: CENTRATOM TRIESTE

SMR/1006 - 28

COURSE ON "OCEAN-ATMOSPHERE INTERACTIONS IN THE TROPICS"
26 May - 6 June 1997

"Climate Variability Simulated in GCMs"

"ENSO & ENSO-related Predictability. Part I: Prediction of Equatorial Pacific Sea Surface Temperature with a Hybrid Coupled Ocean-Atmosphere Model"

presented by

P. CHANG
Physical Oceanography
Texas A&M University
College Station, TX
USA

Please note: These are preliminary notes intended for internal distribution only.

19

Climate variability simulated in GCMs

Ngar-Cheung Lau

19.1 Introduction

One of the most striking characteristics of the Earth's climate system is its variability on a broad range of time scales. The temporal changes that immediately come to mind are those associated with the climatological seasonal and diurnal cycles. Superimposed on these periodic phenomena are many different types of irregular variations. Such departures from the long-term means are often referred to as "anomalies". We shall focus on the numerical simulation of such anomalous fluctuations in this chapter. The pertinent model results will be discussed mostly from a meteorological perspective. This approach is motivated by the important role of the atmospheric circulation in climate variability, and by the devotion of a substantial portion of our modeling efforts to atmospheric simulations. However, we must bear in mind that the atmospheric variability described here is intimately linked to the behavior of other components of the climate system. We shall consider only a subset of these interactions here, namely those involving the atmosphere and the underlying land and ocean surfaces. For a more in-depth treatment of the connections between various climatic components, the reader is referred to other relevant chapters in this book, particularly those in Parts 2 and 4.

As an illustration of the richness of the frequency spectrum for the atmospheric component of the climate system, typical time series of the observed daily and monthly fluctuations of surface air temperature are displayed in Fig. 19.1. The top panel of this diagram depicts day-to-day temperature changes during the winter of 1984/85 at 40°N, 75°W (incidentally, this particular location is selected for its proximity to Princeton, NJ). This time series indicates the frequent occurrence of temperature rises and falls on time scales of less than a week. A closer inspection of this panel reveals the occasional tendency for the rapid temperature changes to "ride" on more slow varying fluctuations. Examples of the latter, longer-term events include the warm spells from November 22 to December 4, and from December 8 to 24, as well as the persistent cold episode lasting from January 8 to February 10. The bottom panel of Fig. 19.1 describes the variations of the monthly averaged, Northern

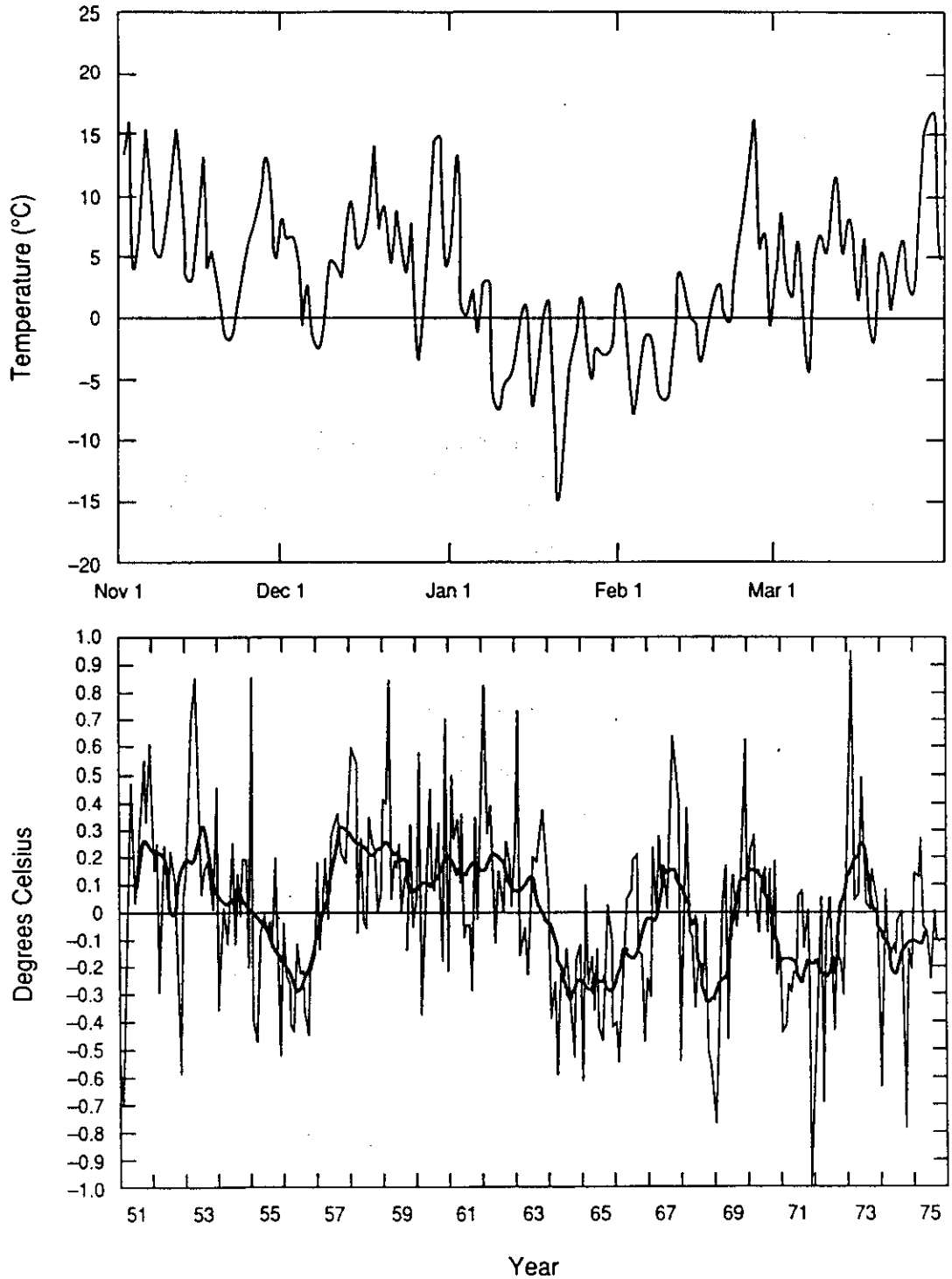

Fig. 19.1 Time series of daily mean 1,000 mb temperature at the gridpoint 40°N 75°W for the period November 1984–March 1985 (top panel), and monthly (light curve) and 12-month running mean (heavy curve) Northern Hemisphere average surface air temperature anomalies for the period 1951–1975 (bottom panel). Data sources: European Centre for Medium-Range Weather Forecasts analyses for top panel; and Yamamoto et al. (1975) and Manabe and Hahn (1981) for bottom panel.

Hemisphere mean temperature anomalies in a 25-year period. The averaged temperatures for individual months (light curve) exhibit notable departures from the climatological mean. The amplitudes of such perturbations are considerably lower than those associated with the daily and local changes portrayed in the top panel. In analogy with the daily temperature record, the monthly means displayed in the bottom panel are modulated by fluctuations with time scales of several years, as highlighted by the time series of the 12-month running means (heavy curve). Of particular interest is the prolonged warm period from 1957 to 1963, and the prominent temperature oscillations from 1965 to 1975 with typical periods of 2–4 years. Turning our attention now to the variability on even longer time scales, it is seen from global temperature variations (IPCC, 1990a) that the year-to-year perturbations are superposed on secular changes with even longer time scales. The warming trend from the beginning of the twentieth century to 1940, and the cooling trend in the 1960s are particularly evident (see Fig. 1.4).

The atmospheric variability in a particular portion of the frequency spectrum is often linked to a specific family of meteorological phenomena, which are, in turn, associated with a distinct set of dynamical and physical processes. In studying the behavior of the climate system, it is essential to have a clear understanding of the nature and origin of atmospheric variability on different time scales. As demonstrated in the preceding paragraph, the characteristic atmospheric time scales which are worth consideration include:

- *Periods of several days*

  Fluctuations on such short periods (referred by many meteorologists as the "synoptic" time scales) are often manifestations of the passage of transient weather systems. These circulation features possess distinct structural and propagation characteristics, and primarily owe their existence to internal atmospheric processes, such as hydrodynamic instability and convection.

- *Periods ranging from about 10 days to a season*

  This time range is particularly relevant to medium- and long-range weather forecasting. The atmospheric variability on this time scale is linked to both the inherent atmospheric variations and interactions with other parts of the climate system. From a meteorological standpoint, the latter interactions affect the atmosphere through alterations of the "boundary conditions" or "boundary forcing" at various interfaces. Some of the atmospheric phenomena in this category, such as persistent high pressure centers in the extratropics, exert a considerable influence on the trajectory and intensity of synoptic-scale systems for extended periods of time. The prevalence of such long-lived meteorological patterns over a given region is often associated with notable changes in the local climate

on subseasonal time scales, such as the occurrence of droughts, floods, and temperature extremes (see examples in the top panel of Fig. 19.1).

- *Periods of several years*

  The roles of different processes operating at various interfaces with the atmosphere become more important for these time scales. In view of the long "memory" embedded in many maritime and land processes, the efforts in understanding interannual variability of the climate system have mostly concentrated on interactions of the atmospheric circulation with the underlying ocean and continental surfaces.

- *Periods of decades and beyond*

  Decadal and centennial climate variability may be attributed to the effects of processes with even longer characteristic time scales, such as those accompanying atmospheric interactions with the deep ocean or the cryosphere, secular changes in the concentration of chemical constituents in the atmosphere, and variations in the Earth's orbital parameters.

During the past decade, the modeling community has performed many investigations aimed at simulating the myriad phenomena associated with the entire range of time scales listed above. The primary tools for such endeavors are the current generation of General Circulation Models (GCMs) at various research centers. A general description of the atmospheric GCMs is given in Chapter 10. Integrations with these GCMs provide a controlled environment in which the contributions of specific internal and external processes to atmospheric variability can be diagnosed in a systematic manner. Most of these model variability studies have been conducted using one of the following experimental designs:

- *Atmospheric GCM runs with fixed, climatological boundary conditions*

  These integrations are particularly suited for studying the nature of model variability in the absence of certain factors which are considered to be external to the atmosphere, such as the influences of sea surface temperature anomalies. The variability in these experiments with climatological setting can mostly be attributed to dynamical and physical processes operating in the atmospheric interior.

- *Atmospheric GCM runs with perturbed boundary conditions*

  This class of experiments entails the prescription of anomalous conditions at certain interfaces between the atmosphere and other components of the climate system. These integrations allow for the boundary conditions to affect the atmosphere, but do not permit the atmosphere to change the boundary conditions. The sensitivity of the model atmosphere to the boundary conditions in question can be assessed by contrasting the output from such experiments with the output from "control" runs subjected to climatological forcing.

- *Coupled experiments with full interactions between the atmosphere and other subsystems*

  The variability of the atmosphere as well as other climatic components (e.g., ocean, cryosphere, ground hydrology) is modeled explicitly in these integrations. Two-way interactions (or "feedbacks") between the atmosphere and other components are incorporated in these coupled models.

Model studies of atmospheric variability performed to date have mostly focused on time scales of several years and less. The emphasis on the high-frequency end of the atmospheric spectrum is somewhat dictated by the availability of computer resources, which, until very recently, were only able to accommodate experiments with durations not longer than several decades. Phenomena and processes with time scales of a decade or more are therefore not sufficiently sampled in such simulations. Moreover, contemporary empirical and theoretical studies have fostered a rapid advance of our knowledge of atmospheric fluctuations with subseasonal and interannual time scales. On the other hand, our understanding of ultra-long period variations of the climate system is hindered by the scarcity of long and reliable observational records, as well as the lack of physical insights into the processes pertinent to these time scales.

The present chapter presents an overview of the different facets of model-simulated climate variability. Emphasis is placed on the baseline levels of variability of the atmosphere–ocean–land–cryosphere subsystem, in the absence of perturbations that might be ascribed to human activity, such as the increase of greenhouse gases. The following presentation is organized according to the typical time scales of the phenomena of interest, which range from periods shorter than a season (Sec. 19.2), to several years (Sec. 19.3), and to a decade and longer (Sec. 19.4). Since some processes and phenomena have a wide span of time scales, some overlap among the discussions in these individual sections is unavoidable.

For a more elaborate discussion of atmospheric and oceanic variability, the interested reader is encouraged to peruse the review articles in the monograph edited by Cattle (1987). Many of the lectures given at the NCAR Summer Colloquium (1987) on the dynamics of low-frequency phenomena in the atmosphere are also relevant to our subject matter. The notes from these presentations (available as a three-volume publication from NCAR) provide a comprehensive survey of the pertinent literature.

19.2 Variability on daily and monthly time scales

19.2.1 Phenomena with periods of several days

At first glance, the typical periods of these circulation features may appear to be too short to have any noticeable impact on the behavior

of the climate system. Nonetheless, these short-lived phenomena do play a crucial role in the long-term balances of energy, momentum and water vapor in the atmospheric branch of the climate system. As will be elaborated later in this chapter, these high-frequency disturbances are also capable of influencing the more slowly varying flow patterns through mutual dynamical interactions, and by communicating the effects of anomalous boundary forcings to the quasi-stationary component of the atmospheric circulation. Moreover, the synoptic climatology (such as the seasonal dependence of precipitation amounts and temperature extremes) of many geographical sites is partially determined by the frequency of occurrence of these weather-scale features. The day-to-day (or "synoptic scale") fluctuations at a midlatitude site (such as those described in the top panel of Fig. 19.1) are mostly associated with migratory cyclones and anticyclones. The preferred trajectories of these disturbances are often referred to as "storm tracks" in the meteorological literature, and have been identified in the extratropical oceans of both the Northern and Southern Hemispheres (Blackmon, 1976; Trenberth, 1981). During the winter season, these zonally elongated sites of eddy activity are located downstream and slightly poleward of the quasi-stationary jet streams (narrow zones of high wind speed). Many observational studies of the structural and transport characteristics of the transient fluctuations residing in the storm tracks have been performed. These empirical results reveal many similarities with those associated with the life-cycle of unstable waves, as produced in simplified mechanistic models (e.g., Simmons and Hoskins, 1978). In particular, vigorous heat and momentum transports by the cyclone waves take place along the storm tracks, thus resulting in enhanced energy exchanges between the transient disturbances and the more slowly varying background flow.

The ability of the GCMs to reproduce the essential characteristics of the extratropical storm tracks has been the subject of many investigations. Most of these studies are concerned with the geographical distribution of temporal variance and covariance statistics based on time-filtered model data. As an illustration of the capability of the current generation of GCMs to simulate the storm track properties, the wintertime distributions of the root-mean-squares of the local height of the 500 mb surface are shown in Fig. 19.2. The height data have been filtered (Blackmon, 1976) to retain fluctuations with time scales between 2.5 and 6 days. Maxima in these charts indicate the occurrence of enhanced variability on subweekly time scales in the nearby regions. It is evident that the geographical locations of the observed sites of synoptic activity over the North Pacific and North Atlantic, as well as the typical eddy amplitude therein, are well simulated in the model atmosphere.

Synoptic-scale weather systems are found not only in the temperate latitudes. Summertime wavelike disturbances with periods of several days are also observed to be active in certain tropical zones (Lau and Lau, 1990). Such transient fluctuations are mostly westward moving, and exhibit well-

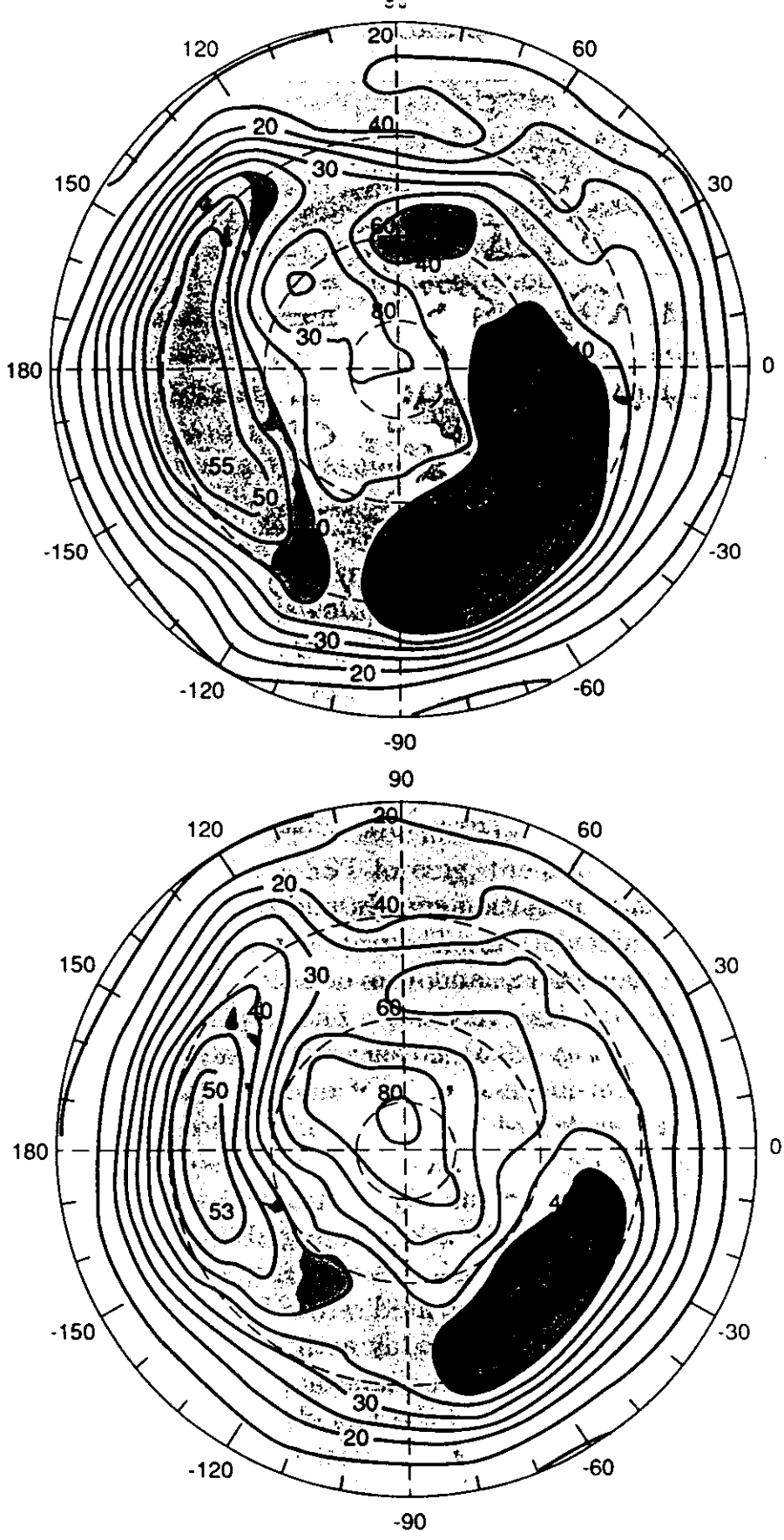

Fig. 19.2 Distributions of the observed (top panel) and model-simulated (bottom panel) root-mean-squares of wintertime 500 mb height data which have been filtered to retain fluctuations with periods between 2.5 and 6 days. Contour interval: 5 m. From Lau and Nath (1987).

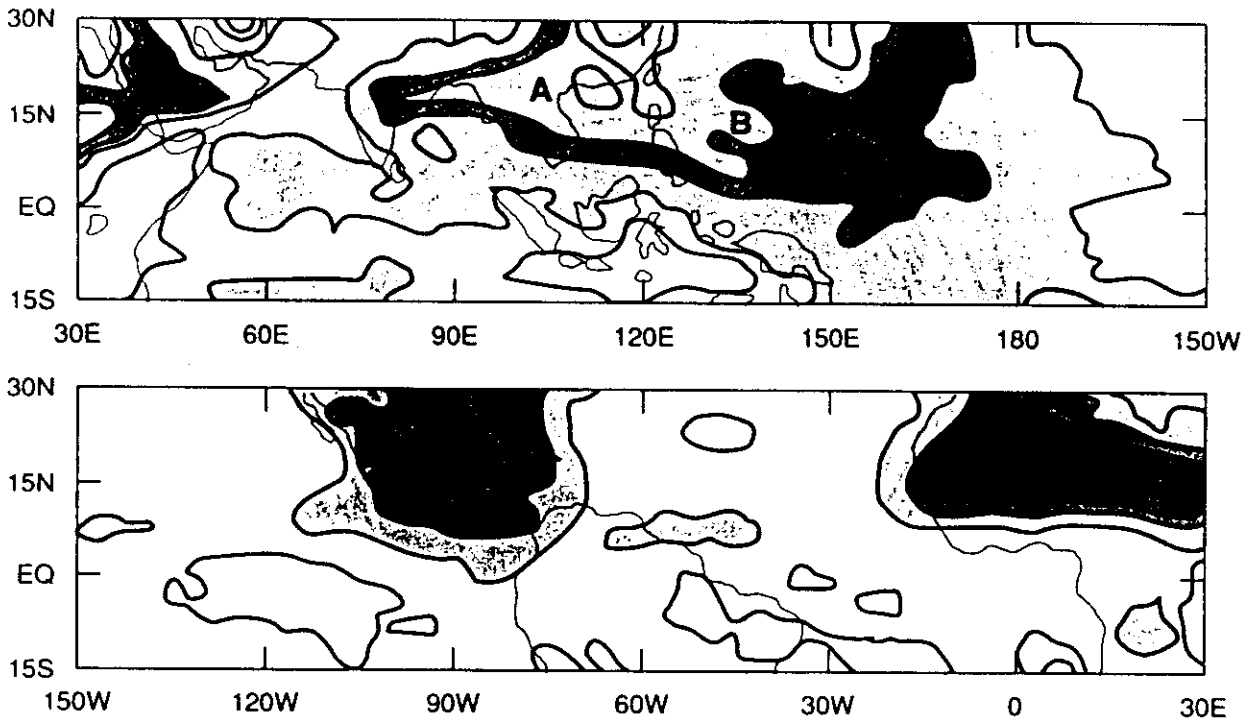

Fig. 19.3 Distribution of the model-simulated root-mean-squares of unfiltered 850 mb vorticity during the northern summer. Contour interval: 4×10^{-6} s^{-1}. Light, medium, and dense shading indicate values of 10–14 $\times 10^{-6}$ s^{-1}, 14–18 $\times 10^{-6}$ s^{-1}, and $> 18 \times 10^{-6}$ s^{-1}, respectively. From Lau (1991).

defined wavelengths, propagation speeds, and spatial relationships with the ambient large-scale circulation. They appear to be intimately associated with deep moist convection, and are occasionally accompanied by the formation of severe tropical vortices. The appearance of these tropical features in a GCM (Fig. 19.3) is shown by the northern summertime distribution of the root-mean-squares of daily fluctuations in the 850 mb vorticity, which is a measure of the rotation of the flow. This pattern clearly illustrates the occurrence in the model atmosphere of enhanced variability over the Bay of Bengal/Indochina region, tropical western Pacific, Central America and northern Africa (marked in Fig. 19.3 by the labels A, B, C and D, respectively). The disturbances over the Asian monsoon regions in sites A and B appear to be associated with the local semipermanent low pressure zone during summer. The eddy activity over northern Africa bears a strong relationship with the local climatological easterly jet stream. The locations of various active sites in the model tropics, and their association with the seasonally averaged circulation features, are in agreement with the corresponding observational results.

19.2.2 Phenomena with periods ranging from 10 days to a season

The processes contributing to atmospheric variability on this time scale may be classified under two broad categories – internal atmospheric

dynamics and forcing by anomalous boundary conditions. A comprehensive review of the nature of various internal and boundary mechanisms has been offered by Wallace and Blackmon (1983). The internal atmospheric processes relevant to this range include nonlinear interactions among different atmospheric wave components, and forcing by high-frequency transients (such as those described in the previous subsection). The second class of processes entails the forcing of the atmospheric circulation by the slowly varying changes in the properties of the land and ocean surfaces. Among the various interactive processes between the atmosphere and other components of the climate system, particular emphasis has been placed on the impact of sea surface temperature (SST) conditions on the atmospheric circulation. To date, the diagnosis of subseasonal variability has mostly been performed on GCM experiments with fixed, climatological SST conditions (see Sec. 19.1 of this chapter for a general discussion on experimental designs). A majority of the simulations with prescribed anomalous forcing is concerned with atmospheric changes on time scales of a season and longer. To simplify the presentation, we shall limit our attention to the role of internal atmospheric processes in this subsection, and defer the discussion on boundary forcing to the next section.

A detailed statistical analysis of the atmospheric variability simulated in a 15-year integration of a GCM (Manabe and Hahn, 1981) shows that, even in the absence of any anomalous SST forcing, the amplitudes of pressure and temperature fluctuations on monthly time scales in the model extratropics approach those of the observed atmosphere. The wintertime hemispheric distributions of model and observed root-mean-squares of 500 mb height values which have been filtered to retain fluctuations with periods between 10 days and a season (Fig. 19.4) reveal that the observed sites of enhanced variability on this time scale over the North Pacific and North Atlantic are mimicked by the model atmosphere, with the simulated amplitudes reaching to 70–80% of the observed values.

The output from Manabe and Hahn's experiment provides additional evidence that the model atmosphere with climatological SST forcing can reproduce the frequency dependence of the three-dimensional structure and temporal evolution of observed midlatitude phenomena with subseasonal time scales (Lau, 1981; Lau and Nath, 1987). In particular, some of the best-known recurrent circulation anomalies (often referred to as "teleconnection patterns") are discernible in the model atmosphere. The space-time evolution of model features with time scales of 10–30 days is similar to that associated with the dispersion of wave energy, with little or no phase propagation, whereas perturbations with periods longer than a month are organized in dipolar structures in the Northern Hemisphere. This distinction between the simulated eddy behavior in the two period ranges is in agreement with observational analyses (e.g., see Blackmon et al., 1984). The structural and energetic behavior of both observed and simulated

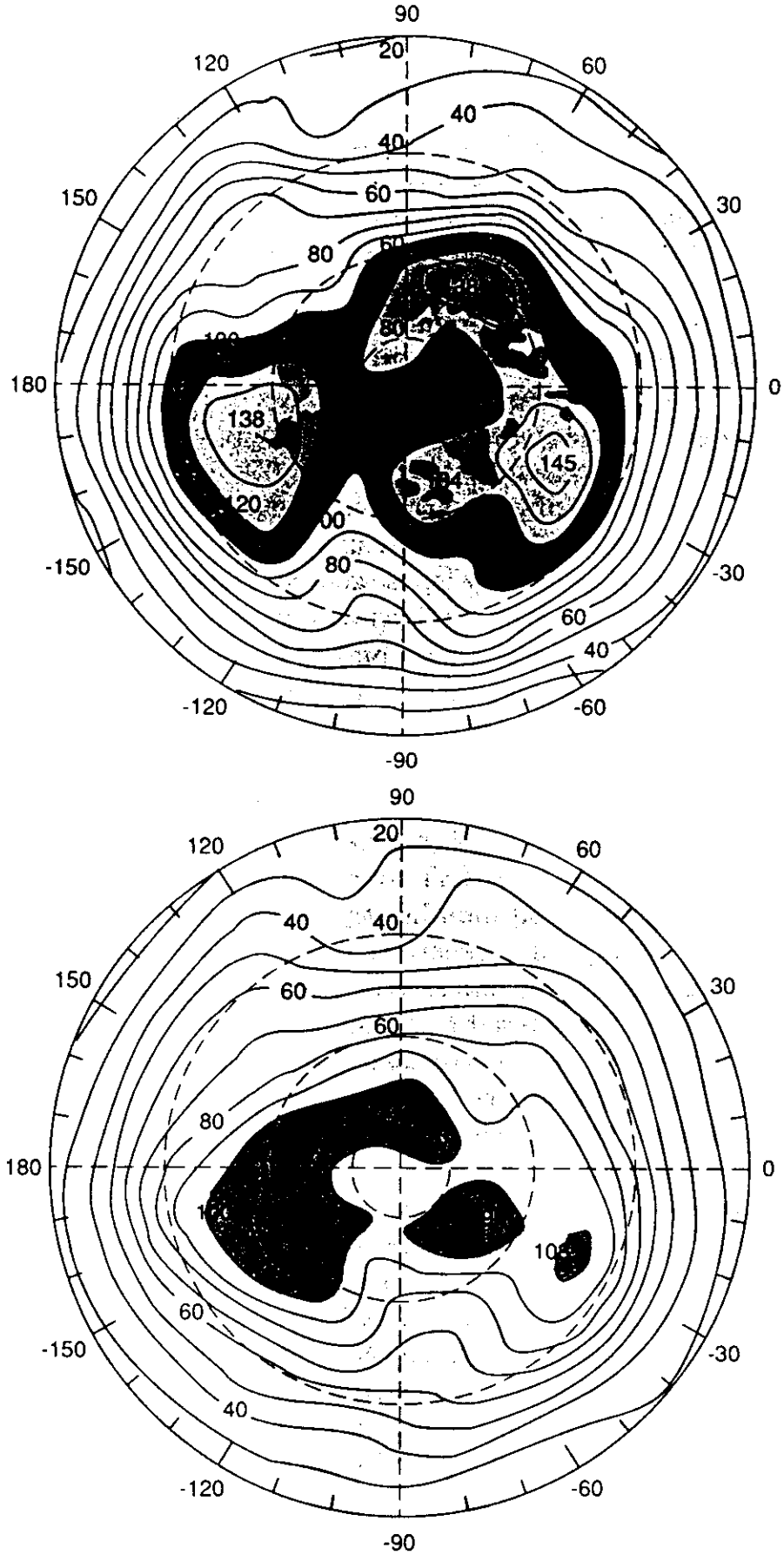

Fig. 19.4 Distributions of the observed (top panel) and model-simulated (bottom panel) root-mean-squares of wintertime 500 mb height data which have been filtered to retain fluctuations with periods between 10 days and a season. Contour interval: 10 m. From Lau and Nath (1987).

perturbations with monthly time scales tend to be elongated in the east-west direction, and thereby extract kinetic energy from the time-averaged jet streams (Wallace and Lau, 1985).

The largely statistical description in the preceding paragraphs is complemented by case-study approaches aimed at highlighting specific classes of model phenomena with weekly and monthly time scales. Of particular interest is the simulation of long-lived, quasi-stationary high pressure centers (often referred to as "blocking highs") in the extratropics. The climatology of blocking events appearing in a 1,200-day wintertime experiment with a GCM subjected to fixed boundary conditions (Blackmon et al., 1986) shows that the structural characteristics of the blocking highs in the model atmosphere are in agreement with the observations. For instance, the composite pattern of simulated blocking highs over the North Pacific bears a striking resemblance to its observed counterpart (Fig. 19.5). In the charts shown, the air flow is oriented approximately parallel to the contours. The set of parabola-shaped contours in the vicinity of 160–170°W represents a marked impediment to the normal west-to-east flow (hence the term "blocking"). Examples of model blocks occurring in conjunction with explosive cyclone formation or strong interactions with synoptic-scale eddies were also presented. The realistic simulation of the blocking episodes in a model environment with climatological boundary conditions led these investigators to suggest that internal atmospheric dynamics and physics could play an important role in the formation and maintenance of such phenomena. The heat and vorticity budgets as well as the transient eddy forcing of the model-generated blocking anticyclones were analyzed (Mullen, 1986). These results highlight the association of blocking events with systematic displacements of the tracks of synoptic-scale disturbances, and with well-defined changes in the heat and momentum transport properties of the high-frequency eddies. Many of the relationships between the simulated storm tracks and the slowly varying circulation are consistent with those pertaining to the observed atmosphere.

Another family of intraseasonal phenomena that has attracted considerable attention in the modeling community is the eastward propagating, planetary-scale "Madden–Julian" oscillation in the tropical troposphere, with a characteristic period of 40–50 days. This feature is associated with observed large-scale variations in pressure, wind, and convective activity near the equator (Madden and Julian, 1972). The origin of this oscillation has been linked to the interaction between moist convection and various wave modes which are preferentially excited in the deep tropics (e.g., Lau and Peng, 1987). A multitude of model diagnostic studies have demonstrated that some of the essential characteristics of the tropical intraseasonal oscillations are captured by GCMs subjected to nonvarying boundary forcing. An example of the model-simulated perturbations in precipitation (contours) and upper-level divergence (stippling) associated

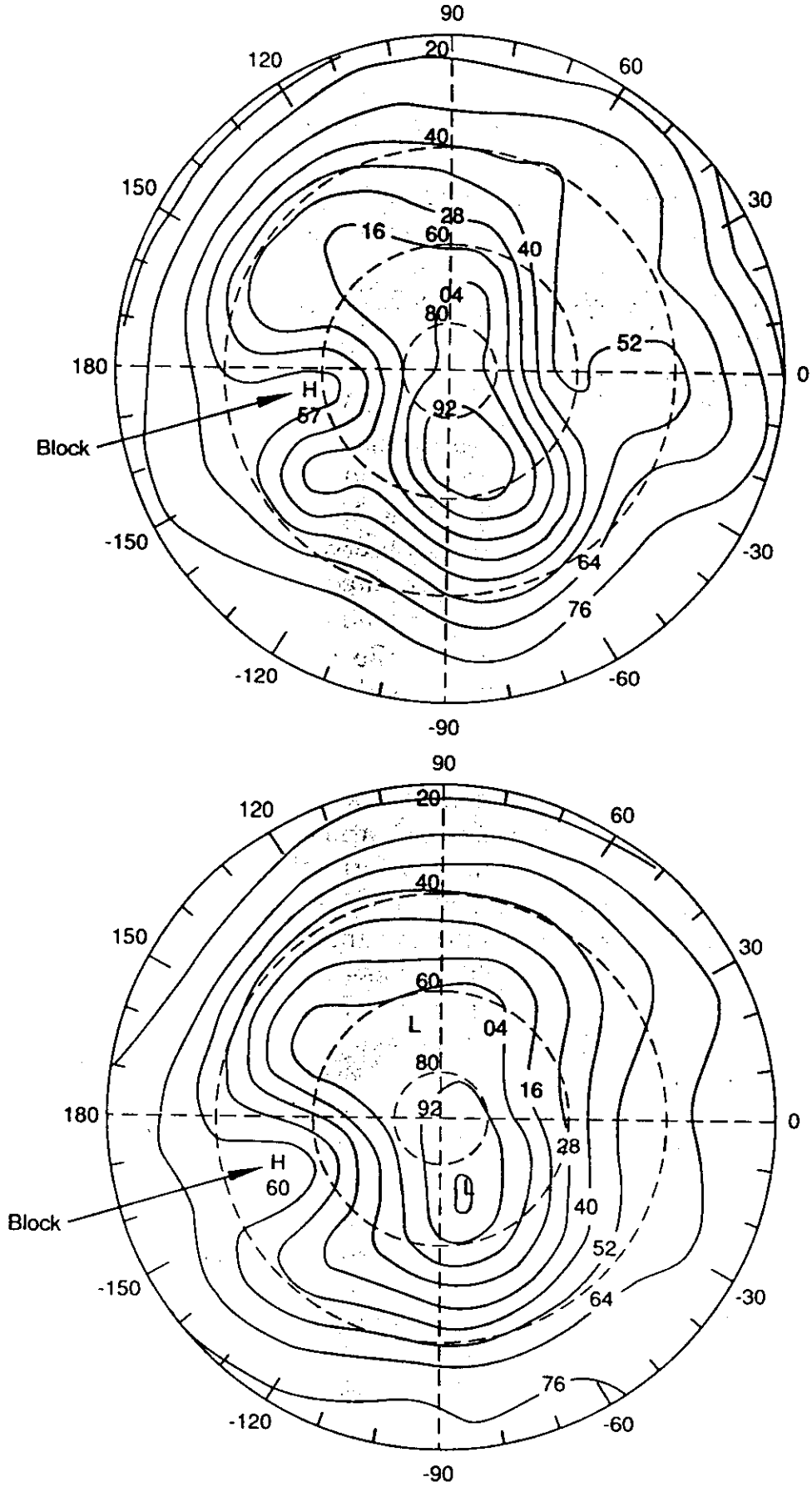

Fig. 19.5 Composite distribution of 500 mb height for observed (top panel) and model-simulated (bottom panel) blocking events over the North Pacific. Contour interval: 120 m. From Blackmon et al. (1986). Note the high pressure region (labelled as "Block") near 160–170°W.

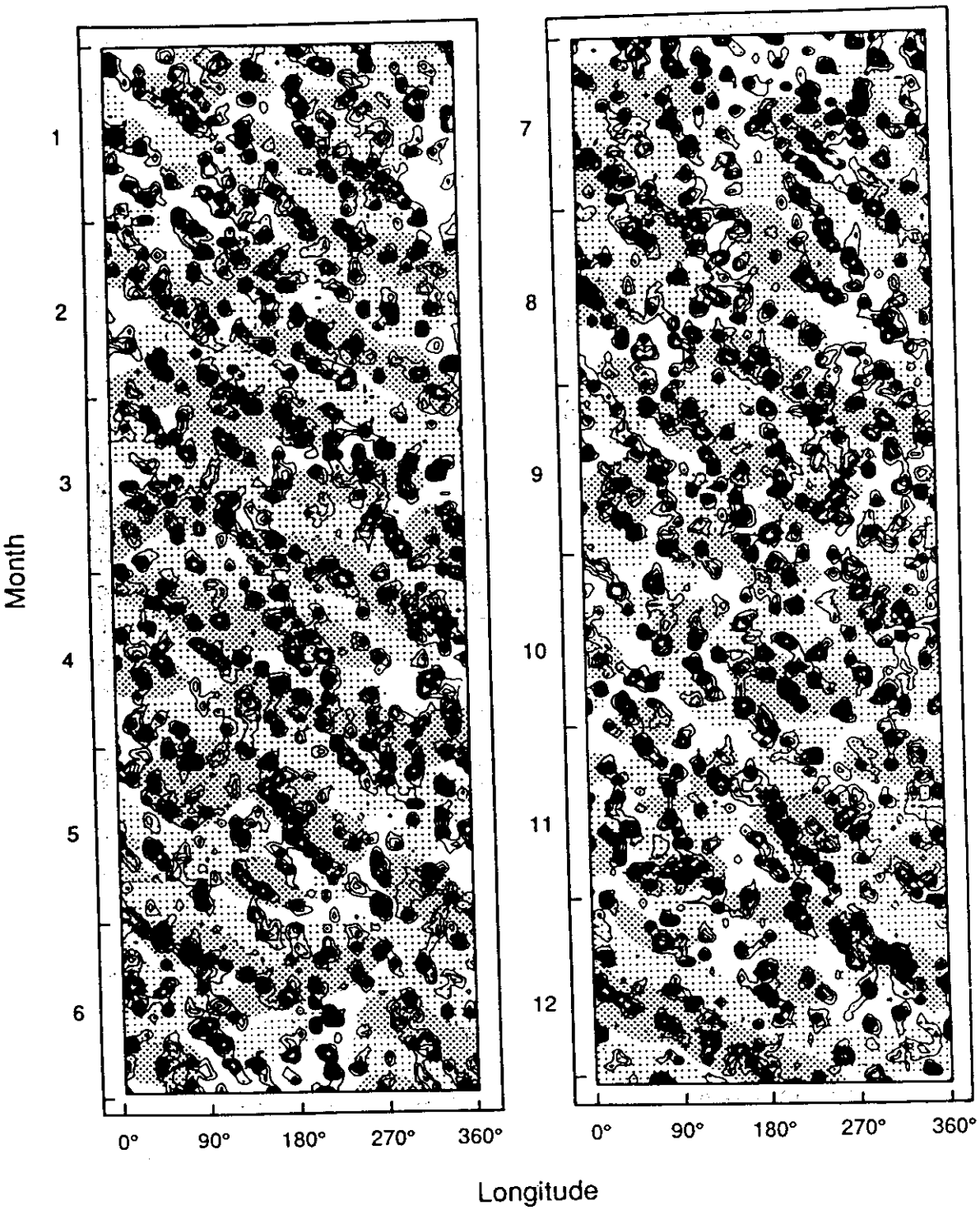

Fig. 19.6 Time–longitude distribution of model-simulated daily precipitation rate near the equator. Contour interval: 4 mm day^{-1}. Light and dense stippling indicate large-scale convergence and divergence near the tropopause, respectively. From Lau et al. (1988).

with this propagating phenomenon extracted from a 1,400-day integration using an idealized GCM with a zonally symmetric climate is displayed in Fig. 19.6. Note the tendency for most of the precipitation signals to migrate towards increasing longitude as one scans down the time axis. This diagram hence illustrates the prevalence of organized, eastward-traveling convective

cells and divergence centers along the equatorial belt. Analogously, dry episodes are typically accompanied by upper-level convergence. The typical period of this oscillation in the model atmosphere is about 20–30 days. The notably shorter periods (as compared with the observations) seen here appear to be a deficiency shared by many GCMs. The phase speeds of these oscillations are seen to be sensitive to the details of model parameterizations of static stability and penetrative cumulus convection.

19.3 Variability on time scales ranging from months to several years

Simulations of atmospheric variability on time scales of several months to several years have mostly been concerned with the roles of interactive processes taking place at the air–sea and air–land interfaces. We shall therefore devote this section to describing phenomena associated with atmospheric interactions with the underlying boundaries. As pointed out in Sec. 19.2.2, conditions at the land and ocean surfaces may influence the atmospheric circulation on time scales even shorter than a season. Hence part of the following discussion has relevance to some of the subseasonal circulation features mentioned in Sec. 19.2.2.

19.3.1 Phenomena associated with air–sea interaction in the tropics

A substantial fraction of the modeling activity on the impact of tropical SST anomalies is focused on the atmosphere/ocean behavior during El Niño–Southern Oscillation (ENSO) episodes in the Pacific. These ENSO cycles have a typical time scale of several years, and are accompanied by coherent changes in many elements of the climate system. For instance, the interannual variations in Northern Hemisphere mean temperature previously noted in the bottom panel of Fig. 19.1 are rather well correlated with the timing of ENSO events in the same era. In view of the widespread influences of ENSO-related processes, secular changes in the frequency of occurrence of such episodes may complicate attempts to detect global warming due to increasing greenhouse gases (Trenberth, 1990). For a more detailed description of the important role of air–sea coupling in generating various ENSO phenomena, the reader is referred to Chapter 18.

Many simulations of the atmospheric phenomena related to ENSO have been conducted by prescribing a perturbed SST forcing at the lower boundary which is *spatially and temporally fixed.* Such experiments are hence primarily aimed at studying the *steady-state* response of the model atmosphere to a set of anomalous (but constant) boundary conditions. An additional degree of realism was built into the series of model runs analyzed by Lau (1985), in which the observed month-to-month changes

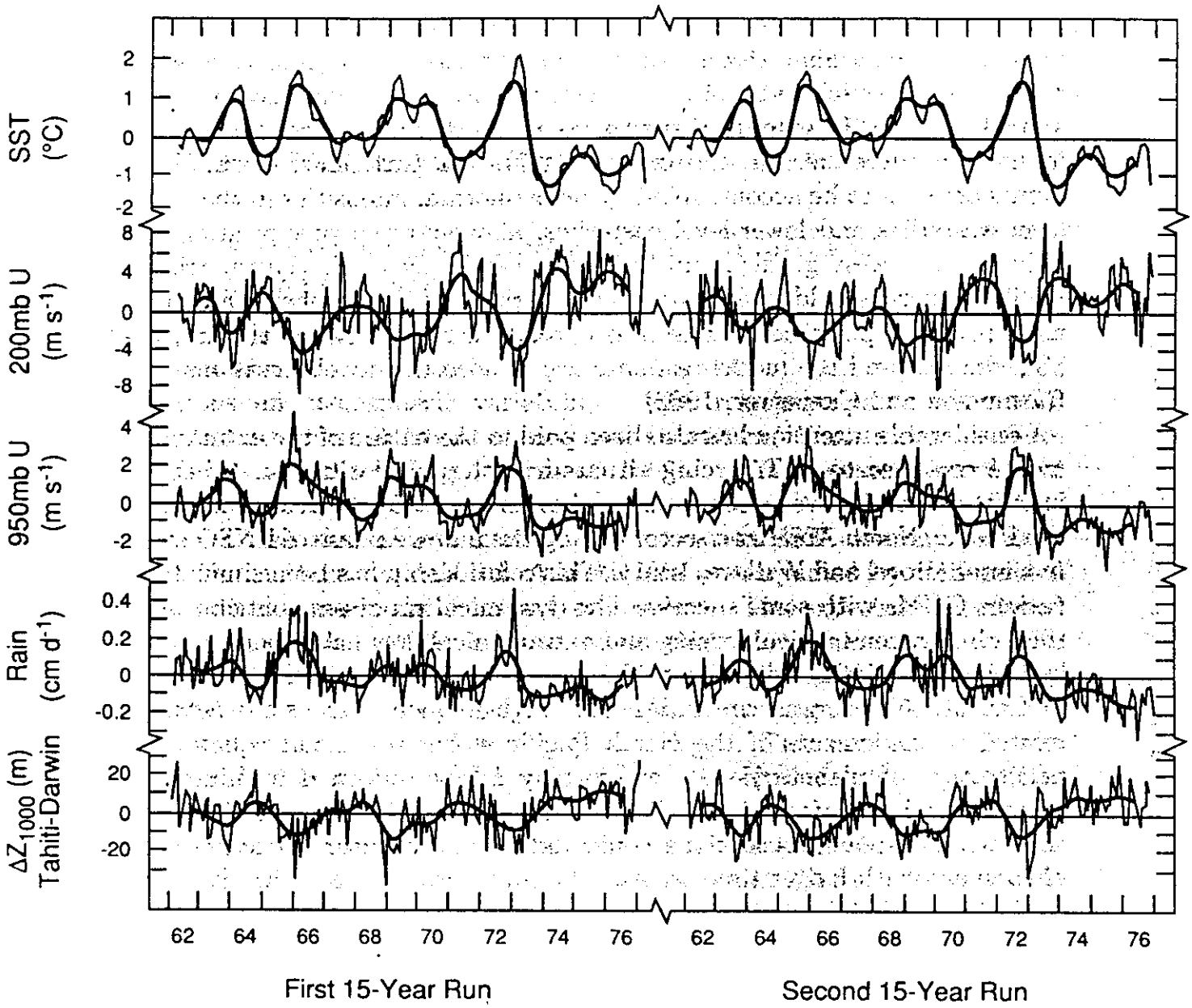

Fig. 19.7 Time series of monthly (light curves) and lowpass filtered (heavy curves) anomalies of sea surface temperature, zonal wind at 200 and 950 mb, precipitation rate, and difference in 1,000 mb height between Tahiti and Darwin, for two independent 15-year model simulations. The tropical indices are computed using data for the central equatorial Pacific. From Lau (1985).

in the tropical Pacific SST field were specified, so that the lower boundary forcing of the atmospheric circulation varies in both space and time. The latter experimental design allows for a more detailed simulation of the *time-varying* atmospheric response in different phases of the ENSO cycle.

In Lau (1985), experiments were initiated using two independent sets of atmospheric conditions, but were subjected to the identical sequence of anomalous SST forcing observed during the 1962–1976 period. The time series of representative indices of the atmospheric circulation in a pair of 15-year integrations (Fig. 19.7) indicate that the interannual component of the

model variability (heavy curves) is rather similar in the two runs. However, it is also evident that the month-to-month fluctuations (thin curves) are not reproducible in the two 15-year integrations. The model fluctuations on annual time scales exhibit a strong correlation with the concurrent SST input (see curves at the top of Fig. 19.7). In particular, warm ENSO events are seen to be accompanied by below-normal intensities in the upper-level westerlies and lower-level easterlies, above-normal precipitation, and reduced east–west gradient in 1,000 mb height over the central tropical Pacific, whereas cold events are characterized by atmospheric anomalies with reversed polarities. The above relationships between the imposed SST changes and the model response are in accord with observations (e.g., Rasmusson and Carpenter, 1982).

Considerable attention has also been paid to the nature of the *extratropical* model response to SST forcing situated in the low latitudes. Of special interest is the observed occurrence of a prominent teleconnection pattern in the Pacific/North American sector during the mature phase of ENSO events in winter (Horel and Wallace, 1981). This relationship has been simulated in various GCMs with some success. The dynamical processes contributing to the link between tropical forcing and extratropical flow have been examined by Held et al. (1989) using the model output from the experiments described in Lau (1985). It was concluded that high-frequency transient activities related to movements of the North Pacific storm track and equatorward penetration of planetary-scale waves play a key role in determining the extratropical response. This finding reinforces the earlier claim in Sec. 19.2.1 that synoptic-scale fluctuations could influence the nature of atmospheric phenomena with longer time scales.

Manabe and Hahn (1981) have pointed out that their model experiment with climatological SST forcing produces lower levels of variability in the tropics than observed. The variance statistics of their "control" experiment have been compared with those derived from the model run with prescribed SST changes (Lau, 1985). It is seen that the presence of changing SST boundary conditions leads to a significant enhancement in the amplitude of variability in the model tropics. Hence a large fraction of tropical variability may be attributed to air–sea interactions.

Some GCM experiments have also been performed to evaluate the role of SST anomalies in the occurrence of severe droughts. The prescription of a dipole-like SST anomaly in the tropical Atlantic produced drought-like conditions in northeastern Brazil (Moura and Shukla, 1981). Model evidence on the importance of worldwide SST anomalies in the incidence of prolonged dry periods in the Sahel region of Africa has been presented (Folland et al., 1986). The possible causes of the North American drought in the summer of 1988 have been analyzed (Trenberth et al., 1988). It was concluded in the latter study that this event was primarily brought about by an anomalous circulation pattern, which in turn was a forced response

to the distribution of atmospheric heating associated with perturbed SST conditions in the tropical Pacific. The 30-day experiments conducted with operational models at various centers (Palmer and Brankovic, 1989; Kálnay et al., 1990) appear to lend some support to this proposed link between the cold phase of ENSO and the summer drought in 1988.

19.3.2 Phenomena associated with air–sea interaction in the extratropics

The current emphasis on SST anomalies in the equatorial zone has somewhat overshadowed the potential effects of *extratropical* oceanic conditions on atmospheric variability. The relationships between SST variations in the midlatitude oceans and short-term climate changes have long been recognized (e.g., Namias, 1969). The research interest in this issue has recently been revived by new observational and modeling results. These studies demonstrate that recurrent SST anomaly patterns in the North Pacific and North Atlantic are accompanied by well-defined circulation changes in the overlying atmosphere. The experiment analyzed by Pitcher et al. (1988) indicates that the atmospheric responses to prescribed midlatitude SST forcings exhibit a notable degree of nonlinearity, i.e., the response does not undergo a straightforward sign reversal when the polarity of the imposed SST anomaly is changed. This nonlinear behavior is also evident in similar model runs analyzed by Kushnir and Lau (1992).

The relative contributions of SST anomalies in the tropics and the extratropics to atmospheric variability on interannual time scales were evaluated with a 30-year integration (Lau and Nath, 1990). The experimental design of this model run is similar to that used in Lau (1985), except that the domain of prescribed (and temporally varying) SST anomalies has been extended to all maritime gridpoints lying north of 40°S, so as to incorporate the boundary forcing in the North Pacific and North Atlantic as well as the tropical oceans. A global survey of the model output indicates that the seasonally averaged circulation during the northern winter exhibits strong covariability with the thermal conditions at two specific ocean sites in the extratropics, namely, the regions just south of Newfoundland and to the northwest of Hawaii. The distributions of regression coefficients of model-simulated 515 mb height versus the SST input at these two forcing locations (Fig. 19.8) depict the amplitude and polarity of typical pressure changes at various gridpoints corresponding to an SST increase of 1°C at the forcing site (indicated by a solid dot). The spatial pattern of the model response with respect to the SST forcing is in accord with the observational results. Lau and Nath also reported that the circulation in the Pacific/North American sector of the model atmosphere is more sensitive to in situ SST variations in the North Pacific than to remote forcing from the tropical ENSO region. The same conclusion was

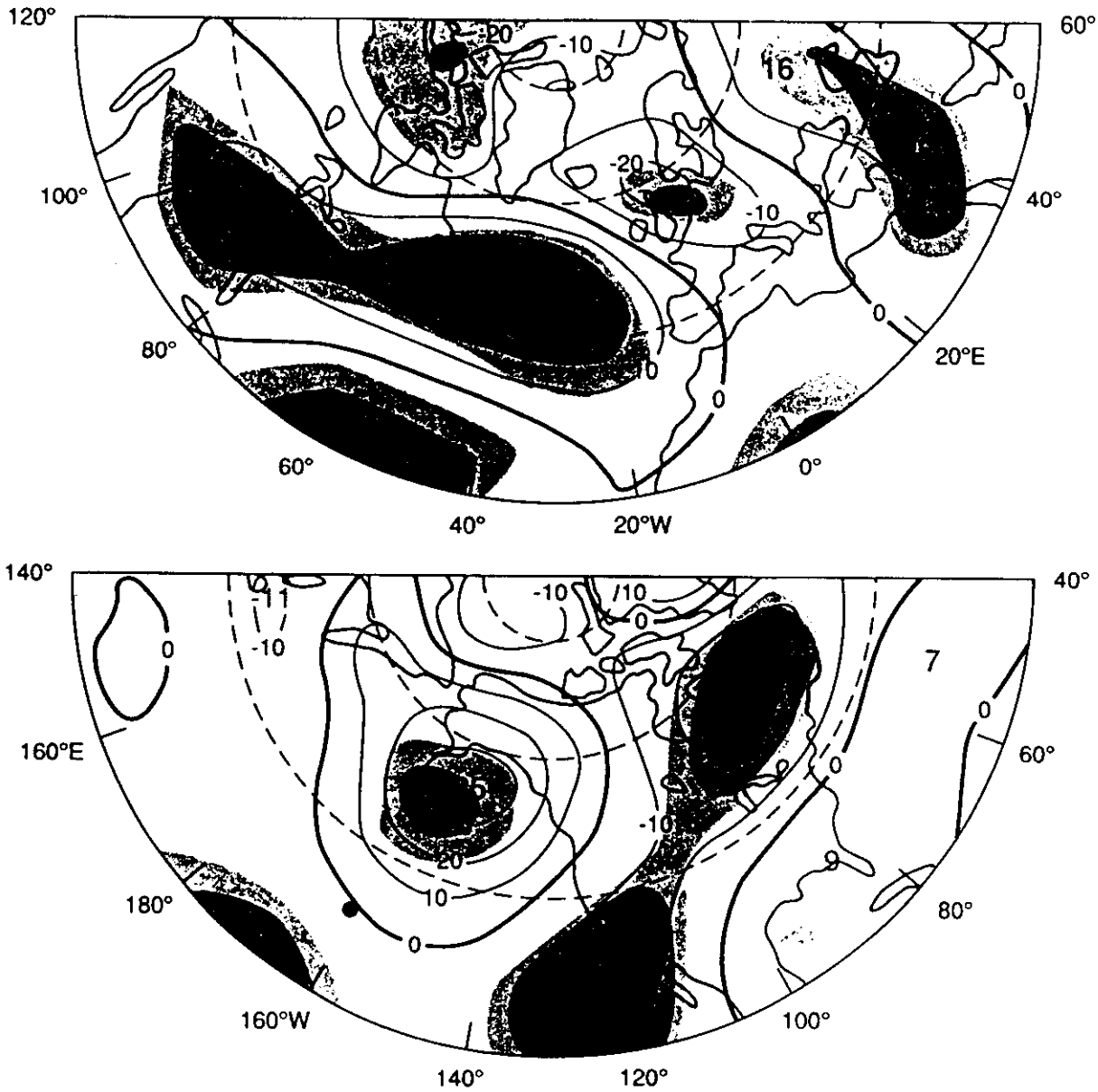

Fig. 19.8 Distributions of the linear regression coefficients between model-simulated, seasonally averaged 515 mb height at individual gridpoints and the imposed sea surface temperature anomalies at 45°N 56°W (top panel) and 31.5°N 161°W (bottom panel). The locations of the sea surface temperature forcing sites are indicated by solid dots. Significant regression values at the 90%, 95% and 99% levels are indicated by light, medium and dense shading, respectively. Contour interval: 10 m per °C. From Lau and Nath (1990).

reached earlier in the observational analysis by Wallace and Jiang (1987). A comprehensive treatment of climate variability must therefore take into account the effects of extratropical air–sea interaction.

Diagnosis of the model output by Palmer and Sun (1985) and Lau and Nath (1990) indicates that not only do the seasonally averaged flow patterns respond to the imposed oceanic forcing, the preferred sites of synoptic-scale disturbances are also noticeably altered due to relocations of the zones of strong temperature gradient at the lower boundary. The displacements of

the storm tracks, in turn, exert a strong influence on the distributions of precipitation (and hence atmospheric heating) anomalies, as well as the spatial patterns of heat and moisture fluxes across the air–sea interface. Moreover, realignments of the storm tracks lead to notable changes in the dynamical interaction between the quasi-stationary circulation and the synoptic-scale eddies. Here is yet another example of the strong relationships between storm track dynamics and atmospheric behavior on lower frequencies.

In addition to the *simultaneous* relationships between midlatitude SST anomalies and the atmospheric circulation described above, there also exists some empirical evidence on the tendency for the atmospheric flow to *lead* the oceanic changes by one to several months (Davis, 1976; Wallace et al., 1990). Such results suggest that fluctuations in the extratropical oceans may actually be the result, rather than the initiator, of air–sea interactions. The asynchronous relationships have been investigated by the present author on the basis of an experiment in which an atmospheric GCM was coupled to a motionless mixed ocean layer of uniform thickness. The temperature of this ocean layer was allowed to vary according to the intensity of local heat fluxes across the air–sea boundary. Fluctuations of the latter fluxes are largely determined by the surface wind speed and air-to-sea temperature differences. Analysis of the model output indicates that even such a simple coupled system is capable of reproducing some of the observed spatial modes of SST and sea level pressure variability. Moreover, the simulated atmospheric changes typically lead the changes in the mixed layer temperature by approximately one month. It thus appears that, even in the absence of detailed ocean dynamics, the extratropical mixed layer in this simplified coupled model responds to local changes in the air–sea heat exchange in a rather realistic manner. These model results further substantiate the notion that the driving of the ocean by the atmospheric circulation plays a significant role in the extratropical variability of the coupled system. However, by virtue of the strong degree of temporal persistence of the oceanic fluctuations, a given SST anomaly produced several months earlier might last long enough to affect the current atmospheric state. It is therefore reasonable that a considerable degree of simultaneous correlation still remains between the variations in the ocean and the atmosphere, as demonstrated in the observational and modeling studies cited earlier in this subsection. Analysis of experiments with fully coupled ocean–atmosphere GCMs should be very helpful in advancing our understanding of the full array of feedback mechanisms involved in extratropical air–sea interaction.

19.3.3 Air–land interaction

One of the most conspicuous properties of the land surface that exhibits marked variability from winter to winter is the latitudinal extent

of continental snow cover (see Chapter 5). Idealized GCM experiments confirm that changes in the snow cover alter the albedo and availability of ground water, and thereby exert a strong influence on the heat and soil moisture budgets of the land surface (Yeh et al., 1983). These model runs further illustrate that the removal of snow cover in late winter results in fluctuations in the climate system that persist well into the following spring and summer, with significant impacts on the thermal and dynamical structure of the atmosphere. Observational evidence on the relationships between seasonal snow cover and the atmospheric circulation (Walsh et al., 1982) shows that the extent of the snow line over North America exhibits a strong correlation with a characteristic teleconnection pattern at 700 mb (top panel of Fig. 19.9). Above-normal snow cover extent at a given longitude coincides with below-normal 700 mb heights directly aloft, and vice versa. The model output from the 15-year experiment of Manabe and Hahn (1981) analyzed by the present author in the same manner shows that the resulting correlation pattern (bottom panel of Fig. 19.9) bears a considerable resemblance to the observations. The lag-correlation statistics indicate that the changes in the atmospheric circulation tend to precede the variations in the snow cover in both model and observations. It thus appears that interactions between continental snow cover and the atmospheric circulation are properly captured by the GCM under investigation. In analogy with the discussion on extratropical air–sea interaction in Section 19.3.2, the nature of the simultaneous and lagged relationships between the atmospheric changes and the snow cover anomaly suggests that the atmospheric circulation could exert a considerable influence on the extent of continental snow cover. The persistence of the snow cover anomalies on monthly time scales could in turn allow for such anomalies to modify the present atmospheric flow.

Another property of the land surface affecting climate variability on interannual time scales is soil moisture. Diagnosis of GCM experiments with idealized geography indicates that soil moisture anomalies can persist for at least several months (Yeh et al., 1984). The length of this persistence time scale exhibits a latitudinal dependence, and is governed by the interplay of various hydrological processes such as evaporation, precipitation, runoff, and atmospheric moisture transport. It was also demonstrated that the soil moisture changes result in notable perturbations of the atmospheric circulation. Experimentation with a two-level GCM allowing for atmospheric interactions with the soil moisture content (Gordon and Hunt, 1987; Hunt and Gordon, 1988) reveals that, even in the absence of anomalous SST forcing, annual and multi-annual droughts do occur in selected geographical regions in the model climate. When compared with observed droughts, the simulated events tend to be more locally confined.

The summertime response of model atmospheres with realistic geography to imposed soil moisture perturbations demonstrate that the prescribed soil moisture changes have noticeable effects on the temperature and

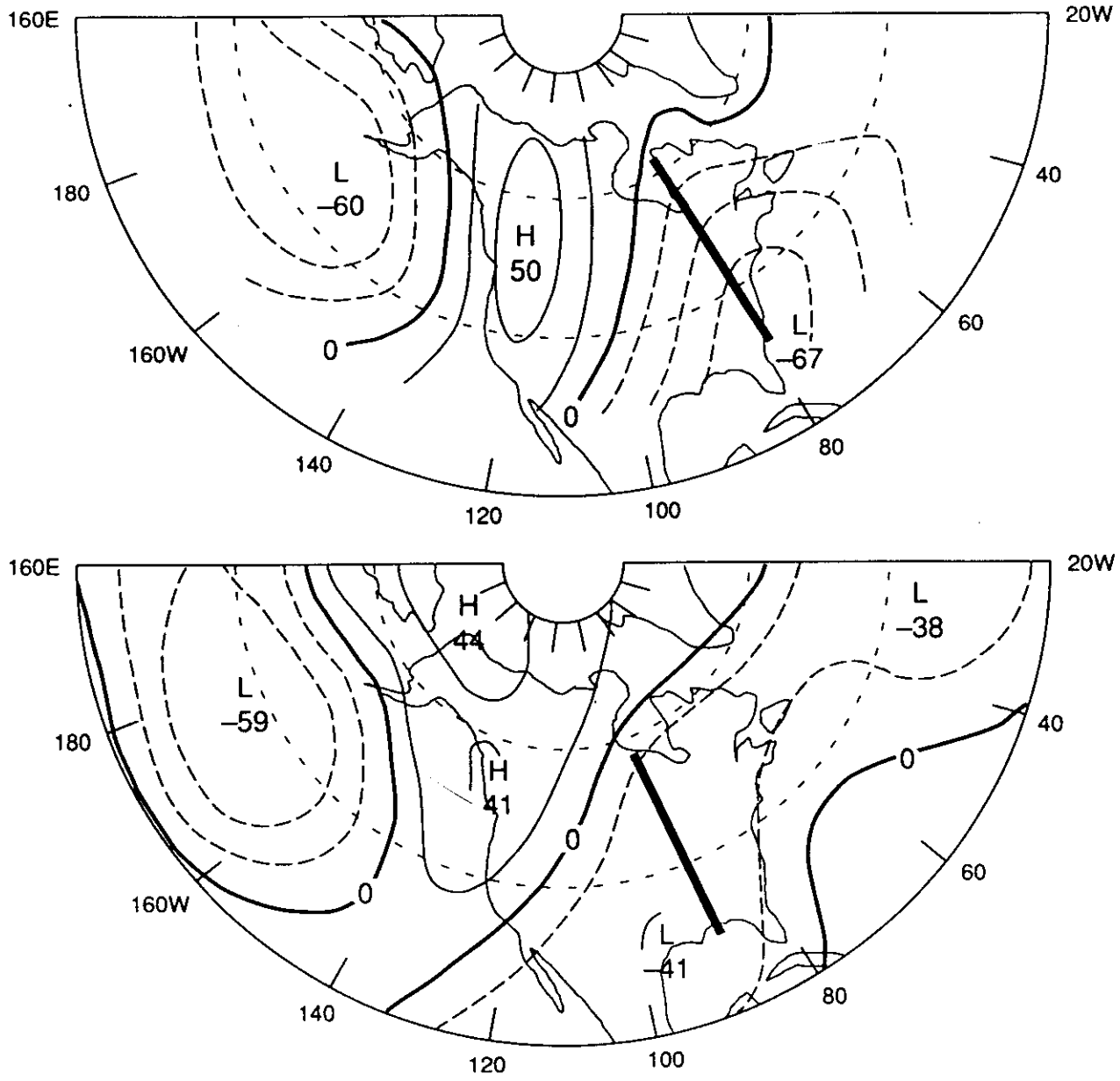

Fig. 19.9. Distributions of the correlation coefficients (in percent) between wintertime 700 mb height at individual gridpoints and the latitudinal extent of snow cover near the 80°W meridian, as obtained from observations (top panel, from Walsh et al., 1982), and from the author's analysis of the 15-year model simulation by Manabe and Hahn (bottom panel).

precipitation in the vicinity of the anomaly area (see Rowntree and Bolton (1983) for the European sector, and Rind (1982) and Oglesby and Erickson (1989) for North America). In particular, Oglesby and Erickson (1989) pointed out that reduced soil wetness may contribute to the initiation and sustenance of warm and dry conditions over midlatitude continental interiors, such as those observed over North America in the summer of 1988.

The nature of soil wetness variability and its influences on the near-surface climate were interpreted in a stochastic framework analogous to

that outlined by Hasselmann (1976) in two model studies by Delworth and Manabe (1988, 1989). It was noted that the soil moisture parameterization scheme used in the experiments is a close mathematical analog to a first-order Markov process[1], in which random forcing with a white-noise spectrum (i.e., with variance uniformly spread over all frequencies) could yield a red-noise response (i.e., with more variance residing in lower frequencies). Evaporation serves as the damping term in the linear Markov process; whereas the white-noise forcing is supplied by the sum of rainfall and snowmelt. The soil moisture may hence be viewed as an integrator of random precipitation forcing from the atmosphere, thereby lending an increased low-frequency (red-noise) component to the variability of the ground hydrology. The model evidence presented by Delworth and Manabe confirms that the precipitation forcing is characterized by a white-noise spectrum, whereas the soil moisture response exhibits a distinct red-noise behavior, with half of the total variance residing at periods longer than seven months in the low latitudes, and as much as 13–20 months in the extratropics. It was shown that the persistence time scale of model soil wetness anomalies is inversely proportional to the rate of dissipation of soil wetness anomalies by evaporation. This dissipation rate is dependent on potential evaporation, so that the persistence time scale is longer when potential evaporation is weak (note that potential evaporation decreases poleward in relation to the poleward reduction of solar insolation). The occurrence of frequent runoff in regions where precipitation exceeds the mean potential evaporation rate can substantially reduce the persistence time scale of model soil wetness.

Some of these model findings have been confirmed by Vinnikov and Yeserkepova (1991) using soil moisture measurements taken at an extensive network of stations in the then Soviet Union. Delworth and Manabe have further evaluated the impact of soil processes on atmospheric variability by comparing the model statistics for a 50-year experiment which incorporates full interactions between the land surface and the atmosphere, with the corresponding statistics for a 25-year run in which such interactions are suppressed. It was concluded that soil processes act to increase the characteristic persistence time scale of the atmosphere. Due to influences of the soil wetness on the intensity of latent and sensible heat fluxes through the ground surface, the amplitude of the variability in temperature and relative humidity is also notably increased in the interactive run, particularly in the low latitudes and during the summer season.

19.4 Variability on decadal and centennial time scales

Thus far, only limited observational and modeling efforts have been devoted to climate variability on time scales of decades and longer.

[1] A concise discussion of Markov processes can be found in Chatfield (1984).

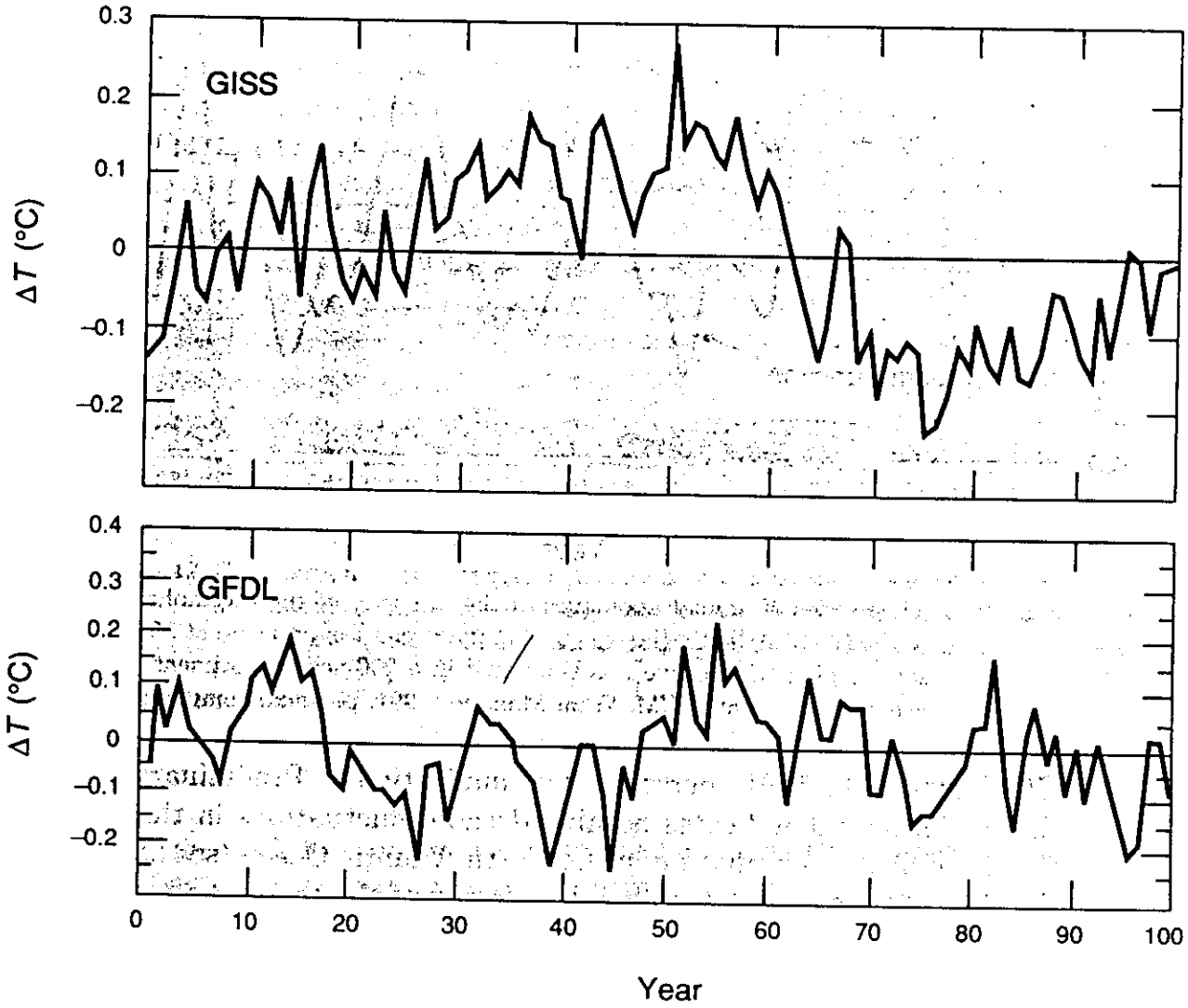

Fig. 19.10 Time series of annual global mean surface air temperature anomalies, as simulated in century-long integrations with coupled models at GISS (top panel, from Hansen and Lebedeff, 1987), and at GFDL (bottom panel, from Manabe et al., 1991).

Our understanding of such ultra-long period fluctuations therefore remains rather inadequate. It is, however, of interest to note the few available century-long integrations of coupled models with fixed external forcing do yield interdecadal variations of the global mean surface temperatures, with typical amplitudes of several tenths of a degree C (Fig. 19.10). In order to comprehend the origin of this low-frequency variability, one must invoke those processes in the climate system with very long time scales.

Since both the specific heat of sea water and the mass of the total water column are very large, the deep ocean has an enormous heat capacity, and exhibits fluctuations on time scales ranging from decades to centuries. Processes associated with the deep ocean circulation should therefore contribute significantly to very low-frequency variability of the climate system. The nature of atmosphere–ocean interactions on decadal time scales has recently been investigated using a 200-year integration of a coupled

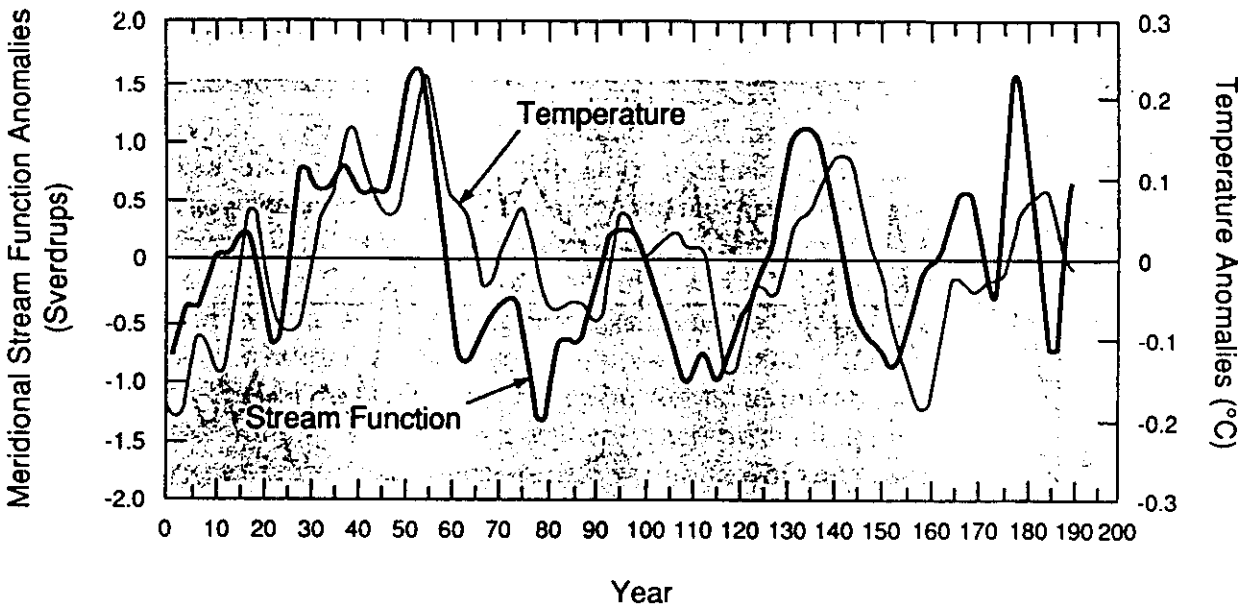

Fig. 19.11 Time series of annual anomalies of the intensity of the thermohaline circulation in the North Atlantic (heavy curve), and ocean temperature at 85 m depth in the same region (thin curve), as simulated in a 200-year experiment with a coupled atmosphere–ocean GCM. From Manabe (1991, personal communication).

GCM (Manabe, 1991, personal communication). Preliminary analysis of the model output indicates notable decadal fluctuations in the intensity of the thermohaline circulation in the North Atlantic Ocean (see heavy curve in Fig. 19.11). For a more detailed description of the thermohaline circulation, the reader is referred to Chapter 17. The changes in the thermohaline circulation are seen to be accompanied by pronounced variations in the subsurface ocean temperature (see thin curve in Fig. 19.11). There exists a distinct tendency for the fluctuations in the thermohaline circulation to lead the temperature anomalies by several years. These findings illustrate a potential role for the thermohaline circulation to modulate the North Atlantic climate on decadal time scales. Diagnosis of the same 200-year experiment also reveals substantial low-frequency variability in the Southern Ocean, with local SST anomalies persisting for several decades. These phenomena are apparently manifestations of long-period fluctuations of the circumpolar deep ocean circulation around Antarctica.

The amplitude of low-frequency variability simulated in the above-mentioned coupled experiment is shown by the distribution of the standard deviation of annually averaged SST, as calculated using data from the first 50 years of the integration (Fig. 19.12). This pattern indicates that enhanced variability is simulated in the North Atlantic, northwestern Pacific and the waters surrounding Antarctica. The maxima in the North Atlantic and the southern oceans coincide well with the sites of pronounced fluctuations in the thermohaline and the circumpolar deep

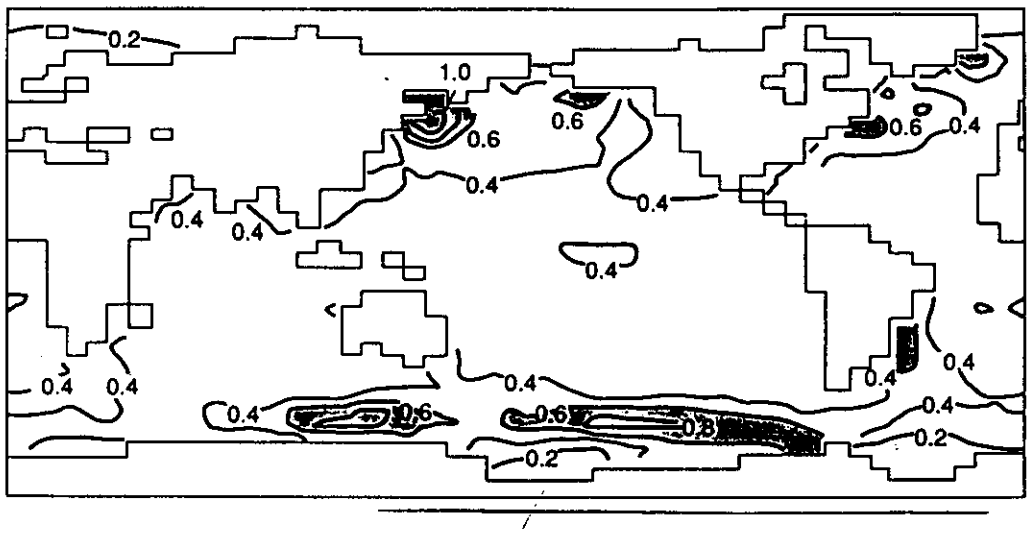

Fig. 19.12 Distribution of the standard deviation of annual mean sea surface temperature, as computed using the first 50 years of a 200-year experiment with a coupled atmosphere–ocean GCM. Contour interval: 0.25°C. From Manabe (1991, personal communication).

ocean circulations, respectively, as discussed in the preceding paragraph. The Northern Hemisphere, extratropical features in Fig. 19.12 are in fair agreement with the observations. The model variability in the tropical Pacific is noticeably weaker than that inferred from ship measurements. The latter discrepancy is primarily a consequence of the low resolution of the ocean GCM used in this experiment, which leads to ENSO events with reduced amplitudes.

In analogy with the discussion of air–land interaction in Sec. 19.3.3, the variability introduced by ocean–atmosphere coupling may also be viewed in a stochastic framework. In the present context, the principal damping mechanism is represented by deep mixing in the ocean interior, whereas the white-noise forcing may be supplied by randomly distributed freshwater fluxes from the atmosphere. This framework was tested using the output of a 4,000-year integration with an ocean model (Mikolajewicz and Maier-Reimer, 1990). Their results suggest that the ocean response to white-noise atmospheric forcing does exhibit a red-noise character for periods of 30 years and less. On even longer time scales, the model behavior is significantly different from that associated with a simple first-order Markov process. Instead, it was shown that the internal dynamics of the model drive a well-defined mode of ocean variability with a typical period of about 320 years. This very low-frequency oscillation is accompanied by coherent changes in the intensity of the basin-wide thermohaline circulation in the Atlantic, and in the mass transport through the Drake Passage.

19.5 Outlook

In this brief survey, it has been demonstrated that the GCMs serve as a powerful tool in expanding our knowledge of the nature of climate variability on a wide range of time scales. Properly designed experiments with these GCMs have provided useful insights on the individual roles and relative importance of different processes in various phenomena occurring within the climate system. With the advent of ever-increasing computational capacity, it will soon be feasible to conduct experiments with coupled systems with durations of a millennium (or even longer) on a routine basis. The model output from such integrations should provide unprecedented details on the ultra low-frequency behavior of the climate system. In fact, the rapidly increasing temporal and spatial coverage of the model-simulated data may soon surpass the corresponding coverage of any conceivable instrumental record of the observed climate system. Thus the array of model tools will in future constitute an unique resource for studying long-term climate change.

Climate modeling activities have always been conducted in conjunction with observational analyses of the real system. The observations provide the ultimate test of model fidelity. Moreover, observational evidence of certain behavior in the climate system often motivates the design and diagnosis of new model experiments. Conversely, model predictions of cause-and-effect relationships or new phenomena often suggest innovative interpretations and analysis procedures of the pertinent observations, or provide useful guidelines for gathering new empirical data. This synergism among model experimentation and real data analysis will hopefully be sustained in future studies of climate variability.

Notwithstanding the immense potential of the numerical models for climate research, it is necessary to bear in mind that a realistic simulation of the climate system is contingent upon the accurate model representation of the complex processes operating within a given component of the system, as well as the interactions among different components. Model development efforts aimed at incorporating the various interactive mechanisms mentioned here are still in a relatively primitive stage. These endeavors would benefit enormously from the bridging of our current research and educational activities across traditional academic disciplines, such as meteorology, oceanography, hydrology, geochemistry and glaciology. The salient relationships between various subsystems of the Earth's climate clearly call for such interdisciplinary approaches.

20

Climate-model responses to increased CO_2 and other greenhouse gases

Warren M. Washington

20.1 Introduction

The Swedish chemist Svante Arrhenius (1896) was the first researcher to express concern about the possible climatic effects of increased concentrations of greenhouse gases, such as carbon dioxide (CO_2). At the same time, the Industrial Revolution of the late 1890s saw a great increase in fossil fuel use, particularly coal, that has led to the observed increases in CO_2 in the atmosphere (Fig. 2.2). Arrhenius concluded that atmospheric CO_2 was important to the Earth's heat balance and that increases in these gases would lead to increased atmospheric temperature. Arrhenius estimated that an increase of 2.5 to 3 times the CO_2 concentration would result in a globally averaged temperature increase of 8–9°C, an effect not too different from that estimated by today's complex computer climate models.

Somewhat earlier, the Irish scientist John Tynall (1861), in his classic paper, *On the absorption and radiation of heat by gases and vapours, and on the physical connexion of radiation, absorption and conduction,* described the effect of increasing CO_2 and other gases, including water vapor, on the Earth's radiative balance. In a greenhouse analogy, solar radiation would be transmitted largely through greenhouse glass while significant terrestrial or infrared radiation would be trapped by the glass.

With simple models, Callendar (1938), Plass (1961), Mitchell (1961), and others tried to link CO_2 increases to temperature change. This chapter discusses model experiments of the response of the climate to increases in greenhouse gases, especially CO_2. Beyond the use of simple models to examine aspects of this problem (Secs. 20.5 and 20.6), there are two main kinds of experiments that have been performed with General Circulation Models (GCMs). The first are equilibrium experiments in which the amount of CO_2 in the model atmosphere is doubled and the differences in resulting climate examined (Sec. 20.7). The second are so-called transient experiments in which the amount of CO_2 is increased slowly in a realistic fashion to examine how the climate adjusts to the slowly increasing greenhouse effect (Sec. 20.8). In all these experiments, it is not just the direct changes in greenhouse radiative heating that are important, but also the myriad of complex feedback effects that must be dealt with

Reprinted from JOURNAL OF CLIMATE, Vol. 6, No. 8, August 1993
American Meteorological Society

ENSO and ENSO-related Predictability. Part I: Prediction of Equatorial Pacific Sea Surface Temperature with a Hybrid Coupled Ocean–Atmosphere Model

T. P. BARNETT,* M. LATIF,** N. GRAHAM,* M. FLÜGEL,** S. PAZAN,* AND W. WHITE*

*Climate Research Division, Scripps Institution of Oceanography, University of California
**Max-Planck-Institut für Meteorologie, Hamburg, Germany

(Manuscript received 1 June 1992, in final form 22 December 1992)

ABSTRACT

A hybrid coupled model (HCM) of the tropical ocean–atmosphere system is described. The ocean component is a fully nonlinear ocean general circulation model (OGCM). The atmospheric element is a statistical model that specifies wind stress from ocean-model sea surface temperatures (SST). The coupled model demonstrates a chaotic behavior during extended integration that is related to slow changes in the background mean state of the ocean. The HCM also reproduces many of the observed variations in the tropical Pacific ocean–atmosphere system.

The physical processes operative in the model together describe a natural mode of climate variability in the tropical Pacific ocean–atmosphere system. The mode is composed of (i) westward-propagating Rossby waves and (ii) an equatorially confined air–sea element that propagates eastward. Additional results showed that the seasonal dependence of the anomalous ocean–atmosphere coupling was vital to the model's ability to both replicate and forecast key features of the tropical Pacific climate system.

A series of hindcast and forecast experiments was conducted with the model. It showed real skill in forecasting fall/winter tropical Pacific SST at a lead time of up to 18 months. This skill was largely confined to the central equatorial Pacific, just the region that is most prominent in teleconnections with the Northern Hemisphere during winter. This result suggests the model forecasts of winter SST at leads times of at least 6 months are good enough to be used with atmospheric models (statistical or OGCM) to attempt long-range winter forecasts for the North American continent. This suggestion is confirmed in Part II of this paper.

1. Introduction

The El Niño–Southern Oscillation (ENSO) represents the largest short-term, interannual climate fluctuation on this planet. Because of this fact, there has been a growing interest in predicting extremes of the ENSO and their impacts outside the tropics. The practical benefit of a successful forecast scheme has oft been documented. However, the ability to forecast these events also implies that we have an understanding of the physics responsible for ENSO and its effect on the midlatitude climate system. Such understanding would be a considerable step forward in our knowledge of global climate dynamics. In this two-part paper, we investigate the predictability of the tropic portion of the ENSO signal (Part I), and then try to extend successful tropic forecasts to midlatitudes (Part II).

There is ample evidence that large ENSO events can be predicted. Rigorous statistical forecast models have been employed to forecast tropical Pacific sea surface temperature (SST), which is a major player in any ENSO event. These models have used near-surface winds and upper-ocean heat content in the tropical Pacific as predictors (Barnett 1977, 1984; Barnett and Hasselmann 1979; Graham et al. 1987a,b; Barnett et al. 1988; Latif et al. 1993) to forecast SST out to 6 months in advance. The near-global sea level pressure field has also been used to predict SST out to lead times of order 1 yr (Graham et al. 1987a,b; Barnett et al. 1988). These empirical results have been complemented by simplified ocean forecast models developed at The Florida State University (FSU) (Busalacchi and O'Brien 1981; Inoue and O'Brien 1984) and driven by observed winds. This system appears to have skill out to 3 months in advance (Inoue and O'Brien 1984; Barnett et al. 1988). More impressive forecast lead times have been obtained by the Lamont group (cf. Cane et al. 1986; Cane and Zebiak 1985; Zebiak and Cane 1987), who have demonstrated skill out to 1 yr in advance or more. This work is especially important, for it represents the first embodiment of a theory for ENSO expressed as a simplified dynamical model of the coupled ocean–atmosphere system in the tropical Pacific. Three of the

Corresponding author address: Dr. Tim P. Barnett, Climate Research Division, Scripps Institution of Oceanography, University of California, San Diego, La Jolla, CA 92093.

aforementioned forecast schemes have been run in quasi-operational mode since 1986. In general, they have experienced a surprisingly high degree of success over a time period when the tropical ocean temperatures underwent very large changes ($\pm 2\sigma$).

Considerable effort has recently been devoted to understanding just why the forecast models have been successful. There are several scenarios that now exist but one that seems well supported by model and empirical studies attributes much of the skill at extended lead times to internal ocean dynamics. The introduction of the delayed oscillator concept by Schopf and Suarez (1988) (see also Graham and White 1988; Battisti 1988) was perhaps the first expression that internal ocean waves, once generated, could propagate slowly across great distance, eventually being funneled into the equatorial waveguide to initiate an ENSO event. Another important link involves a strong, local air–sea interaction that amplifies unstably to produce the main ENSO signal, for example, Neelin (1991). Recent results suggest the atmosphere is driven principally by direct ocean forcing (Barnett et al. 1991), a result consistent with the use of a steady-state atmospheric component in the Lamont model. Both of these results suggest the need for any forecast scheme to handle the ocean portion of the ENSO cycle as well as possible.

A new type of model has arisen in response to the key role played by the ocean in the ENSO phenomenon. These models have been called hybrid coupled models (HCM), a term apparently originated by Neelin (1989, 1990). Such models are comprised of a complete ocean general circulation model (OGCM) coupled to a simpler atmospheric model—something far short of a full atmospheric general circulation model (AGCM) in sophistication. An example of such a model may be found in Latif and Flügel (1991), where a primitive equation OGCM was coupled to a statistical atmosphere represented by point correlations between SST and wind stress. Graham et al. (1992) describes a more sophisticated approach in which a statistical atmosphere based on the field-to-field relations between SST and surface wind-stress fields was coupled to the oceanic component of the Lamont model.

The present paper explores the abilities of an HCM to predict ENSO events. In our case, the ocean component of the hybrid model will be a full OGCM, while the atmospheric component will be statistical in nature. Section 2 describes the model briefly, as well as methods to overcome the ubiquitous problems associated with physically coupling ocean and atmosphere models. Section 3 describes the behavior of the coupled model, which leads to the suggestion of the existence of a natural mode of variability in the tropical Pacific ocean–atmosphere system. Section 4 demonstrates the forecast skill of the coupled model, while section 5 discusses several of the more interesting aspects of model performance. Section 6 lists our conclusions.

2. The HCM

a. The ocean model

The ocean model is basically that described in Latif (1987) and is a nonlinear primitive equation model that calculates the three-dimensional current field, sea level, and sea surface temperature on an equatorial β plane. The model domain is the tropical Pacific Ocean from 30°S to 30°N and from 130°E to 70°W. The model includes real coastlines but no bottom topography so that the ocean floor is at a constant depth of 4000 m. The zonal resolution is constant with a grid distance of 670 km. The meridional resolution is variable, increasing from 50 km around the equator to about 400 km at northern and southern boundaries. There are 13 levels in the vertical direction, most of them being placed within the upper 300 m. In contrast to Latif (1987), Richardson's number–dependent vertical-mixing coefficients have been adopted in our study. The model is forced by wind stress and a heat flux that enters only in the form of a Newtonian feedback term.

The performance of the ocean model driven by observed winds [FSU product, see Goldenberg and O'Brien (1981)] during an integration that covered the period 1970–85 has been examined in detail (Latif 1987; Barnett et al. 1991; Miller et al. 1992). The OGCM does a creditable job of generating its own climatological seasonal cycle, although the cold tongue is 1°–2°C too strong. The model also did a reasonably good job of reproducing the anomalous sea level, SST, and zonal currents in a band within 10° of the equator. During the 1982–83 warm event, the model reproduces most of the observed features, including the deceleration of the equatorial undercurrent, the evolution of eastward surface currents, and the zonal redistribution of heat associated with the eastward propagation of warm water.

The numerical skill of the OGCM in producing anomalous SST is shown in Fig. 1 (upper right panel, labeled MPI). The model was forced by the observed FSU wind stress over the period 1970–85 and the resulting monthly SST anomalies correlated with the observations. Also shown for comparison is the same skill measure obtained from three other ocean models forced by exactly the same wind field for the same time period. [See Miller et al. (1992) for a full description and intercomparison of models.] Concentrating on the OGCM used in this study, one finds it works best in the central equatorial Pacific. It performs poorly outside the waveguide, say ±8°, but then it has no effective heat-flux forcing, so this behavior is not surprising. It also does less well at the eastern and western edges of the basin. For latter reference, please note that the Lamont ocean model does better than the MPI OGCM along the coast of South America, while the reverse is true in the central ocean. The forecast skill to be dis-

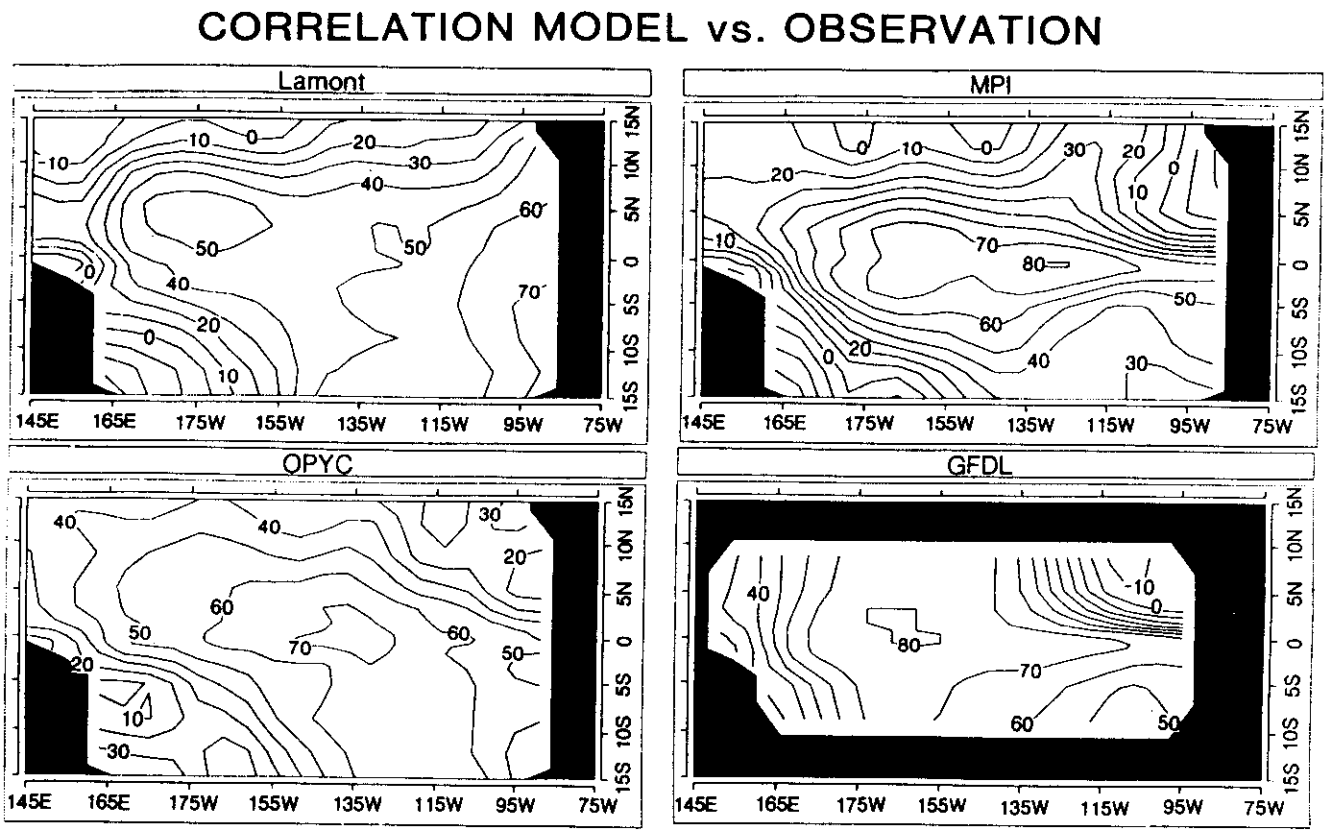

FIG. 1. Intercomparison of the skill of four tropical Pacific Ocean models (after Miller et al. 1992). The models were forced by the identical wind-stress fields for the period 1970–85. Shown is the correlation between anomalous SST from the model versus observation.

cussed later will clearly reflect this model difference. In summary, the model, while comparable in skill to the others shown, clearly has room for improvement, and so the forecast skills discussed below are probably lower limits on what might eventually be expected.

b. *The atmospheric model*

The atmospheric model to be used in this study is an anomaly model and statistical in nature; that is, it is based on the assumption that near-surface wind stress is determined by SST. Thus, the atmosphere effectively responds instantaneously in the planetary boundary layer (PBL) to ocean forcing only. Analysis of AGCM simulations forced by observed SST suggests this is a surprisingly good assumption. Note, however, that any feedback or near-surface circulation from large-scale condensation heating [which drives the main troposphere; Barnett et al. (1991)] will automatically be included in the model in so far as the feedback is reflected in the SST field.

The statistical atmospheric model was based on 19 yr (1967–85) of monthly SST and surface wind-stress data from the tropical Pacific. The SST data are originally from the Comprehensive Oceans Atmosphere Data Set (COADS; Slutz et al. 1985), with additional quality control and processing as described by Barbour (1986). The surface wind-stress data are from the FSU dataset (Goldenberg and O'Brien 1981) and were detrended (e.g., Posmentier et al. 1989) and smoothed with a 5-month running mean filter for this study.

The model, very similar to that described in Graham et al. (1992), was constructed as follows: Given observed SST ($T(x, t)$) and surface wind-stress ($\tau(x, t)$) anomaly datasets, express each in terms of "fixed-phase" empirical orthogonal functions (EOFs) [i.e., a separate set of EOFs for each calendar month; cf. Hasselmann and Barnett (1981)] so that for a specified month

$$T(x, t) = \sum_n \alpha_n(t) e_n(x)$$

$$\tau = \sum_n \beta_n(t) f_n(x). \qquad (1)$$

The domain x was defined to be within 10° of the equator and between 130°E and 90°W, and t refers to the 20 yearly values of, say, January data. Here, α and β are the EOF temporal coefficients and e and f are the spatial coefficients. The use of a fixed phase rather than a "time invariant" formulation (one model for all months) allows some account to be taken of the

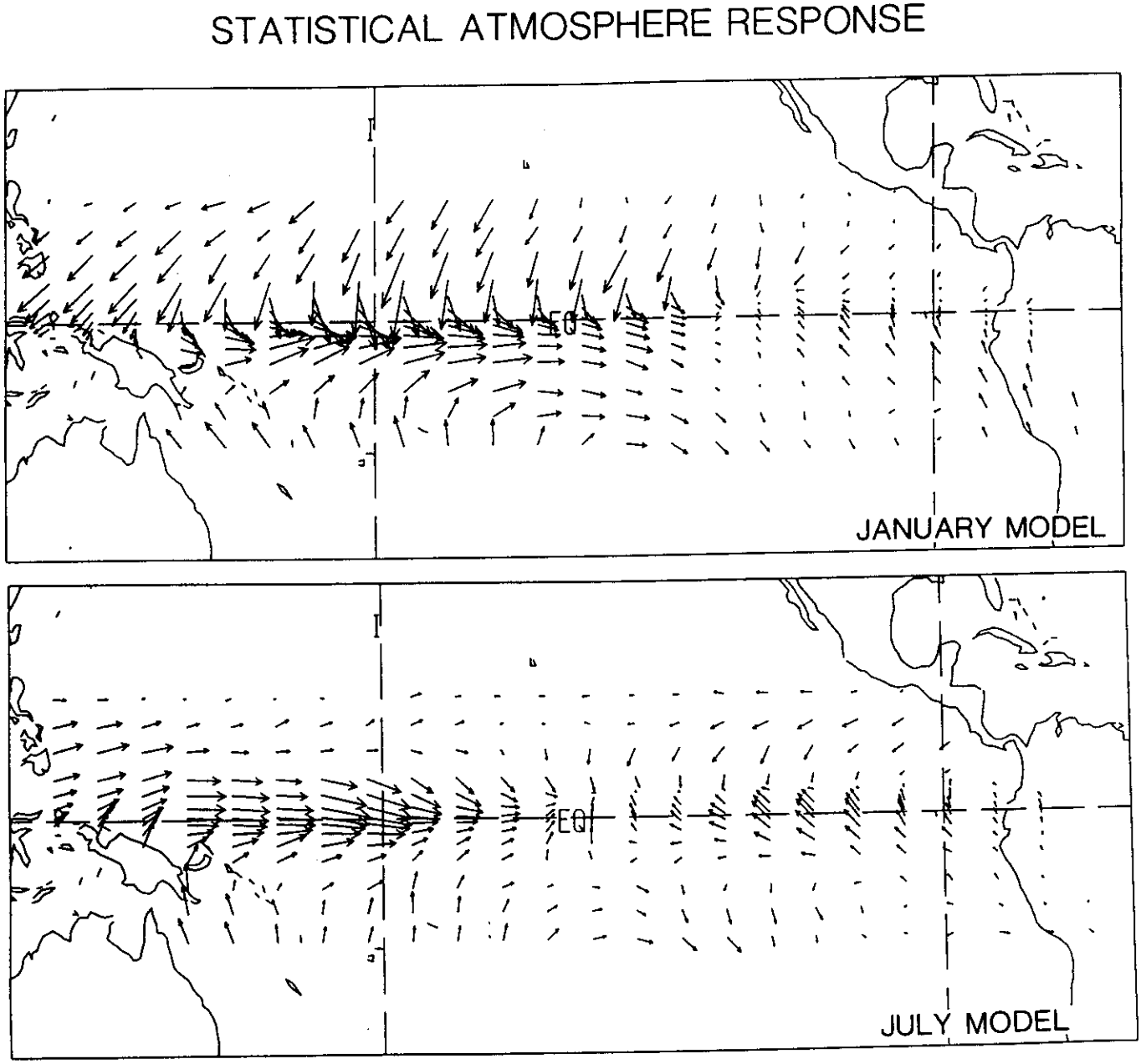

FIG. 2b. Anomalous stress field produced by an observed, warm SST anomaly (February 1992) from the atmospheric model: upper, using January coefficients; lower, using July coefficients.

the OGCM forced by the SST-derived wind stress for the period 1966–85 produced model-estimated monthly SST fields for that period. The difference between these model fields and the observed SST fields for the same period were computed and termed the "error" field, $\epsilon(x, t)$. We next constructed a statistical model of the error by using the model SST ($T_m(x, t)$) and model sea level fields ($h(x, t)$) to "predict" the error field. This statistical model, based on model output statistics (MOS), will be referred to as an "MOS" corrector. In a sense, it represents a near-optimal tuning of the OGCM itself but provides no insight into the nature of the model problems.

The MOS corrector was constructed with the same tools as the atmospheric model, that is, (1)–(5), but with the predictor T replaced by the concatenated dataset for T_m, and h and the predictand, τ, replaced by the model error field ϵ. The concatenation technique for handling multivariate datasets is described in Barnett and Preisendorfer (1987).

In practice, the MOS correction reduces model SST anomalies in the central Pacific while increasing model SST anomalies in the far eastern ocean—an area where model performance is especially weak (Fig. 1). The importance of the corrector variables was interesting. In the central and western part of the ocean model,

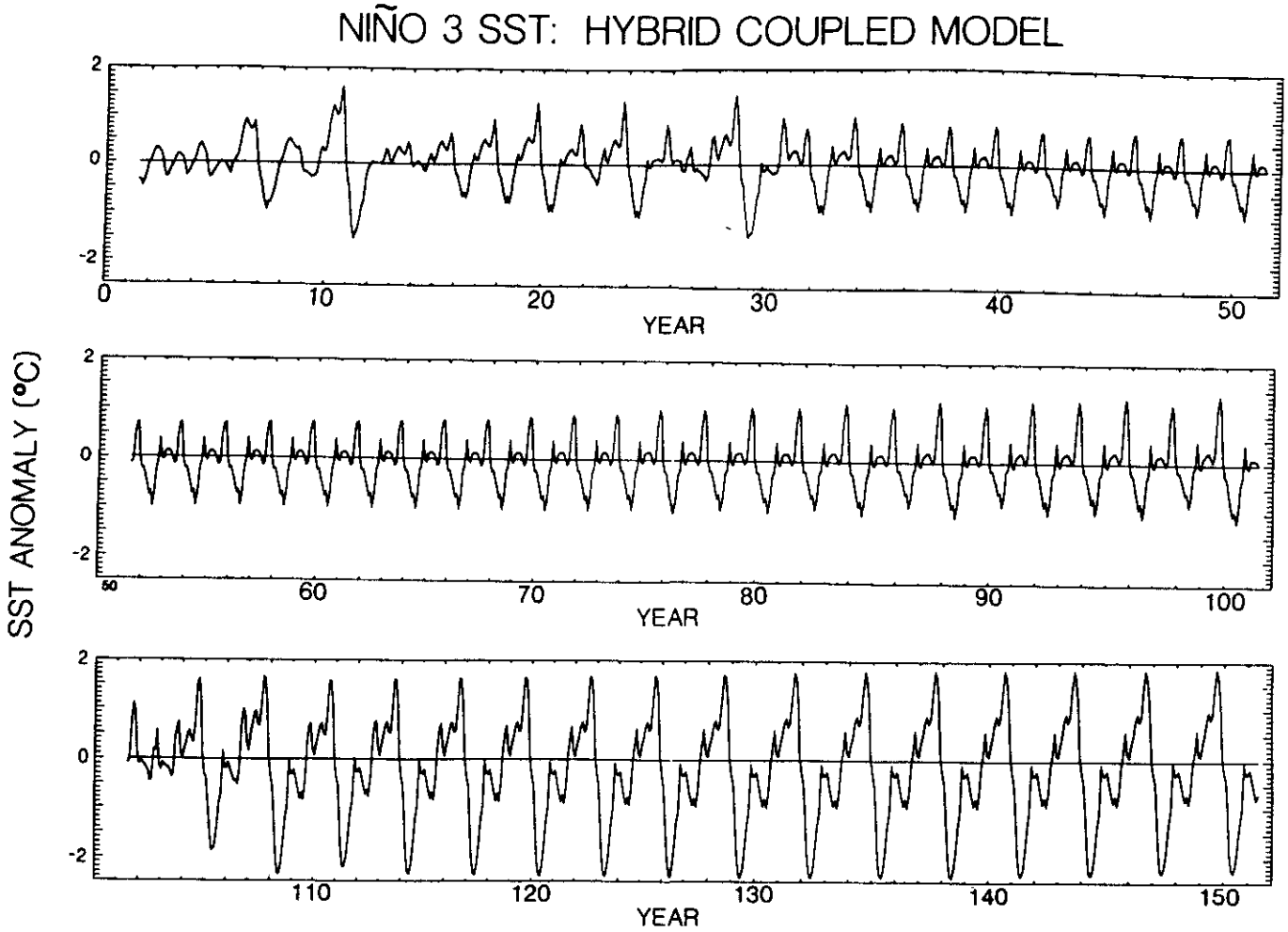

FIG. 3. NIÑO3 SST anomaly for the 150-yr hybrid coupled model control run. Note the change in behavior near years 30 and 100.

SST was the major corrector variable, while in the eastern ocean, the model sea level was the most important; the transition between the two extremes was smooth and well behaved.

The time-dependent MOS expedient, which is a step beyond the flux-correction schemes (Sausen et al. 1988) used in most greenhouse gas coupled model simulations, worked very well, as later results will show. This in turn gives us some confidence that the job of actually fixing the causes of error in the model physics will be worth the effort when it is complete. For now it lets us proceed with the prediction work, which is the main subject of this paper.

3. Coupled model performance

a. Characteristics

The winds derived from the atmospheric model were used to spin up the OGCM to January 1972. The distribution of ocean variables at that time was used as the initial condition for the HCM. The SST anomaly for region NIÑO3 for the subsequent 150 yr of HCM integration is shown on Fig. 3. During the first 30 yr of integration, referred to as epoch 1, the HCM oscillates in an irregular manner with a typical period of 25 months, but ranging in length from 6 to 35 months. Beginning in about year 30, the nature of the oscillation shifts abruptly within one period to a time scale of exactly 24 months. The time period characterized by this mode of variability, referred to below as epoch 2, continues for approximately another 74 yr (36 cycles), at which time the dominate period abruptly shifts to 36 months and continues at that period to the end of the integration (epoch 3). The behavior is reminiscent of a chaotic system characterized by, say, a generalized Hill equation or some other nonlinear differential equation. In this case, the response seems to be in the form of subharmonics of the basic annual forcing.

The spatial distribution of the HCM control-run response in the wind stress, SST, and sea level fields was examined via a simultaneous Principal Oscillator Pattern (POP) analysis of the three variables (Hasselmann

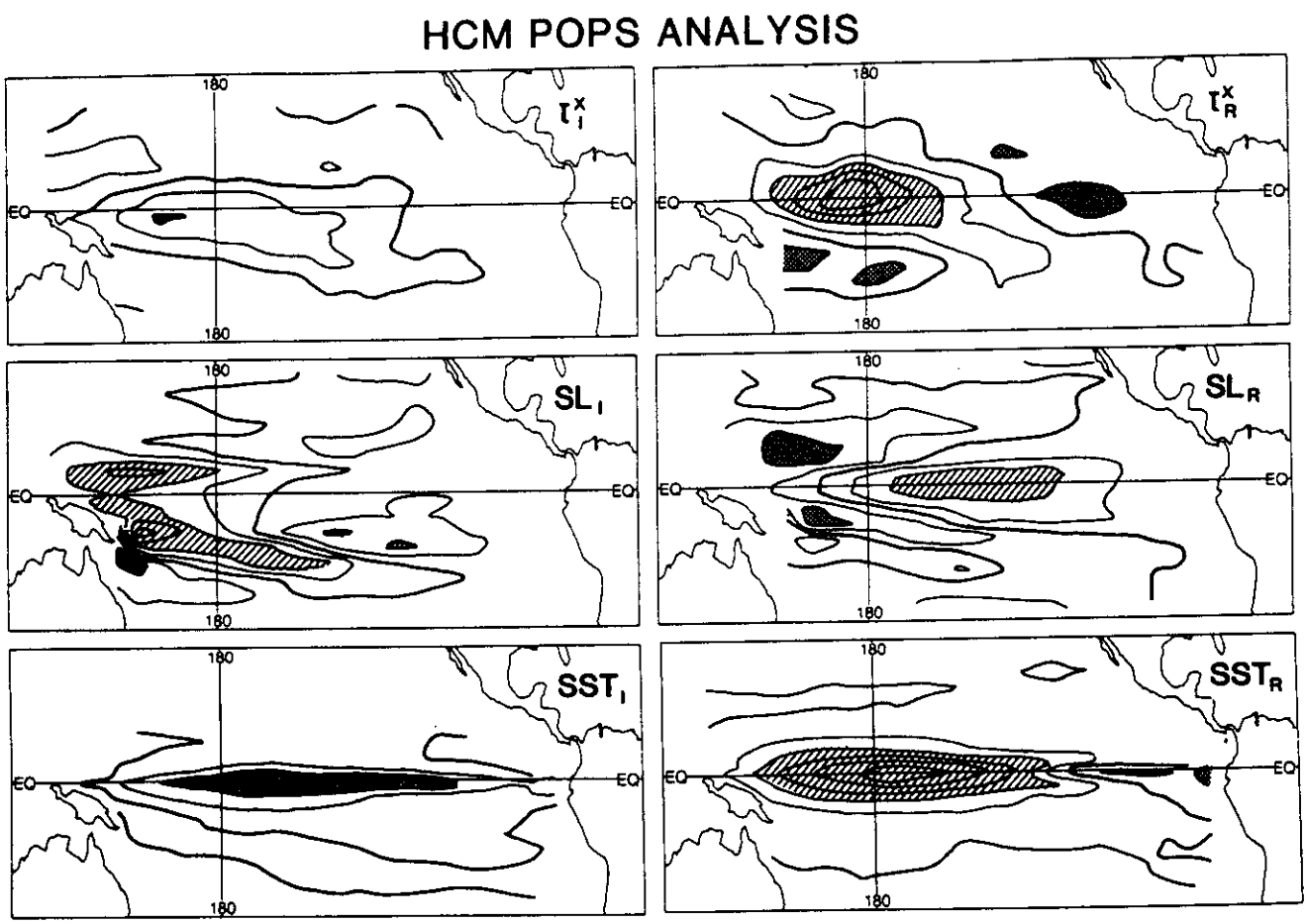

FIG. 4. Simultaneous POPs analysis of the biennial portion (24-month period) of the HCM control run (years 30–104). The decay time is 78 months, and this mode captures approximately 50% of the total variance. The imaginary component (left panels) leads the real component (right panels) by one-quarter of a cycle. Analyzed anomalies are zonal wind stress (upper panels), sea level (middle panels), and SST (lower panels). Hatching refers to regions of positive anomaly, while stipple refers to regions of negative anomaly.

1988; von Storch and Xu 1988) for years 31–104 of the coupled integration. The real and imaginary components of the POPs spatial patterns are shown in Fig. 4. In general, the real parts of the POP show the extreme of the ENSO cycle, while the imaginary parts show a transition phase. The upper pair of panels shows an eastward-directed stress anomaly in the western Pacific (upper left) propagating one-quarter of a cycle later to the eastern Pacific (upper right). At this time, the stress anomaly in the western Pacific has been replaced by a westward-directed anomaly. The associated changes in sea level are shown in the middle panels. Lower-than-normal off-equatorial sea level anomalies are impinging on the western boundary in concert with the positive stress anomalies in the western ocean. This is accompanied by a higher than normal sea level in the central and eastern Pacific (middle left). One-quarter of a cycle later (middle right), a large region of the equatorial Pacific is covered by lower-than-normal sea level, while higher-than-normal off-equatorial stands are found in the western part of the basin. The left column of panels goes with a broad equatorial region of warmer-than-normal SST. The lower-right panel shows that the SST has moved to the eastern ocean with a region of colder than normal SST developing in the central equatorial ocean. All of these patterns and associations have oft been documented in the literature describing the evolution of ENSO in observed data.

Several other interesting facts arose from the POPs analysis.

(i) The 150-yr HCM integration was partitioned at the abrupt transitions, and the resulting three groups of integrations, referred to as epochs above, were considered separately. The spatial POP patterns were *essentially the same* as described above for all three epochs. In each analysis, the leading mode (shown on Fig. 4) captured 54%–58% of the multifield variance and strongly dominated the analysis. Thus, the patterns shown in Fig. 4 represent the coupled, normal modes of the HCM. However, there are some subtle differences between the epochs (see below).

(ii) The associated POPs time series resemble closely the NIÑO3 series shown in Fig. 3. During the three epochs, the characteristic periods of oscillation deter-

mined from the POPs coefficients were 22, 24, and 36 months, respectively. The corresponding decay times were 20, 78, and 107 months, respectively. The long decay times of epochs 2 and 3 relative to their period of oscillation show them to be relatively long-lived modes of the coupled system.

(iii) The principal differences between the epochs referred to in (i) are as follows; years 1–30 show SST and zonal stress to be more in a standing mode while sea level propagates. This might be termed the "delayed action" mode. Between years 31–100, two modes appear to operate simultaneously since all three fields show propagating features. Between years 110–150 the "delayed action" mode appears again, but now the rotation period is longer (3 yr), and all fields have a larger meridional extent. The reasons for these changes are discussed in section 3c.

The most important characteristic of the model for prediction purposes is its temporal behavior. During the first 30 yr of integration, the behavior is irregular in time and, for NIÑO3, not unlike the observations. After year 30, however, the behavior becomes periodic, and in this state, the coupled model would become largely useless for prediction work [unless ENSO happens to be in a 2- (or 3-) yr cycle]. The reasons for these shifts in model behavior are discussed in section 3d.

b. Comparison with observations

We cannot make a direct comparison of the coupled model results with observations in a traditional sense, but we can ask if the spatial distribution of covariability between the model fields is, in a statistical sense, like that found in observations. The manner in which the atmospheric model was constructed assures that the SST–wind stress relation will be as observed (by definition). The key test of the HCM that remains is to see if the forcing from the atmospheric model will produce variations in interior-ocean thermal structure like those observed. This intercomparison was performed in a compact manner as follows. The HCM ocean-temperature anomalies were computed with respect to the HCM control run climatology and were vertically integrated to obtain an estimate of the heat-content field as a function of horizontal position and time. Epoch 2 of the control run, the period of biennial oscillation covering approximately year 31–100, was used initially. (A later study showed we could have used either the first or third epoch from that run and obtained much the same results as shown below.)

We next computed the same vertical integrals from the temperature anomaly field obtained from the Pacific XBT data. This set was constructed by objectively mapping all XBTs taken in the tropical Pacific for the period 1979–88 on to a uniform 2° × 10° grid in space and bimonthly in time. Details of the data that went into this unique set and the methods used to develop it may be found in Pazan et al. (1993). This observed set was subsequently mapped onto the OGCM grid at monthly intervals.

The aforementioned upper-ocean heat content fields were subjected to standard EOF analysis. The two leading eigenmodes from these analyses are shown in Fig. 5. The two eigenmodes from the observed data have nearly equal variance (28% versus 22%). The dis-

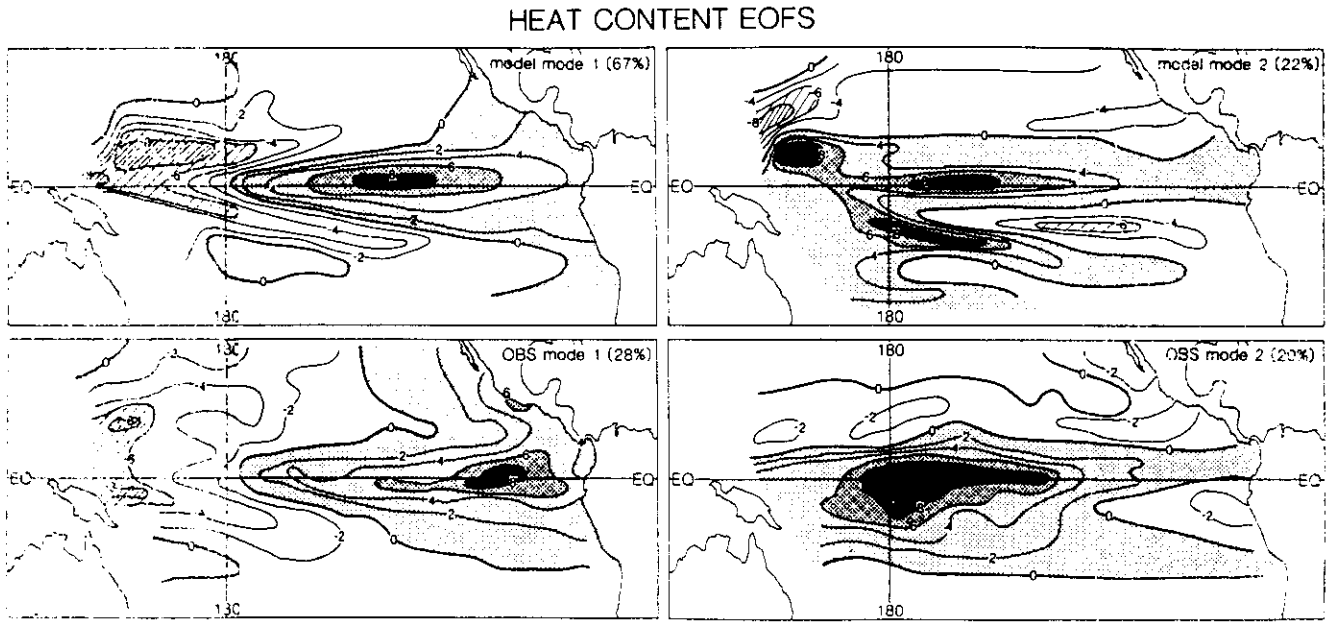

FIG. 5. The first two EOFs of tropical Pacific heat-content anomalies (0–400 m) for the HCM control run (upper panels) and observations (lower panels). Positive regions are stippled and negative values are hatched. The pattern correlation between the first modes is 0.87 and between the second modes it is 0.78, for the region within 15° of the equator.

tribution of variance and associated principal components show propagating heat content anomalies that originate in midocean at off equatorial latitudes (5°–8°) that move westward into the continental boundary and subsequently are channeled back into the equatorial waveguide where they move eastward to the South American coast. The principal components show that the spatial patterns are controlled by events during 1982–83 and 1986–88. The comparable leading EOFs for the HCM integration (Fig. 5, upper) bear a striking similarity to the observed modes. The model EOFs also show the same off-equatorial westward propagation and eastward propagation on the equator seen in the observations. The first and second modes of each analysis spatially correlate at 0.87 and 0.78, respectively, over the domain within 15° of the equator. This leaves little doubt as to the similarity between the patterns of heat-content variability produced by the HCM and those found in the observations.

There are several differences between the model and observed EOFs. The leading model mode accounts for 67% of the field variance versus only 22% for the second mode, so the model does not propagate energy across the Pacific as well as nature. Rather, it adds standing wave energy to what should nearly be a pure progressive wave. The likely reason for this is the generally poor performance of the OGCM in the far eastern and western Pacific, where its resolution precludes an accurate reproduction of the observations. Note also that the model signal is more equatorially confined than the observations. Part of this may be real since the model heat flux, which in the real world is thought to be important outside the waveguide, does not compare well with observations at latitudes outside approximately 8°. Part of the problem may also reside with the observed data, whose sparse nature in large parts of the Pacific will, when objectively mapped, assure large spatial scales that may be unrealistic.

In summary, the agreement between the spatial scale and evolution of the heat-content fields in the HCM and those observed in nature is unexpectedly good. The model successfully captures both the spatial scale and the complicated propagational character of the observations. These facts, together with the assured performance of the ocean-to-atmosphere interaction, suggest the model has a reasonable physical basis for any forecast skill it demonstrates. More importantly, the physical mechanisms that account for the model's behavior are likely to be operative also in the real world.

c. The tropical pacific coupled climate mode

The results of the prior sections clearly show the existence of a principal natural mode of variability in the ocean–atmosphere of the tropical Pacific basin. One element of this mode is associated largely with ocean dynamics and bears a close resemblance to the delayed-action oscillator described by Schopf and Suarez (1988) and Graham and White (1988), among others. It is this component that is associated with the westward, off-equatorial propagation of information in the ocean. The other key component of the mode is a strongly coupled, local ocean–atmospheric interaction in the equatorial zone of the type described by Barnett et al. (1991). This element is characterized by eastward propagation of information along the equator resulting from simple ocean dynamics within the mixed layer and the fact that the overlying atmosphere acts as a slave to (local) oceanic forcing. These items are discussed briefly in the following, with a more extensive discussion deferred to another paper.

In general concept, the natural mode found here is much the same as that described by Graham and White (1988), Battisti (1988), Suarez and Schopf (1989), and Wakata and Sarachik (1991). In detail, the results show the importance of Rossby wave dynamics to the coupled mode as noted by these authors. However, the equatorial element operates differently than previously envisioned, with meridional advection of heat in the ocean and geostrophic convergence onto the equator playing critical roles in the dynamics of this component of the coupled mode. Given the importance of meridional motion in the model physics, this behavior cannot be ascribed to Kelvin wave dynamics alone.

The way these elements of the coupled mode work goes as follows. Start with, say, a warm SST anomaly on the equator. The anomalous SST gradients force an eastward-directed stress anomaly that gives a convergence of mass and heat onto the equator because there is a climatological SST minimum on the equator. Note here the critical role played by the seasonally varying spatial distribution of wind stress. It is only during the symmetric phase occurring in the summer–fall period (Fig. 2b, lower) that the atmosphere can support and maintain this convergence. Geostrophic convergence to the east of the center of mass accumulation will cause the eastern edge of the SST anomaly to warm, while geostrophic divergence to the west will cause a cooling, and the entire SST anomaly will move eastward. Note this is a truly coupled ocean–atmosphere mode that relies for its existence on thermodynamic considerations. This eastward motion is a tenuous behavior that depends critically on a number of ocean–atmosphere parameters, most especially the mean meridional temperature gradient. An interesting discussion and dissection of the possibilities for such modes is given in Neelin (1991), Neelin and Jin (1993), Jin and Neelin (1993), Cane et al. (1990), and Münnich et al. (1991).

As envisioned by Schopf and Suarez (1988), Graham and White (1988), and others, the Ekman pumping associated with the equatorial anomalies will generate Rossby waves of the opposite sense; that is, after moving westward to Asia and eventually back into the waveguide, they will generate local upwelling that will work to either damp the warm SST anomaly if it still

exists or cause the creation of the second half of the cycle, namely, a colder-than-normal equatorial SST field. The cycle is completed by invoking the same physics but with signs of the forcing/response reversed.

d. Chaotic behavior

The abrupt transitions in period of the HCM are related to a slow drift in the model's temperature field. This drift appears as a cooling near the surface and is due to a diffusive transfer of heat to the deeper layers of the model without a compensation by deep, cool water inflow through the northern and southern model boundaries. This failure in the model physics suggests it is most appropriate for integrations not exceeding a few year's duration, which was the purpose of the model in the first place.

The slow changes in SST are shown in Fig. 6 as a difference between the average of the first 30 yr of epoch 3 and the average of the last 30 yr of epoch 2. A comparable difference map for the zonal stress is also shown. The cooling appears as an extension of the cold tongue into the central and western Pacific. Note the cooling is stronger just north of the equator than it is right on the equator. This suggests the mean meridional temperature gradient will be reduced in epoch 3 relative

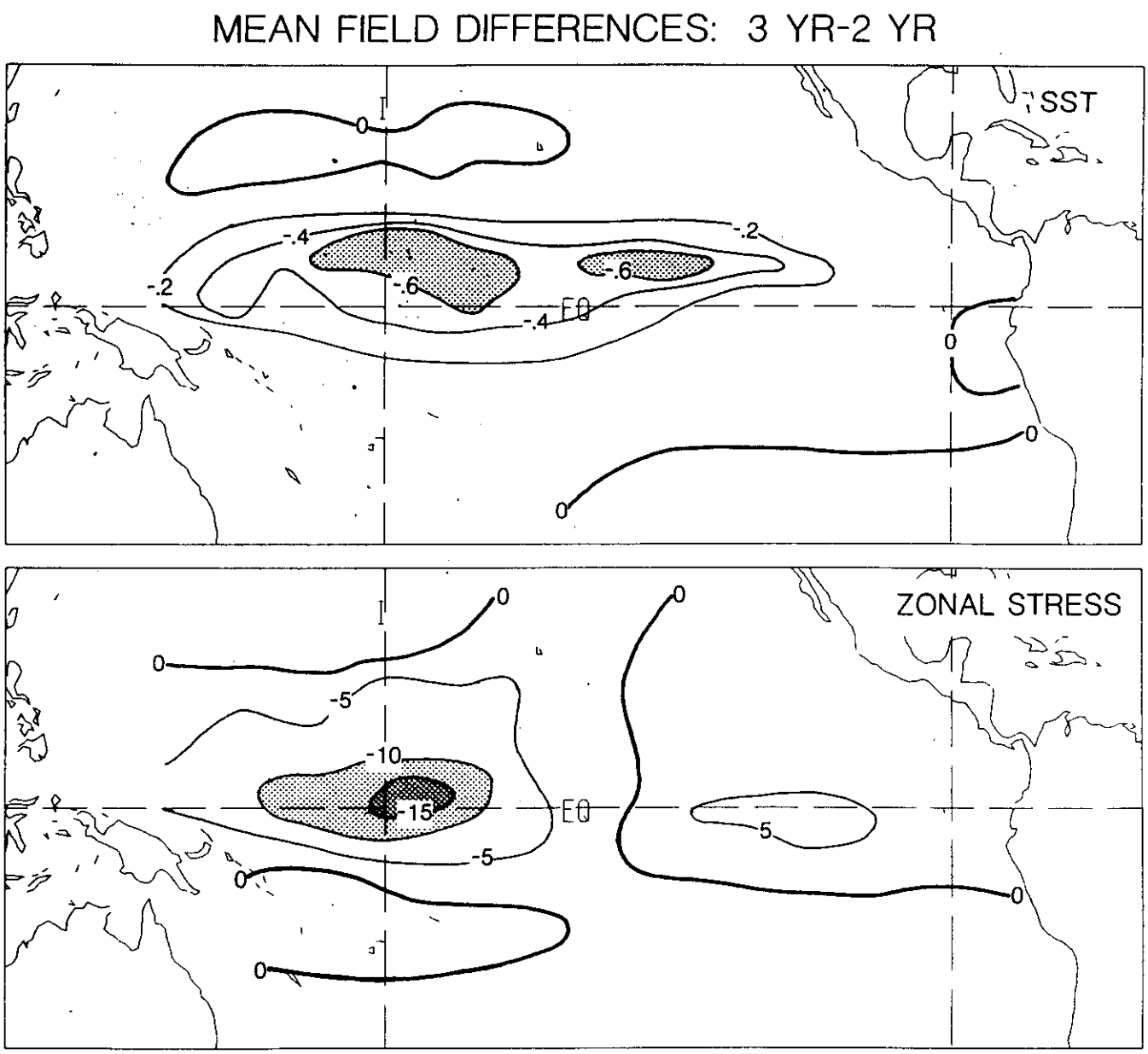

FIG. 6. The difference in SST (°C) between the average of the first 30 yr of epoch 3 and the last 30 yr of epoch 2, upper panel. The lower panel gives the same difference field for the zonal wind stress [mPa].

to epoch 2 and, by the arguments above, result in a slower eastward propagation for the air–sea coupled mode.

The zonal stress strengthens in the central and western ocean but decreases in the eastern ocean. This change in zonal stress between the two epochs results in little change in the curl on the equator. However, as one moves north or south there are significant changes in the stress curl, with the largest values occurring at about latitude 8°. This results in more effective Rossby wave generation at these latitudes during epoch 3, a result confirmed by a shift in off-equator thermal structure variability from about 5° in epoch 2 to 8° in epoch 3. This shift in wave activity will also tend to increase the time it takes to complete one cycle of an event and lead to a 3-yr period versus a 2-yr period. The strong locking of the HCM to the annual cycle (see section 5) seems to require that it oscillate at a subharmonic of that cycle, and hence, the abruptness of the shift from the 2- to 3-yr period.

e. *Summary*

In summary, the physical relations that explain the model variability support the idea of a natural mode of variation in the tropical Pacific ocean–atmosphere system. This natural mode in concept, but not detail, is much like that described by earlier workers. In the current simulations, that mode can be both irregular or self-sustaining and cyclic. The reason for this nonstationary behavior is related to a slow drift of the seasonally averaged mean fields of the HCM. A full exposition of this result is beyond the focus of the present paper but it does suggest that the abilities of models to simulate or predict ENSO events may well depend on their ability to reproduce the background mean state of the tropical ocean. For present purposes, it suffices to say that the natural mode present in the model seems to reproduce well observations from the real world. The scenarios described by both model and data have a basis in theory. It seems reasonable to conclude that the model to be used in the following prediction studies has a reasonable physical basis.

4. Prediction experiment results

In this section we investigate the ability of the HCM to predict changes in the equatorial Pacific SST. The first set of experiments covers the period 1967–85, which will be termed the dependent period, since the statistical atmospheric model was constructed with data from this period. The artificial skill for these hindcasts will be high for very short lead times because we are effectively giving the HCM the observed SST field as an initial condition. Unfortunately, it is not clear how one should estimate the artificial skill for extended-range forecasts during this period, and so we will use an SST persistence model computed over this period as an approximation to the expected artificial skill. A second set of experiments will cover the period 1986–90, a time when many locations in the equatorial ocean underwent changes in SST range of approximately four standard deviations. No data from this period have entered the model construction in any way; we will refer to this as the independent period. The forecast verification for both periods will be against the *observed* data from the COADS set (and the Climate Analysis Center).

a. *Dependent skill*

The OGCM was spun up with winds derived from the statistical atmosphere for the period January 1961 to December 1966. A base run was then made for the period January 1967 through mid-1990, wherein the OGCM was forced by the winds from the statistical atmosphere model, which was, in turn, forced by the observed SST. Restart files for the OGCM for each month were retained and they provided the initial conditions for the prediction experiments. Each hindcast extended from the initial month into the future 18 months.

The success of the hindcasts was evaluated from the simple correlation between the model-predicted values and the observed SST. These skill estimates were computed as functions of lead time, month of the year for which the hindcast was being made, and geographic position. Bias and trend were removed for each lead time, but the forecasts were not MOS corrected before computing the skill scores.

The skill of persistence in hindcasting the 3 months of March, April, and May (MAM) at lead times of 6 and 12 months is shown in Fig. 7, as are the comparable persistence skills for December, January, and February (DJF) for the same lead times. These groups of months were selected since they were the parts of the annual cycle when the HCM performed moderately well and best, respectively. The HCM did poorly for forecasts of summer conditions, and it did about the same in the fall season as it did for MAM. This same seasonal distribution of hindcast–forecast skill has been found previously (e.g., Barnett 1977; Hasselmann and Barnett 1981).

The performance of the HCM for the MAM and DJF time frames is shown in Figs. 8 and 9 for lead times of 0, 6, 12, and 18 months in advance. Inspection of these figures leads to the following conclusions.

(i) The ability of the model to capture the SST field at a lead time of 0 months, a specification, is rather closely confined to the equator; within $+/-10°$. In this region, the highest correlation between observed SST and model hindcast is 0.90 (versus 1.0 expected from persistence). This result is really a reflection of the performance of the atmospheric model (Fig. 2a). The HCM also demonstrates a reasonable ability to capture the SST variability across most of the Pacific. It clearly fails in this regard in both the extreme western

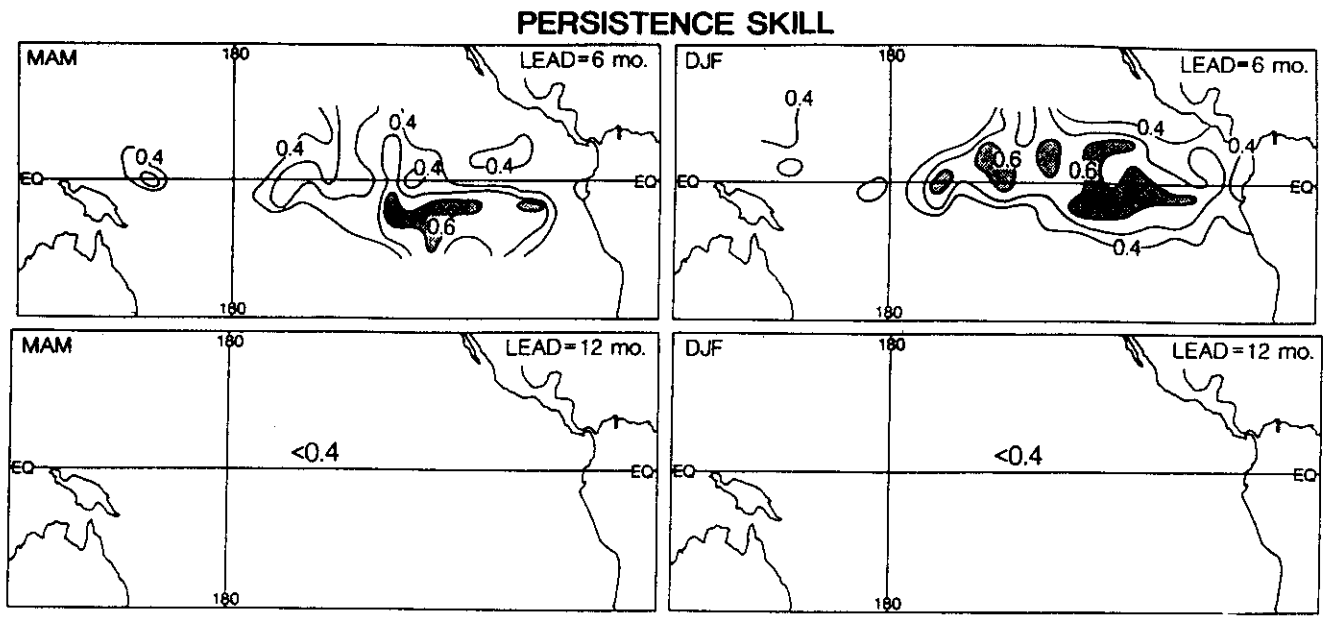

FIG. 7. Skill of persistence, expressed as lag correlation, in hindcasting tropical Pacific SST for March, April, May (MAM) and December, January, February (DJF) over the period 1967–85. Correlations above 0.6 are stippled.

and eastern parts of the basin, a result expected from Fig. 1. The specification skill shown in Figs. 8 and 9 is almost precisely the skill obtained by running the OGCM with the observed FSU stress fields. It is worth noting that had we shown just the comparison for region NIÑO3, the HCM would have a skill (correlation) of 0.88. The spatial distribution of skill is clearly a more informative, although not necessarily a more flattering, measure of model performance.

(ii) At hindcast lead times of 6 months, the regional skill for MAM has shrunk in magnitude to 0.4–0.6 and is confined to the region around the date line. Persistence has little or no skill in this area but is moderately successful in the central eastern Pacific. All in all, persistence generally has the edge over the HCM at this season/lead. During DJF the story is much the same. The model now has larger skill over a larger region, but so does persistence. Other measures of performance (not shown) support these results and lead us to conclude that the HCM is about equivalent, but a bit in-

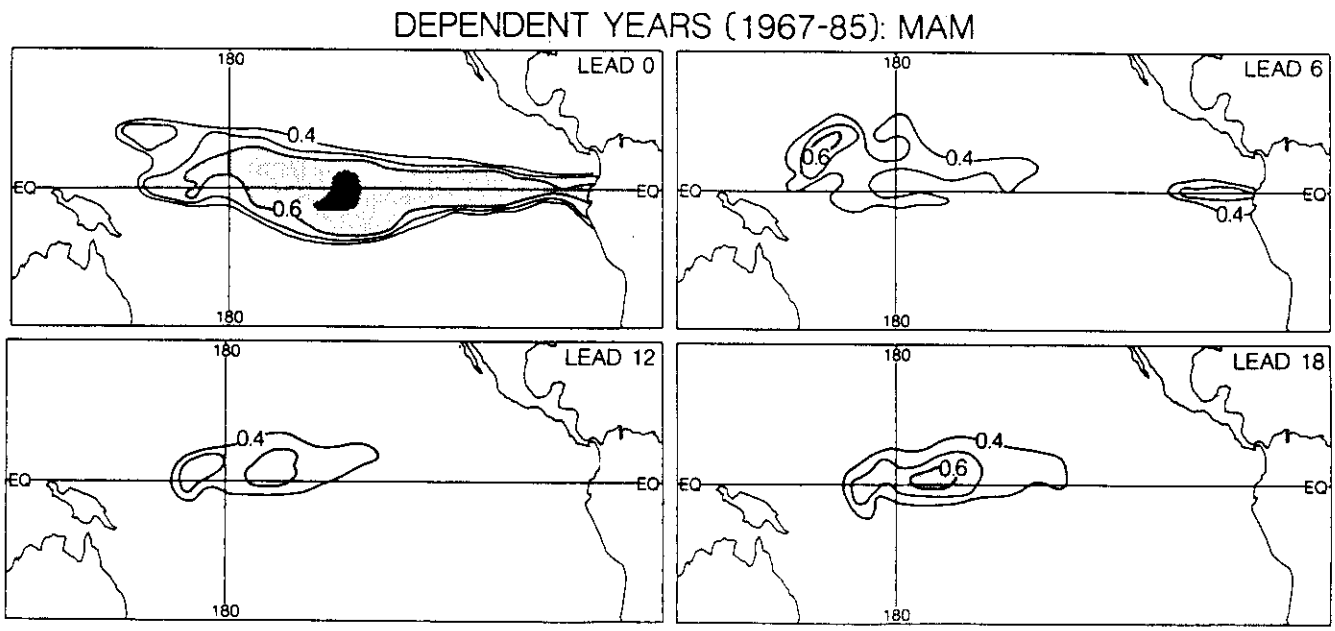

FIG. 8. Skill (correlation) of HCM hindcasts of SST for MAM for 1967–85. Light stipple for values above 0.6 and heavy stipple for values above 0.8. Hindcast lead times are 0, 6, 12, and 18 months.

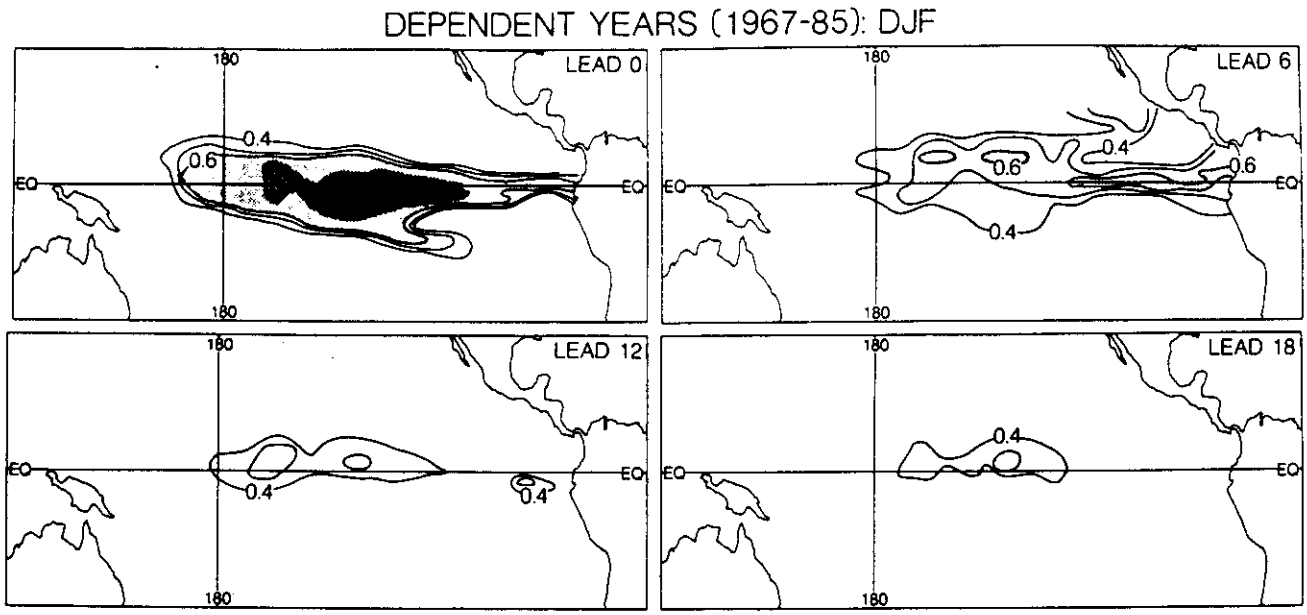

FIG. 9. Same as Fig. 8 but for DJF.

ferior, to persistence at a forecast lead time of 6 months. For longer lead times the HCM outperforms persistence.

(iii) Persistence has no skill at lead times of 12 months and beyond (cf. Fig. 7). The HCM does show some skill at a 12-month lead but only in the region of the date line. The skill values/regional coverage are such as to make these forecasts of limited value *on average*. We shall see below that this is, in one sense, a misleading result since the HCM does well at simulating the largest of the ENSO events.

(iv) The skill of the HCM at a lead time of 18 months improves over the 12-month skill. Correlations exceeding 0.6 are found in the region of the date line for the MAM period, with nearly as large values in the DJF period. The model has clearly been successful in capturing the oscillatory nature of the ENSO process, a result we might have anticipated based on earlier discussion. This in turn suggests that the physics described in the model diagnostic study of section 3 is also operative in the real world.

In summary, the performance of the HCM on the 19-yr hindcast dataset is less skillful than a persistence competitor out to hindcast lead times of approximately 6 months. Beyond that lead time, the model consistently outperforms persistence in the central equatorial Pacific with surprising skill, even at hindcast lead times of 18 months. This increase in skill with lead time can be attributed to the low-frequency ocean dynamics simulated by the model.

b. *Forecast skill*

The model was used to produce forecasts for the independent period of 1986–90. This period is too short to produce stable statistics regarding model performance, but should give an idea if the skill shown above is realistic, since data from this period have not previously entered the analysis. Thus, the results shown in the following are true forecasts.

The skills, computed as above, for the independent period are shown in Figs. 10 and 11 for the same combination of months and leads as used on the hindcast results. A total of 15 separate forecasts are represented in each panel. The following set of conclusions may be drawn from these illustrations.

(i) The skill values are substantially higher and cover a broader region than found in the hindcast study and clearly beat persistence even at a 6-month lead. Some grid points at lead times of both 12 and 18 months have correlation values exceeding 0.80. No doubt, part of this result is due to the shortness of the forecast period and to the occurrence of a large warm event followed by a cold event, which represents a substantial low-frequency signal. However, the sequence of events in the forecast period did occur, and the model captured them surprisingly well. This is particularly impressive since the range in SST between the warm event of 1986–87 and the cold event of 1988 was between three and four standard deviations over much of the equatorial Pacific Ocean.

(ii) The model performed poorly in the same regions it did in the hindcast study—the eastern and western Pacific and for latitudes above about 10° of latitude.

(iii) The performance for extended lead times, 12–18 months, was especially encouraging.

In summary, the HCM's forecast performance on an independent test period was excellent. The fact that

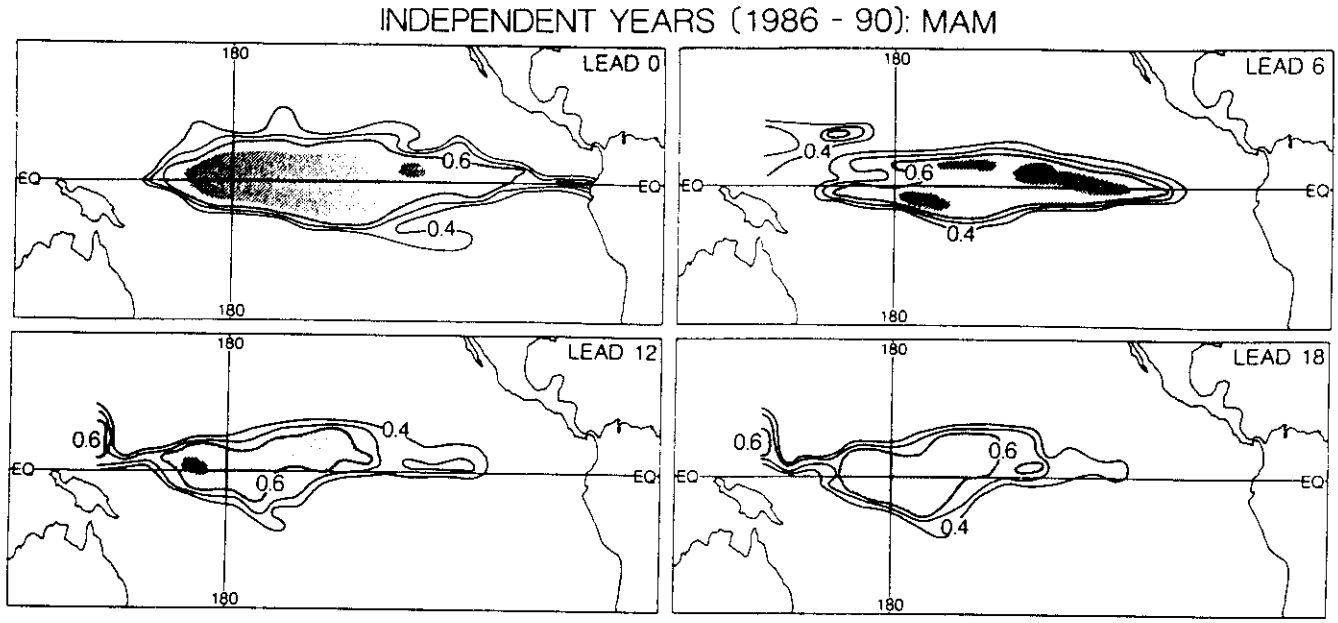

FIG. 10. Same as Fig. 8 but for the independent period 1986–90.

the model did better on this test period is partially due to the shortness of the record. But it must also be attributed to the fact that the test period was dominated by major events. In contrast, the hindcast period contains a far less dense population of major events. This suggests that the model may do big events well but may have little or no skill for lesser fluctuations. If this were true, then the skill scores for the dependent period (section 4a) might be portraying the model abilities in a negative light. This possibility is explored in the following section.

c. *Discrete forecasts*

Three major warm and cold events were selected for specific study. The winter (DJF) SST predicted by the model at a lead time of 6 months, that is, initialization with data ending 1 June or earlier, for these events is compared with the observed SST in Figs. 12 and 13. Note that two of the cold events and one warm event came from the dependent period, while the other three events came from the independent period. The correspondence between prediction and observation is

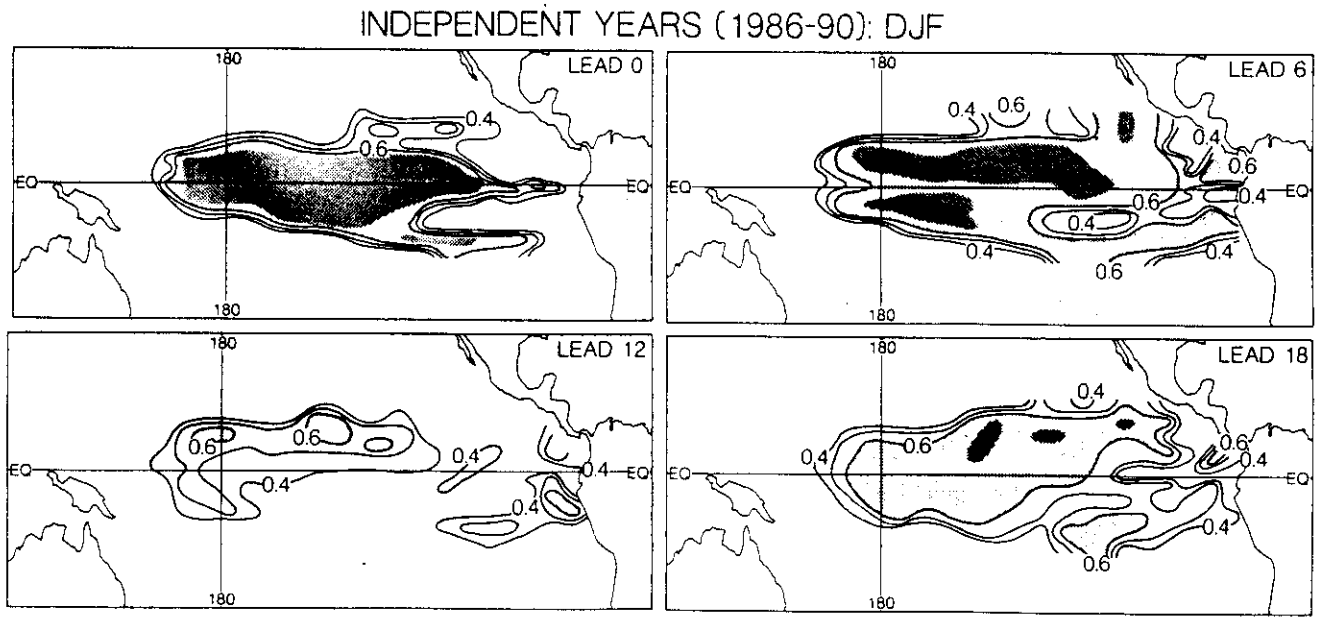

FIG. 11. Same as Fig. 9 but for the independent period 1986–90.

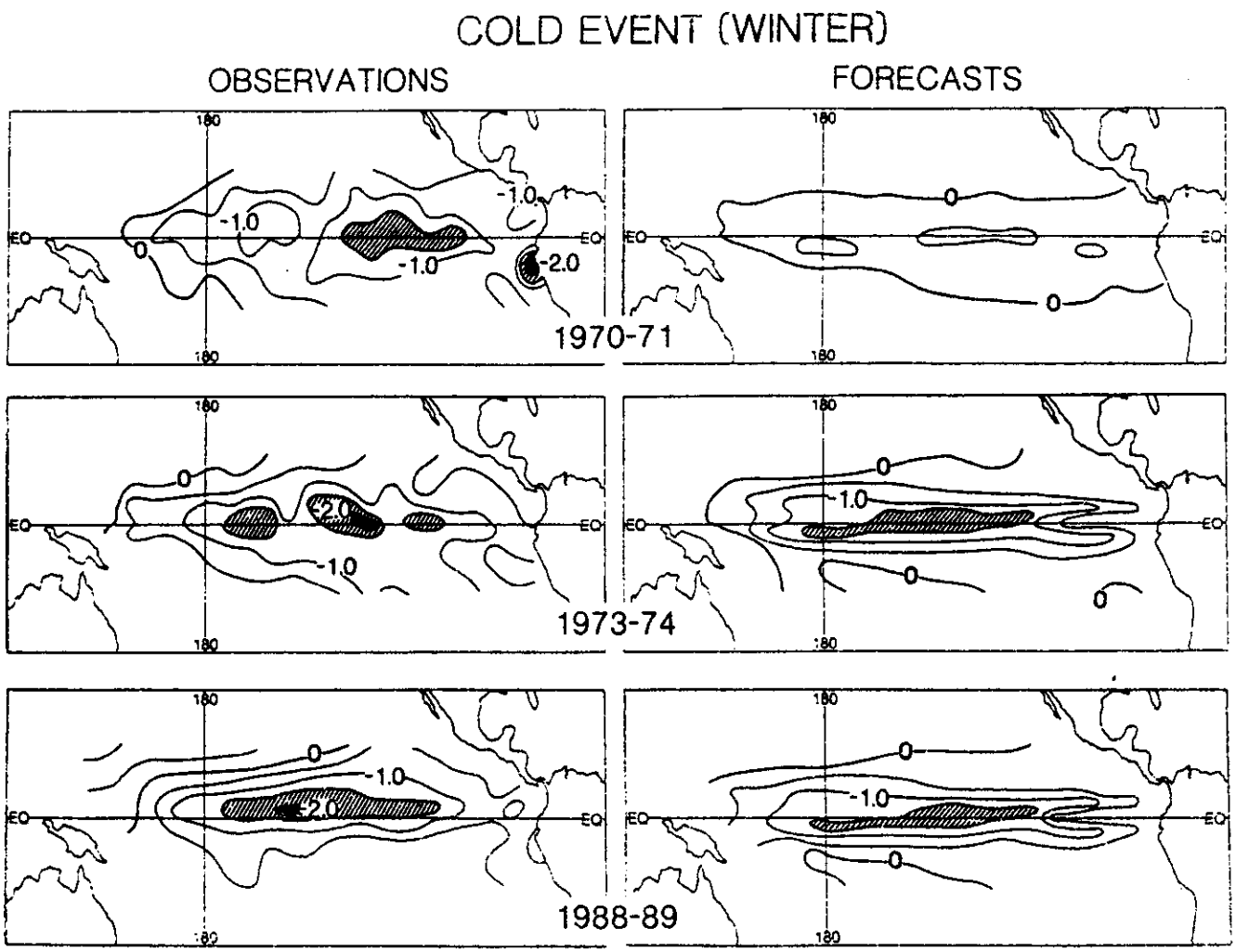

FIG. 12. Six-month lead forecasts and observations for winter for cold events.

generally good. The main exceptions to this conclusion again occur in geographic regions of model weakness, that is, the ocean margins and outside the waveguide. Comparisons with persistence forecasts (not shown) generally favor the HCM forecasts. The following are additional observations.

1) COLD EVENTS

The three cold events shown represent the winter (DJF) SST condition for 1970–71, 1973–74, and 1988–89. The first cold event is underhindcasted in magnitude, but the spatial distribution of SST is adequate. The other events are good with respect to both magnitude and spatial distribution. Note again the relatively narrow region around the equator where model performance is good but not reflective of the broader distribution of anomalies seen in the observations. All in all, the performance for these large, discrete events look better than one might have guessed from the statistical skill estimate alone.

2) WARM EVENTS

The forecasts for the warm events give much the same impression as those noted immediately above. The forecasts for 1986–87 and 1991–92 are approximately centered in the correct locations. The correct magnitude is forecast for 1986–87, but the 1991–92 event is underestimated. The 1982–83 event is rather poorly represented by the model. The model places the event much farther to the west than it actually occurred, and it seriously underestimated the actual magnitude. This performance was expected a priori since the observations show the real event to be centered in the eastern part of the basin, an area where the model does not perform well (as noted above).

In summary, the HCM performed on the large events somewhat better than one would have guessed from the statistical analysis alone. The two cases where the model did not do so well were from the dependent period. The poor showing on the 1982–83 event, given its magnitude, surely had a major impact on the sta-

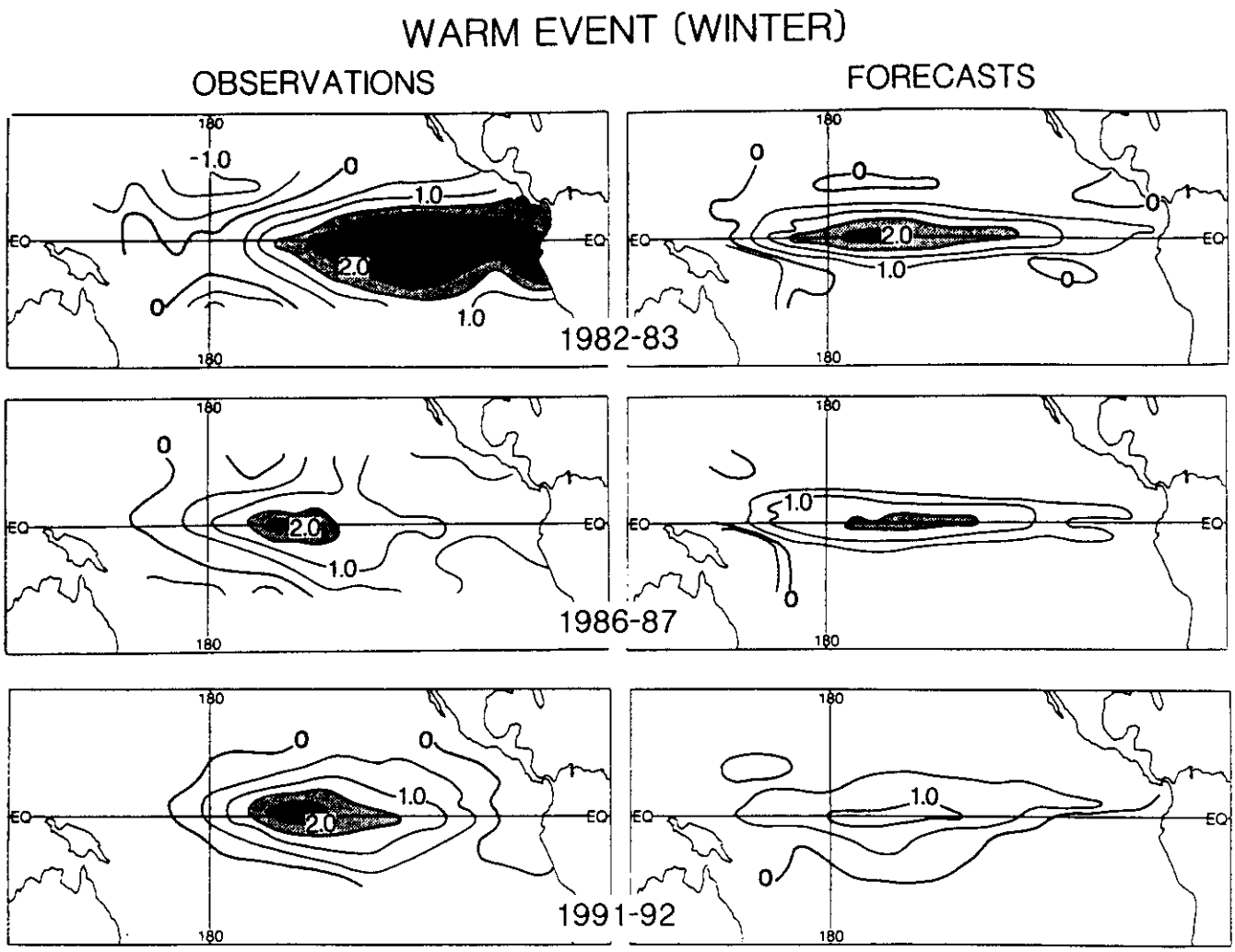

FIG. 13. Same as Fig. 12 but for winter for three warm events.

tistical skill scores for the dependent period. At any rate, it appears the 6-month lead forecasts of individual, large events have enough skill to be used in a statistical or AGCM forecast scheme for the subsequent winter. The results of this former effort are given in Part II, while the results of the latter effort will be reported elsewhere.

5. Discussion

The purpose of this section is to discuss some of the more interesting issues raised by the forecast result presented above. It is also of interest to compare the skill of the HCM with several of the other ENSO prediction methods now in semioperational use.

1) REGIONALIZATION OF SKILL

The forecast skills had a distinctive regional characteristic. The reasons for this are rather straightforward. Prior studies have shown that SST in the region of the waveguide is determined mainly by ocean dynamics. In this region air–sea heat exchange plays the role of a damping mechanism, trying to return the ocean to its climatological mean state (e.g., Barnett et al. 1991). In most tropical-ocean models, including the one used here, these fluxes are parameterized with a "Newtonian" formalism, so the operative physics is reasonably well represented. Outside the waveguide, say 10° or more away from the equator, and in the western Pacific, the near-surface heat budget is determined largely by air–sea exchange and not simply ocean dynamics. Thus, a good representation of these fluxes will be required to simulate the SST variation in these regions. This type of physics is not in the HCM. Finally, we note that the horizontal and, especially, vertical resolution of the OGCM is not adequate to resolve the climatological thermal structure in the eastern basin, and so the model shortcomings in this area were expected.

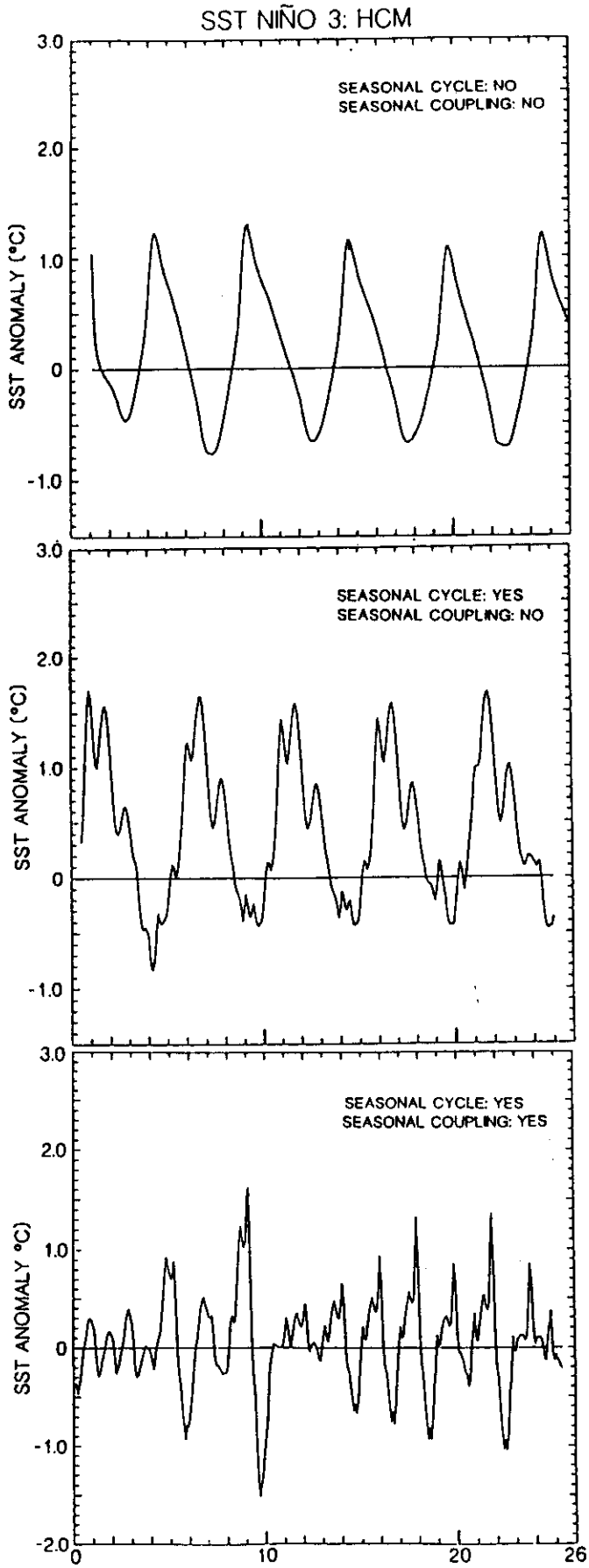

2) Seasonally varying physics

In an earlier study, Latif and Flügel (1991) carried out numerical experiments with a model much like that used here, but their results with regard to predictive skill were lower than found in the present study, particularly for long lead times. Part of the reason for this is that they did not detrend their hindcasts before computing the skill. However, their atmospheric model was based on a local regression between SST and wind stress. Recent work shows that the near-equatorial wind responds to the SST gradient, not just to the absolute value of the SST (Lindzen and Nigam 1987; Barnett et al. 1991), and so their model failed to capture some of the key physics necessary to explain ENSO, especially the off-equator wind-field relation needed to successfully capture Rossby wave activity. Perhaps more importantly, their atmospheric model was time invariant, and so the degree of air–sea coupling was independent of the seasonal cycle. In fact, their coupled model did not oscillate under extended integration as did the HCM unless random forcing was applied in addition to the anomalous forcing from the atmospheric model.

We tested the importance of the cyclostationary atmospheric–ocean interaction via three versions of the HCM. In the first case, the HCM was run in a perpetual July mode; that is, the phase of the annual cycle was fixed at July for both the climatological forcing and the anomalous wind forcing from the statistical atmospheric model. During extended integration, the model oscillated but now at a period of about 5 yr instead of the 2–3-yr periods noted earlier (Fig. 14, upper). In this case, addition of random forcing (noise) to the anomalous forcing still did not produce the 2–3-yr oscillations. In a second simulation, seasonal cycle forcing was permitted but the atmospheric model was held in perpetual July (Fig. 14, middle). A 5-yr period plus an annual cycle were produced by the HCM under this circumstance. Only with seasonality in both the climatological and anomalous forcing did the model produce 2–3-yr oscillations. For present purposes, we conclude that the seasonal cycle and cyclostationary character of the anomalous ocean–atmosphere coupling is critical to the ENSO process.

We also repeated the forecasts for the period 1986–90 using a time-invariant version of the atmospheric model; that is, while the seasonal cycle was allowed to evolve during the 18-month forecasts, the wind-stress anomaly calculation was done with the coefficients ap-

FIG. 14. Time series of NIÑO3 SST anomaly from HCM runs with various forms of seasonal wind forcing: no seasonal cycle and no seasonal dependence in ocean–atmosphere coupling (upper); seasonal-cycle forcing from climatology and no seasonal dependence in ocean–atmospheric coupling (middle); seasonal-cycle forcing from climatology and seasonal dependence in ocean–atmosphere coupling (lower).

propriate to the month of the initial condition. Thus, the importance of the seasonal variations in anomalous ocean–atmosphere coupling to the forecast problem was tested directly. The forecast skill for these time-invariant forecasts diverged steadily from those made with full seasonal information. At a lead time of about 8 months, the time-invariant forecast skills were about one-half those with seasonal cycle-dependent coupling. By lead time of 18 months, the former had values of under 0.2 compared with numerous 0.7–0.8 values for the seasonally varying coupling case. The disparity was most pronounced in the eastern half of the basin. The clear message from these experiments is that ENSO forecast models need seasonally varying physics to realize their full potential.

In summary, the models we have used strongly suggest that an important feature of the ENSO process involves the seasonally varying coupling between the ocean and the atmosphere. This same characteristic is seen in many statistical analyses of ENSO-related observational data (e.g., Rasmussen and Carpenter 1982; Wright 1984; Wright et al. 1985; Hasselmann and Barnett 1981; to name but a few). Interestingly, some tropical Pacific ocean–atmosphere models have been made to oscillate without taking any account of the seasonal cycle (e.g., Philander et al. 1992; Lau et al. 1992). However, the vast bulk of observational studies and other modeling studies suggest that the seasonal cycle is a critical element in ENSO, and so support the results found here.

3) Comparison of forecast skills

It is of interest to compare the hindcast–forecast skill described above with other ENSO prediction methods. An advanced statistical technique (Barnett et al. 1988; Graham et al. 1987a,b) and the coupled dynamical model from Lamont (Cane and Zebiak 1985; Zebiak and Cane 1987) produced forecasts for the NIÑO3 region for the independent forecast period 1986–91. These are shown along with the HCM forecasts and observed SST in Fig. 15 for a lead time of 9 months. All methods appear about equally skillful in that all capture the extended warm event early in the period, the intense cold event of 1988, and the subsequent, gradual warming to the recent warm event. One can pick minor disagreements between observations and predictions, but on the whole, the forecasts—and all were true forecasts—are rather good.

The Lamont model was also run over the dependent period and the results displayed (Fig. 16) in a manner comparable with those of the HCM (compare with Figs. 8 and 9). The comparison illustrates both the strong and weak points of both models. In general, the Lamont does better at all leads and seasons in the eastern part of the basin, while the HCM is superior in the central basin. The HCM does better at very short lead times because it is essentially initialized with observed SST. At lead times near 6 months the Lamont model is better during MAM, but during DJF both models are comparable. At lead times of 12 months, the regional characteristic of the model skills is most evident with the Lamont model, giving an encouraging performance in the eastern basin, and the HCM doing moderately well in the central ocean. The dichotomy in regional abilities suggests the obvious possibility of combining the predictions from the two models at a lead time approaching a year or beyond. At lead times of 18 months, the main regional features are still in evidence, but the HCM is slightly better, although the difference is small.

In summary, the forecast skill of the HCM is comparable with the statistical method but only during the winter season when the latter method has maximum ability. During the other seasons, the HCM is better (except summer when both models do poorly). The HCM is comparable with the Lamont model in forecast skill, but there is a major dissimilarity between the two. The former model works best in forecasting central ocean SST, while the latter does best forecasting SST in the eastern part of the basin. Although the record is too short to be definitive, during the independent test period of 1986–90 the Lamont model appears to have a slight edge. Since the HCM has had almost no "tuning," this small advantage in skill should be easy to overcome, but it seems more important at this stage to understand why the models differ so in their spatial forecast ability and to remedy what appears to be a legitimate difference in model physics rather than adjust coefficients to "best fit" a limited dataset.

4) Averaging forecasts

The forecast skills computed from the Lamont model (and used above) benefit immensely from the averaging of six consecutive forecasts (Cane et al. 1986; Graham et al. 1992). We tried the same strategy with

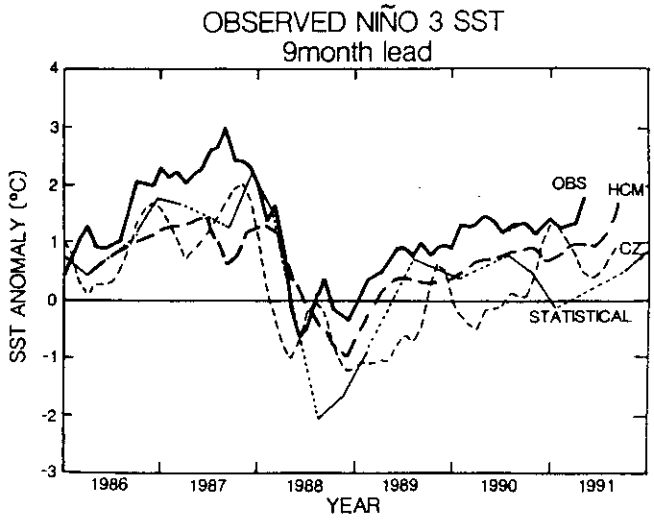

FIG. 15. NIÑO3 SST forecast by three models versus observations.

the HCM, but found no increase in skill. Indeed, the forecasts made for a specific month but at a different lead reproduced each other surprisingly well, a finding consistent with that of Graham et al. (1992). In other words, the forecast trajectories in phase space for the HCM are very stable and tend to trace each other. In the Lamont model, the forecasts from different initial conditions are really variable, and averaging helps to define the region of the phase space that best defines the forecast. Apparently the HCM is somewhat more deterministic, but it is unclear if this is good and/or a better/worse representation of the real world.

6. Conclusions

A new HCM of the tropical ocean–atmosphere system has been constructed. The ocean component of the model is a fully nonlinear OGCM confined to the tropical strip developed at the Max-Planck Institute in Hamburg (Latif 1987). The atmospheric component is a statistical model that uses OGCM SST to derive the wind-stress forcing for the ocean model. The atmosphere responds directly and immediately to only the SST field. A novel feature of the HCM is a statistical interface between the two components designed specifically to compensate for flaws in the OGCM.

The model has been run in the coupled mode for a 150-yr simulation. Sea surface temperature in the central equatorial Pacific serves as a good index for model behavior. The anomalous SST time series showed a chaotic behavior with irregular oscillations for the first 30 yr of integration. This was followed by a 2-yr and, later in the run, a 3-yr oscillation. The transition between regimes was abrupt, generally occurring within one cycle. Analysis of the control run led to the following conclusions.

(i) The space–time evolution of the key model variables (SST, sea level, and wind stress) showed systematic propagational characteristics that agree well with previous observational studies. The heat content of the upper 400 m in the model also showed a good correspondence to the spatial patterns of variations of a new observation set of the same quantity. In short, the HCM seems to have reproduced the important observed variations of the Pacific ocean–atmosphere system.

(ii) The model physics is well characterized by a single, natural mode of oscillation of the tropical Pacific

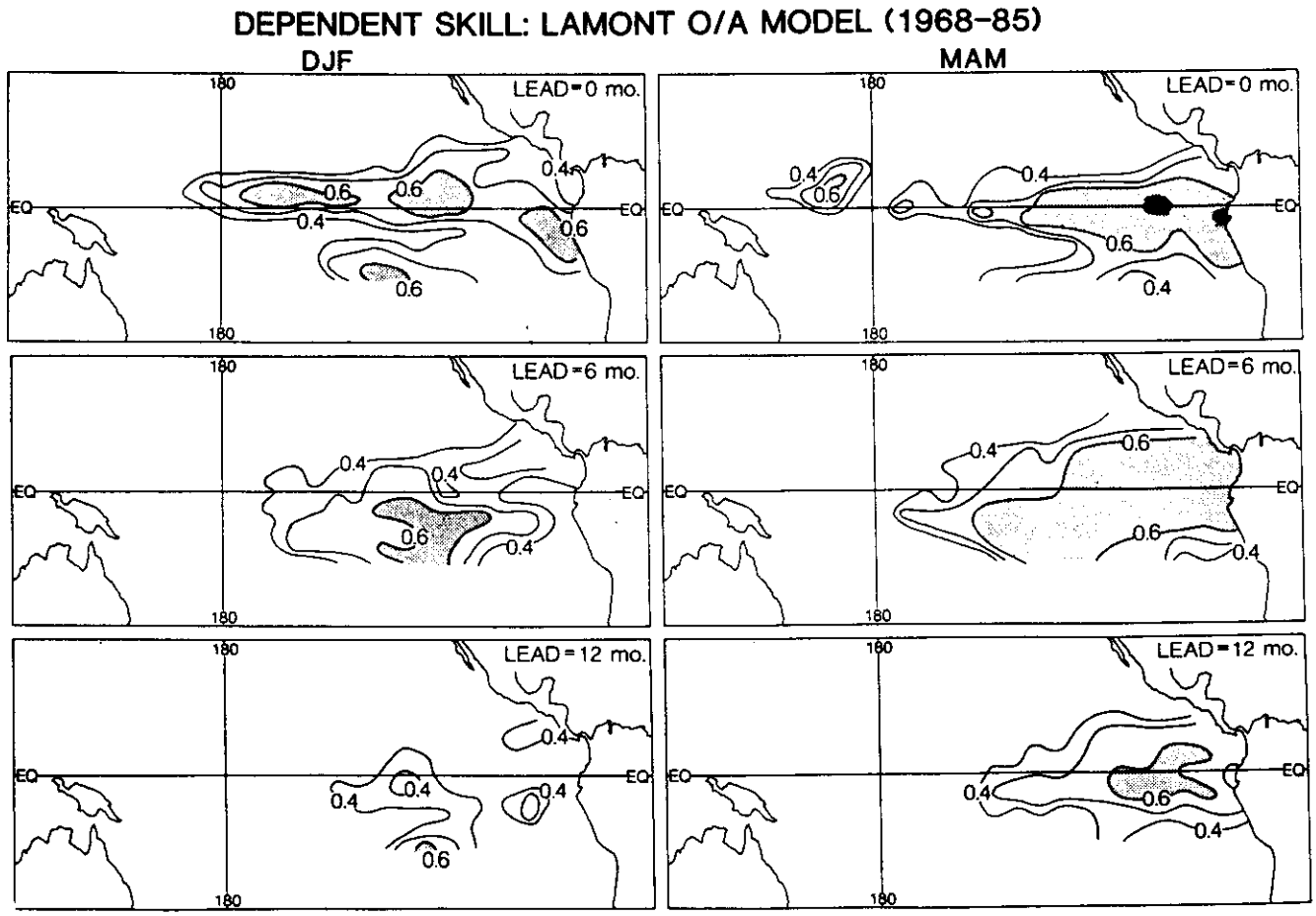

FIG. 16. Skill (correlation) of Lamont model hindcasts for DJF and MAM for the period 1968–85 at leads of 0, 6, and 12 months. Stipple convention as in Fig. 8.

ocean–atmosphere system. One element of this mode is the so-called delayed action oscillator and consists of westward propagation of Rossby waves. The second critical element is a slow air–sea interaction mode that propagates eastward along the equator. The physics of this mode, which is substantially different than those expected from Kelvin wave dynamics, has been described by Barnett et al. 1991.

(iii) The chaotic behavior in the HCM was attributed to a slow drift in the mean state of the ocean. This, in turn, suggests the importance to ENSO prediction of correctly simulating the mean background state of the tropical Pacific.

The HCM was used to make an extended series of hindcasts of Pacific SST for the period 1967–85 and a set of true forecasts for the period 1986–90. Analysis of the results of these numerical experiments led to the following conclusions.

(i) The HCM demonstrated real skill at forecasting SST out to lead times of 18 months, especially during the independent forecast period. A part of this later result is due to the shortness of the test period, but part of the skill is also due to the fact that this period is heavily populated by large events. A separate study suggested that the model best forecasts larger events but not smaller ones.

(ii) The main area of model skill was confined to the central equatorial ocean and to latitudes within 8°–10° of the equator. The model did poorly poleward of this band. It also did poorly in the eastern and western edges of the basin. The model shortcomings that account for the poor regional performance are partially due to OGCM resolution (too coarse) and to an inadequate representation of air–sea heat exchange in regions where this process dominates the upper-ocean heat balance.

(iii) The forecast skill of the HCM is comparable to that of a sophisticated statistical competitor and to the Lamont coupled model. It possesses both strengths and weaknesses compared to these competitors; that is, the Lamont model works well in the eastern ocean but not the central ocean, while the HCM had just the opposite characteristics. This is encouraging, for a thorough analysis of both models should allow us to produce a new coupled model that will be superior to both of its predecessors.

(iv) The regions where the HCM is most successful are just those that both modeling and empirical studies have shown are most strongly related to Northern Hemisphere winter climate anomalies. This, in turn, suggests that the HCM forecasts of tropical Pacific winter SST can be used in conjunction with either a statistical model or a full AGCM to provide useful forecasts for the tropics and those parts of the Northern Hemisphere that possesses a strong regional correlation to ENSO events. Forecast experiments using this former approach are described in Part II of this paper.

(v) A key element in the success of the HCM was its inclusion of seasonal variability in the degree of anomalous ocean and atmospheric coupling. Excluding the seasonal character oi this coupling produced poor forecasts and also poor simulations of the typical oceans seasonal mean state. It seems important to consider the seasonality of ocean–atmosphere interaction when attempting to realistically simulate ENSO.

Acknowledgments. The majority of this work was supported by the National Science Foundation through Grant ATM88-14571-03. The NOAA Experimental Climate Forecast Center at Scripps Institution of Oceanography also provided support (NOAA NA86AA-D-CP104), as did the Scripps Institution of Oceanography and the NOAA TOGA Program of Prediction (T-POP) through Grant NA 26GP0078-01. Mojib Latif's visit to La Jolla to complete this work was sponsored by the Department of Energy under Contract DOE DE-FG03-91ER61198. Tony Tubbs carried through the computational parts of the program. Special thanks are also due to Mike Jue and Andy Charman who contributed to the early phases of our attempts to construct coupled ocean–atmosphere models and who experienced firsthand the vagaries of these creatures. Jean Seifert helped produce the manuscript.

REFERENCES

Barbour, P., 1986: Construction of a monthly sea surface temperature for the global ocean: 1950–1979, SIO reference series 86-26, 5. [Available from Climate Research Division, Scripps Institution of Oceanography, University of California, San Diego, La Jolla, CA 92093.]

Barnett, T. P., 1977: An attempt to verify some theories of El Niño. *J. Phys. Oceanogr.*, 7, 633–647.

——, 1981: Statistical prediction of North American air temperatures from Pacific predictors. *Mon. Wea. Rev.*, **109**, 1021–1041.

——, 1984: Prediction of the El Niño of 1982–83. *Mon. Wea. Rev.*, **112**, 1403–1407.

——, and K. Hasselmann, 1979: Techniques of Linear Prediction with Application to Oceanic and Atmospheric Fields in the Tropical Pacific. *Rev. Geophys. Space Phys.*, **17**, 949–968.

——, and R. W. Preisendorfer, 1987: Origins and levels of monthly and seasonal forecast skill for United States air temperatures determined by canonical correlation analysis. *Mon. Wea. Rev.*, **115**, 1825–1850.

——, M. Latif, E. Kirk, and E. Roeckner, 1991: On ENSO Physics. *J. Climate*, **4**, 487–515.

——, N. Graham, M. Cane, S. Zebiak, S. Dolan, J. O'Brien, and D. Legler, 1988: On the prediction of the El Niño of 1986–1987. *Science*, **241**, 192–196.

Battisti, D. S., 1991: Reply. *J. Phys. Oceanogr.*, **21**, 461–465.

——, 1988: Dynamics and thermodynamics of a warming event in a coupled tropical atmosphere–ocean model. *J. Atmos. Sci.*, **45**, 2889–2919.

——, and A. C. Hirst, 1989: Interannual variability in a tropical atmosphere–ocean model: Influence of the basic state, ocean geometry and nonlinearity. *J. Atmos. Sci.*, **46**, 1687–1712.

Betts, A. K., and W. Ridgway, 1989: Climatic equilibrium of the atmospheric convective boundary layer over a tropical ocean. *J. Atmos. Sci.*, **46**, 2621–2641.

Busalacchi, A. J., and J. J. O'Brien, 1981: Interannual variability of the equatorial Pacific in the 1960's. *J. Geophys. Res.*, **86**, 10 901–10 907.

Cane, M. A., and S. E. Zebiak, 1985: A theory for El Niño and the Southern Oscillation. *Science*, **228**, 1085–1087.
——, S. E. Zebiak, and S. C. Dolan, 1986: Experimental forecasts of El Niño. *Nature*, **321**, 827–832.
——, M. Münnich, and S. E. Zebiak, 1990: A study of self-excited oscillations of the tropical ocean–atmosphere. Part I: Linear analysis. *J. Atmos. Sci.*, **47**, 1562–1577.
Gaffen, D., T. P. Barnett, and W. P. Elliott, 1991: Space and time scales of global tropospheric moisture. *J. Climate*, **4**, 989–1008.
Goldenberg, S., and J. O'Brien, 1981: Time and space variability of the tropical Pacific wind stress. *Mon. Wea. Rev.*, **109**, 1190–1207.
Goswami, B. N., and J. Shukla, 1991: Predictability of a coupled ocean–atmosphere model. *J. Climate*, **4**, 3–22.
Graham, N. E., 1992: Decadal-scale changes in winter Northern Hemisphere circulation during the 1970s and 1980s: Some observations and model results. *Proc. of the Fifth Conf. on Climate Variations*, Denver, CO.
——, and T. P. Barnett, 1987: Sea surface temperature, surface wind divergence, and convection over tropical oceans. *Science*, **238**, 657–659.
——, and W. B. White, 1988: The El Niño cycle: A natural oscillator of the Pacific ocean–atmosphere system. *Science*, **24**, 1293–1302.
——, and ——, 1990: The role of the western boundary in the ENSO cycle: Experiments with coupled models. *J. Phys. Oceanogr.*, **20**, 1935–1948.
——, and ——, 1991: Comments on "On the role of off-equatorial oceanic Rossby waves during ENSO." *J. Phys. Oceanogr.*, **21**, 453–460.
——, J. Michaelsen, and T. P. Barnett, 1987a: An investigation of the ENSO cycle with statistical models. Part I: Predictor field characteristics. *J. Geophys. Res., Oceans*, **92**, 14 251–14 270.
——, ——, and ——, 1987b: An investigation of the ENSO cycle with statistical models. Part II: Model results. *J. Geophys. Res.*, **92**, 14 271–14 290.
——, T. P. Barnett, and M. Latif, 1992: Considerations of the predictability of ENSO with a low-order coupled model. *Proc. of the 16th Annual Climate Diagnostics Workshop*, Los Angeles, NOAA, 323–327. [Available from National Oceanic and Atmospheric Administration, National Technical Information Service, U.S. Department of Commerce, Sills Building, 5285 Port Royal Road, Springfield, VA 22161.]
Hasselmann, K., 1988: PIPs and POPs: The reduction of complex dynamical systems using principal interaction and oscillation patterns. *J. Geophys. Res.*, **93**, 11 015–11 021.
——, and T. P. Barnett, 1981: Techniques of linear prediction for systems with periodic statistics. *J. Atmos. Sci.*, **38**, 2275–2283.
Inoue, M., and J. J. O'Brien, 1984: A forecasting model for the onset of a major El Niño. *Mon. Wea. Rev.*, **112**, 2326–2337.
Jin, F-F, and J. D. Neelin, 1993: Modes of interannual tropical ocean–atmosphere interaction—A unified view. Part III: Analytical results in fully coupled cases. *J. Atmos. Sci.*, **50**, (21) in press.
Kessler, W. S., 1991: Can reflected extra-equatorial Rossby Waves drive ENSO? *J. Phys. Oceanogr.*, **21**, 444–452.
Latif, M., 1987: Tropical ocean circulation experiments. *J. Phys. Oceanogr.*, **17**, 246–263.
——, and M. Flügel, 1991: An investigation of short-range climate predictability in the Tropical Pacific. *J. Geophys. Res.*, **96**, 2661–2673.
——, A. Sterl, E. Maier-Reimer, and M. M. Jaye, 1993: Structure and predictability of the El Niño/Southern Oscillation phenomenon in a coupled GCM. *J. Climate*, **6**, 700–708.
——, J. Biercamp, H. von Storch, M. J. McPhaden, and E. Kirk, 1990: Simulation of ENSO-related surface wind anomalies with an atmospheric GCM forced by observed SST. *J. Climate*, **3**, 509–521.
Lau, N. G., S. G. H. Philander, and M. J. Nath, 1992: Simulation of El Nino/Southern Oscillation phenomena with a low-resolution coupled general circulation model of the global ocean and atmosphere. *J. Climate*, **5**, 284–307.
Lindzen, R. S., and S. Nigam, 1987: On the role of sea surface temperature gradients in forcing low level winds and convergence in the tropics. *J. Atmos. Sci.*, **44**, 2418–2436.
McCreary, J. P., Jr., and D. L. T. Anderson, 1991: An overview of coupled ocean–atmosphere models of El Niño and the Southern Oscillation. *J. Geophys. Res.*, **96**, 3125–3150.
Miller, A. J., J. Oberhuber, N. E. Graham, and T. P. Barnett, 1992: Tropical Pacific Ocean response to observed winds in a layered general circulation model. *J. Geophys. Res. Oceans*, **97**(C5), 7317–7340.
Münnich, M., M. A. Cane, and S. E. Zebiak, 1991: A study of self-excited oscillations of the tropical ocean–atmosphere system. Part II: Nonlinear Cases. *J. Atmos. Sci.*, **48**, 1238–1248.
Neelin, J. D., 1989: Interannual oscillations in an ocean general circulation model coupled to a simple atmosphere model. *Phil. Trans. Roy. Soc. London*, **329A**, 189–205.
——, 1990: A hybrid coupled general circulation model for El Niño studies. *J. Atmos. Sci.*, **47**, 674–693.
——, 1991: The slow sea surface temperature mode and the fast-wave limit: Analytic theory for tropical interannual oscillations and experiments in a hybrid coupled model. *J. Atmos. Sci.*, **48**, 584–606.
——, and F-F. Jin, 1993: Modes of interannual tropical ocean–atmosphere interaction—A unified view. Part II: Analytical results in the weak-coupling limit. *J. Atmos. Sci.*, **50**, (21) in press.
Pazan, S. E., W. B. White, and R. Molinari, 1993: Global variability in the upper ocean thermal structure. Part I: The long-term mean and annual cycle, 1979–88. *J. Phys. Oceanogr.*, **23**,
Philander, S. G. H., R. C. Pacanowski, N. C. Lau, and M. J. Nath, 1992: A simulation of the Southern Oscillation with a global atmospheric GCM coupled to a high-resolution, tropical Pacific Ocean GCM. *J. Climate*, **5**, 308–329.
Posmentier, E. S., M. A. Cane, and S. E. Zebiak, 1989: Tropical Pacific climate trends since 1960. *J. Climate*, **2**, 731–736.
Preisendorfer, R. W., 1988: *Principal Component Analysis in Meteorology and Oceanography*. Elsevier, 425 pp.
Rasmusson, E., and T. Carpenter, 1982: Variations in tropical sea surface temperature and surface winds associated with the Southern Oscillation/El Niño. *Mon. Wea. Rev.*, **110**, 354–384.
Sausen, R., K. Barthel, and K. Hasselmann, 1988: Coupled ocean–atmosphere models with flux corrections. *Climate Dyn.*, **2**, 145–163.
Schopf, P. S., and M. J. Suarez, 1988: Vacillations in a coupled atmosphere–ocean model. *J. Atmos. Sci.*, **45**, 549–566.
Slutz, R., S. Lubker, J. Hiscoz, S. Woodruff, R. Jenning, D. Joseph, P. Steurer, and D. J. Elms, 1985: The comprehensive ocean–atmosphere data set release. I: Climate Research Program, ERL/NOAA, Boulder, CO, 39 pp.
Suarez, M. J., and P. S. Schopf, 1989: A delayed action oscillator for ENSO. *J. Atmos. Sci.*, **45**, 3283–3287.
Trenberth, K. E., 1990: Recent observed interdecadal climate changes in the Northern Hemisphere. *Bull. Amer. Meteor. Soc.*, **71**, 988–993.
von Storch, H., and J. Xu, 1990: Principal oscillation pattern analysis of the 30- to 60-day oscillation in the tropical troposphere. Part I: Definition of an index and its prediction. *Climate Dyn.*, **4**, 175–190.
Wakata, Y., and E. S. Sarachik, 1991: On the role of equatorial ocean modes in the ENSO cycle. *J. Phys. Oceanogr.*, **21**, 434–443.
Waliser, D. D., and Graham, N. E., 1992: Convective cloud systems, and warm-pool SSTs: Coupled interactions and self-regulation. *J. Geophys. Res.*, in press.
Wright, P., 1984: Relationships between indices of the Southern Oscillation. *Mon. Wea. Rev.*, **112**, 1913–1919.
——, T. P. Mitchell, and J. M. Wallace, 1985: Relationships between surface observations over the global oceans and the Southern Oscillation. NOAA Data Report, ERL PMEL-12, 21.
Xu, J. S., and H. von Storch, 1990: Principal oscillation patterns—The state of the ENSO cycle. *J. Climate*, **3**, 1316–1329.
Zebiak, S., and M. Cane, 1987: A model El Niño/Southern Oscillation. *Mon. Wea. Rev.*, **115**, 2262–2278.

Observed wind speed annual cycle (x)

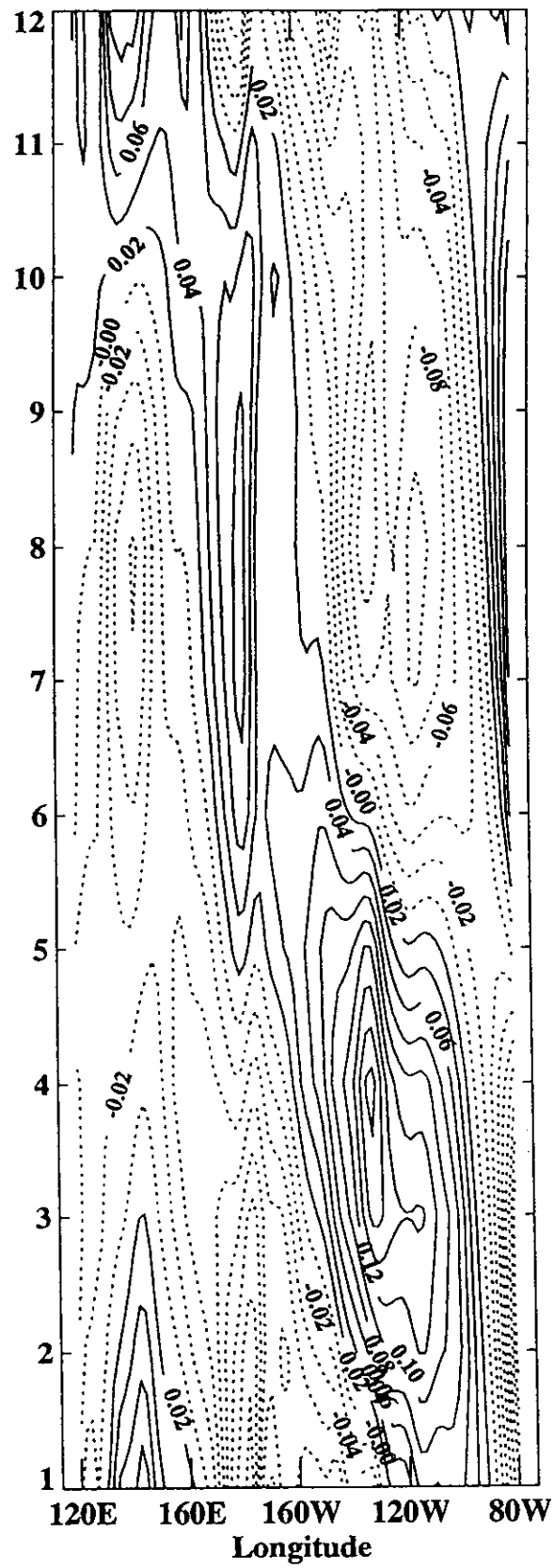

Atmospheric model data

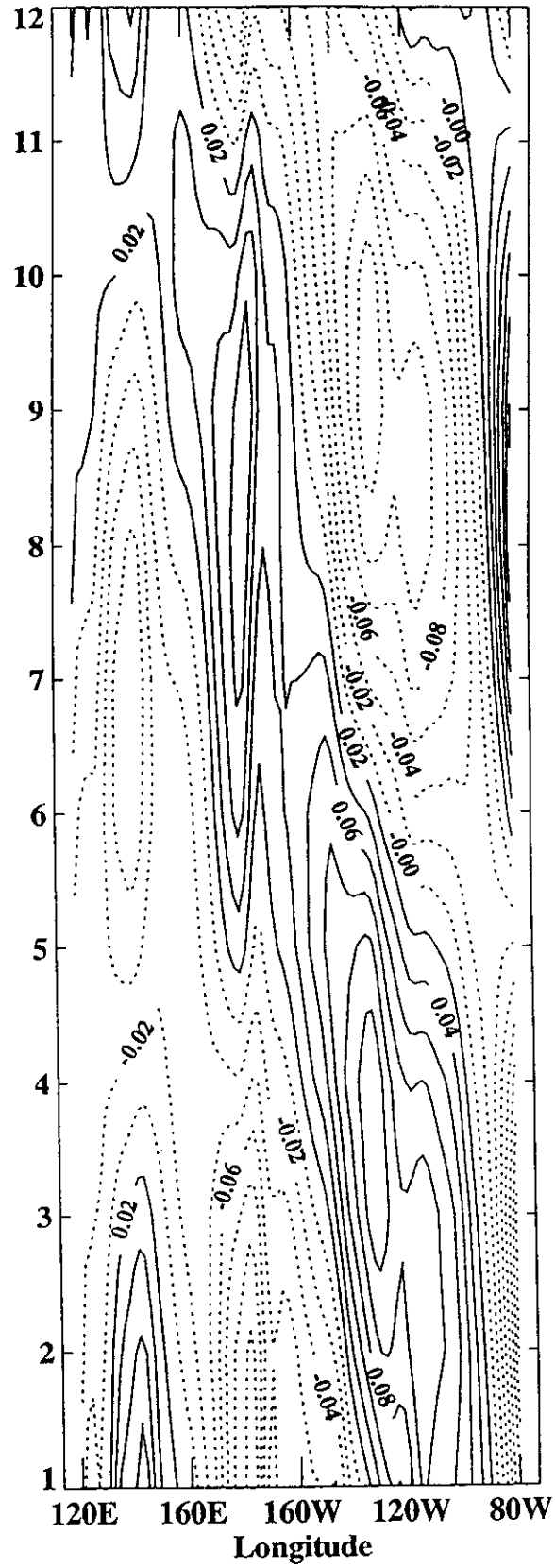

Giese stress data, 8 eigenvetors used, with interpolation and 5-month filter

Observed wind stress anomaly (x)

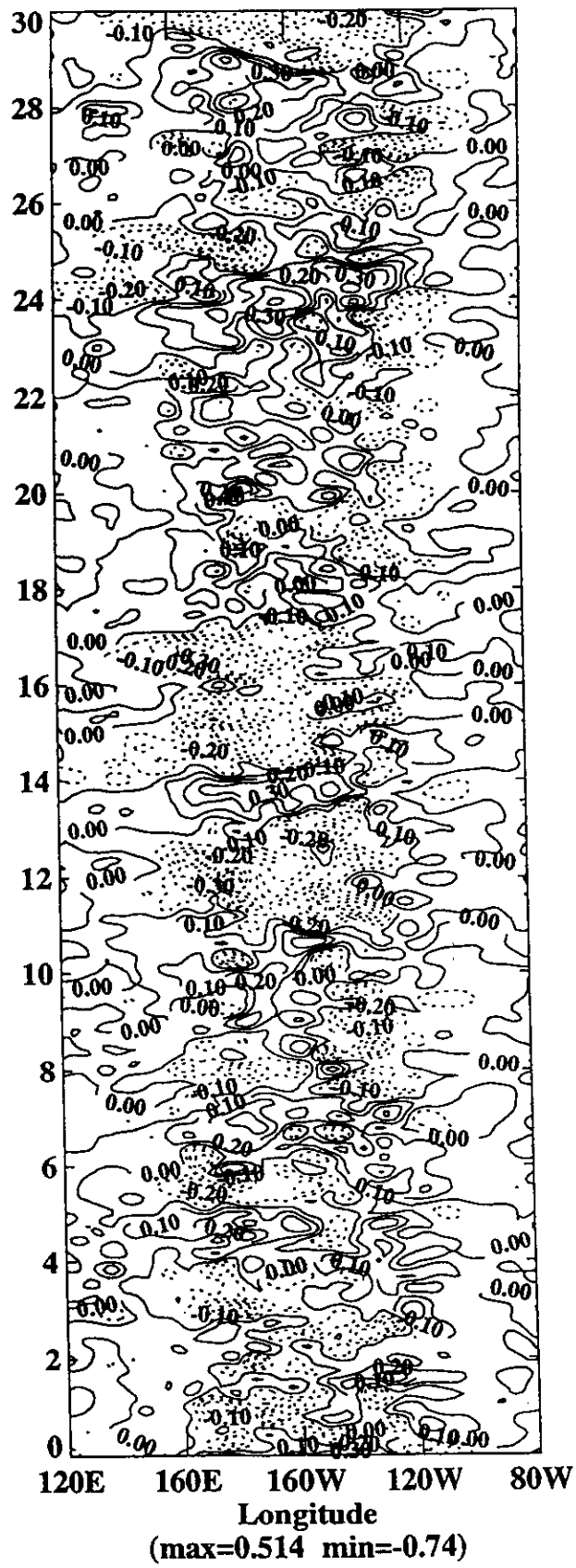

Atmospheric model data(x)

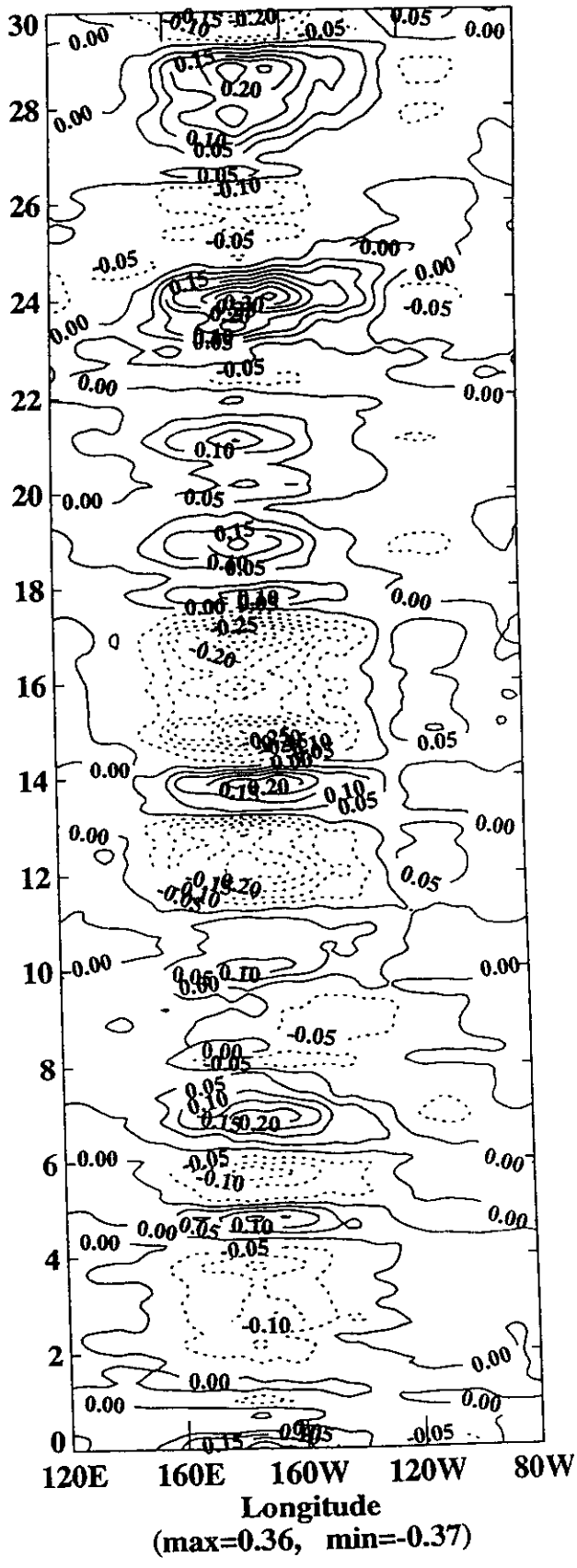

Giese stress data, 8 eigenvetors used, with interpolation and 5-month filter

Observed wind speed annual cycle (x)

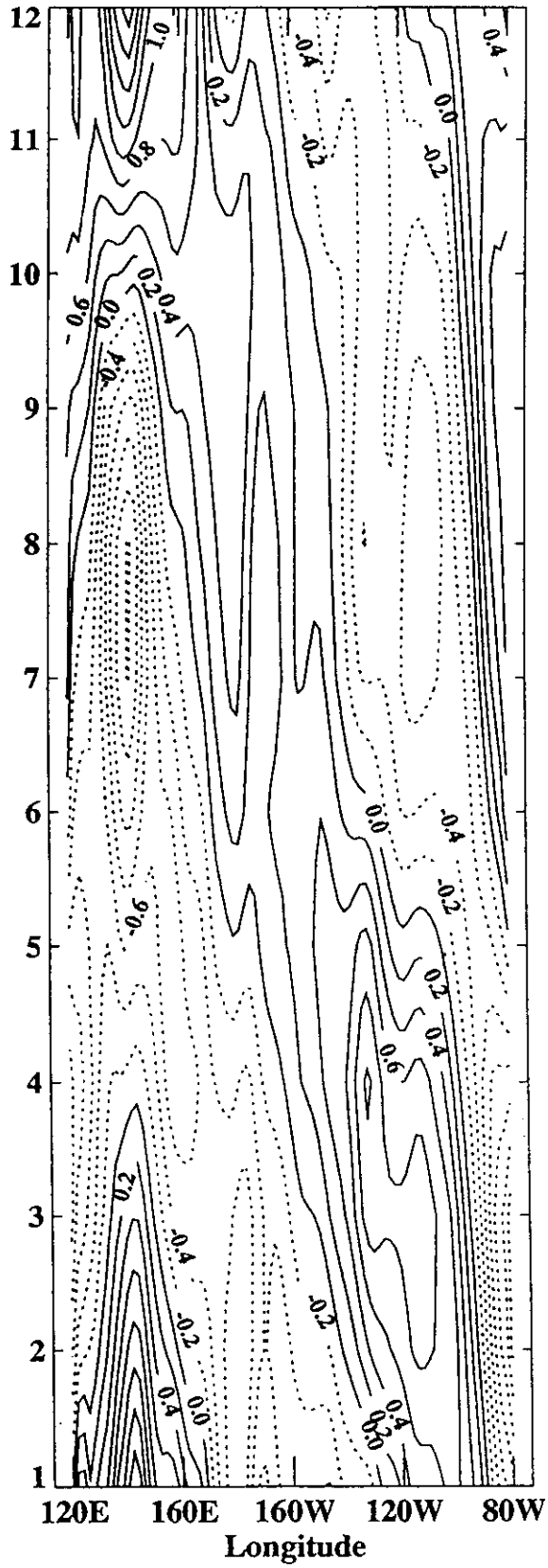

Atmospheric model data

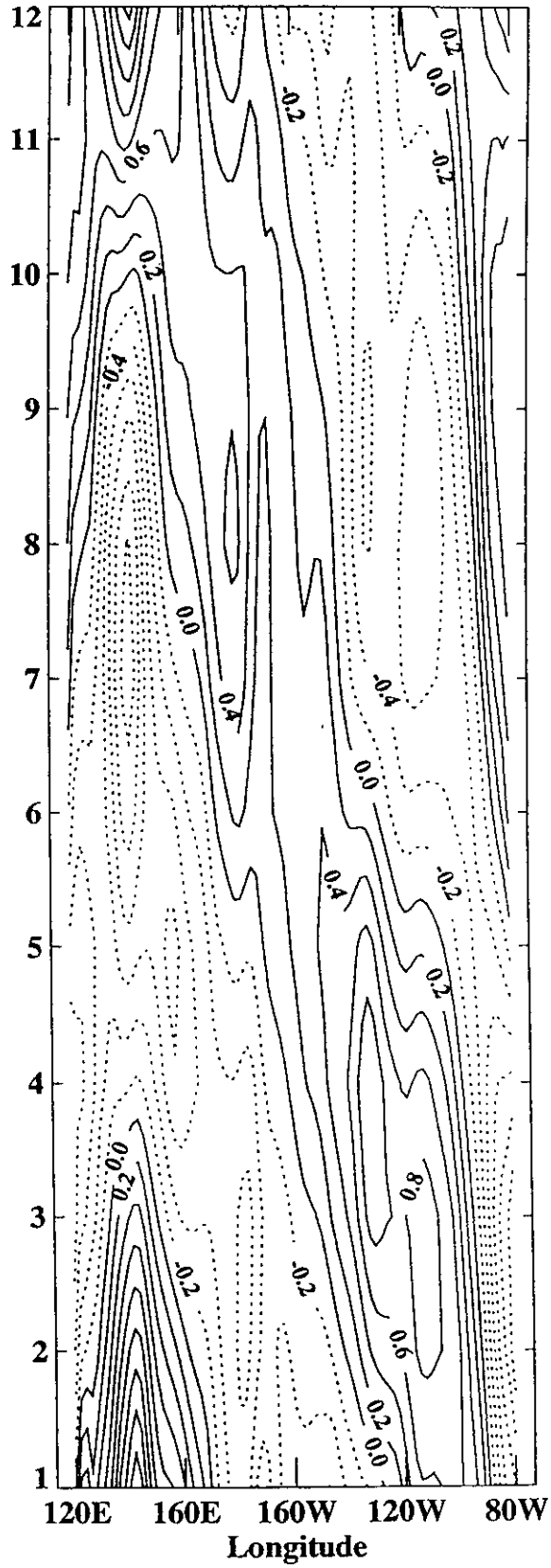

Giese speed data, 40 eigenvetors used, with interpolation and 5-month filter

Observed wind speed anomaly (x)

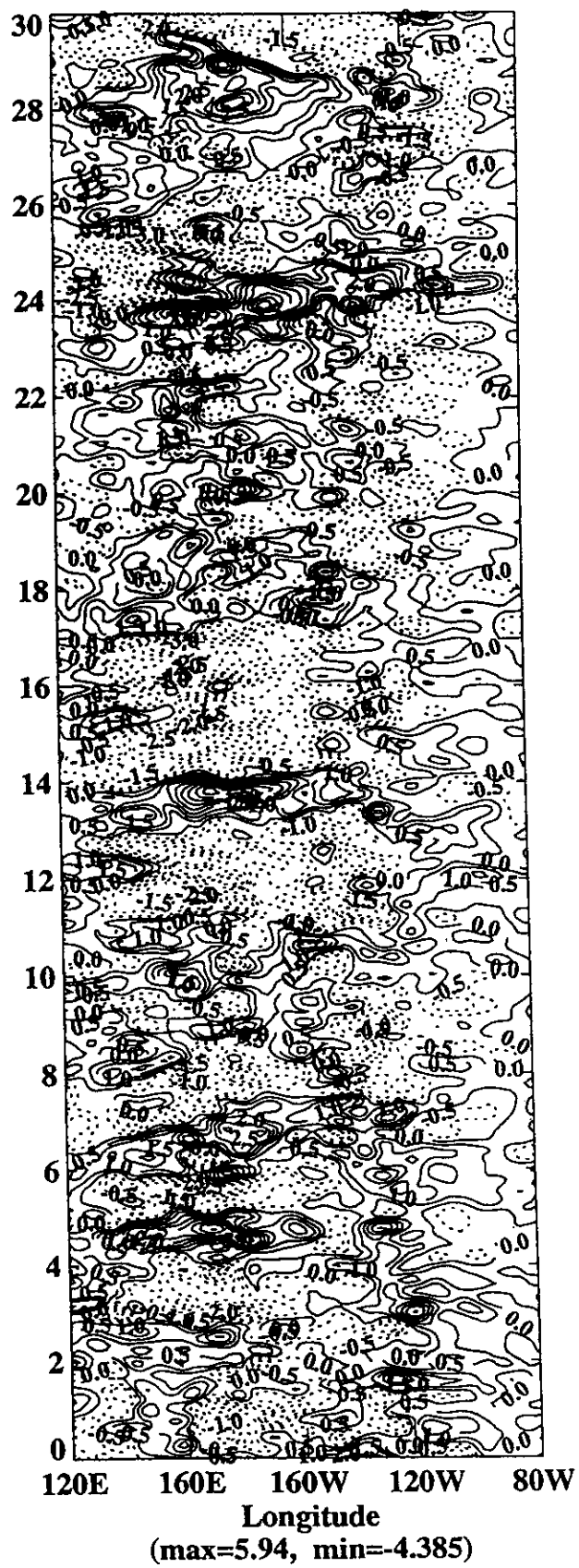

(max=5.94, min=-4.385)

Atmospheric model data(x)

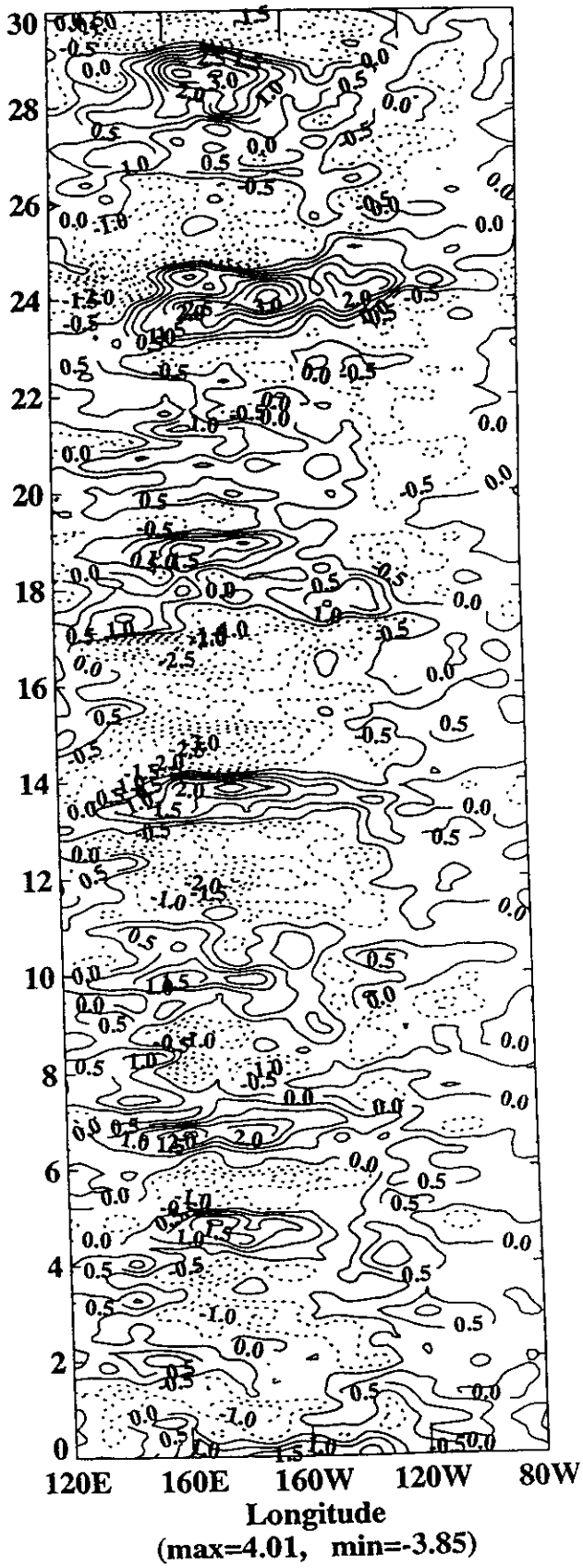

(max=4.01, min=-3.85)

Giese speed data, 40 eigenvetors used, with interpolation and 5-month filter

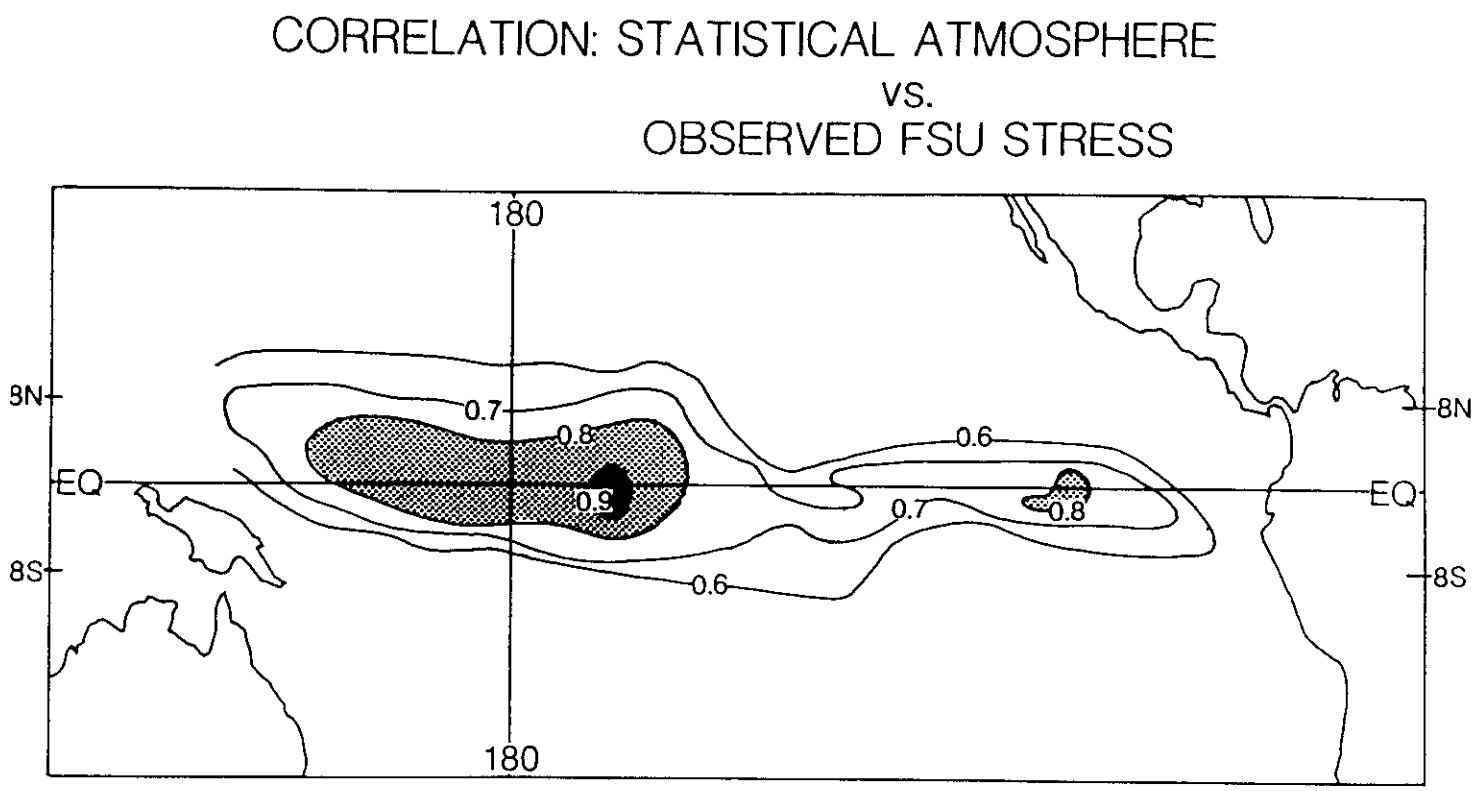

FIG. 2a. Correlation between atmospheric-model zonal stress and observed zonal stress over the period 1965–1985. Values above 0.8 are stippled and above 0.9 are heavily stippled.